BMP-modulated extracellular matrix mechanics in the early phase of fracture healing

Inaugural-Dissertation

to obtain the academic degree

Doctor rerum naturalium (Dr. rer. nat.)

Submitted to the Department of Biology, Chemistry and Pharmacy

of Freie Universität Berlin

by

Erik Brauer

Berlin, June 2019

The work presented in this thesis was performed between November 2013 and June 2019 in the group of Cellular Biomechanics from the Julius Wolff Institute under supervision of Prof. Dr. Georg N. Duda.

This thesis was realized within the framework of the Berlin-Brandenburg School for Regenerative Therapies (BSRT) and the Berlin-Brandenburg Center for Regenerative Therapies (BCRT) in active collaboration with the group of Prof. Dr. Petra Knaus from the Institute for Chemistry and Biochemistry of Freie Universität Berlin.

1. Gutachter:	Prof. Dr. Petra Knaus
2. Gutachter:	Prof. Dr. Georg N. Duda
Disputation date:	09.12.2019

Für meine Familie, Freunde, Kollegen und ganz besonders für meine Frau und meinen Sohn. Ich danke euch für alles.

Abstract

Regenerative medicine aims to re-establish full functionality of tissues and organs after injury through the stimulation of the body's endogenous repair mechanisms. In higher mammals, bone is one of the few tissues that shows a natural self-healing capacity and therefore can be used as a model system to describe regenerative processes. A detailed understanding eventually can be translated to other tissues and organs with an intrinsically poor healing outcome such as tendon, cartilage, cardiac and skeletal muscle. But even for bone the natural regenerative capacity can be exceeded, especially when large quantities of tissue need to be restored. Approximately 10% of all fractures result in a delayed healing or even a non-union which requires clinical intervention and follow-up.

Bone morphogenetic proteins (BMPs) are potent osteoinductive growth factors with clinical approval for usage in open tibial fractures and spinal fusions. Despite its beneficial effect on the overall healing outcome, the supra-physiological amounts lead to various side effects. While it is generally believed that BMPs mostly affect cell migration and differentiation, only limited information is available how early extracellular matrix formation and patterning is influenced.

This thesis investigated the process of tissue formation *in vitro* using a soft macroporous collagen scaffold and how BMP stimulation affected this process. Tissue formation and tensioning was found to strongly depend on the presence of collagen fibers. It could be demonstrated that tissue forming cells incrementally transfer and store cellular forces inside a tensioned fibrillar collagen network which led to a multiplication of macroscopic tension. Stimulation with BMP during the process of tissue formation led to an acceleration of contraction and an increased stiffening which was followed by a matrix metalloproteinase-mediated remodeling and softening. Collagen scaffolds of varying stiffness were finally used as a model system to investigate the influence of an altered mechanical environment on BMP signaling. Cells showed an increased BMP responsiveness when cultured inside very soft collagen scaffolds (0.5kPa) compared to stiffer environments (>4kPa). Intriguingly, cellular migration within soft scaffolds led to a systemic deformation of the underlying biomaterial which might be responsible for an inter-cell communication through substrate deformation.

Taken together, this thesis provided insights into formerly unknown aspects of tissue formation as well as how BMP stimulation modulates and signaling response itself becomes modulated by this process. These findings are expected to contribute to future biomaterial design in order to overcome limitations of current treatment options for bone defects as well as to increase safety and efficacy of BMPs in clinical applications.

Zusammenfassung

Regenerative Medizin verfolgt die Wiederherstellung der vollen Funktionalität von Geweben und Organen nach Verletzung durch die Aktivierung körpereigener Reparaturmechanismen. In höheren Säugetieren weist Knochen als eines der wenigen Gewebe des Körpers eine natürliche Fähigkeit zur Selbstheilung auf und kann damit als Modellsystem für regenerative Prozesse genutzt werden. Ein tiefgreifendes Verständnis dieser ließe sich eventuell auf andere Gewebetypen, wie z.B. Sehnen, Knorpel, Skelett- und Herzmuskel, übertragen, welche über eine verringerte Fähigkeit zur Selbstheilung verfügen. Jedoch kann in manchen Fällen selbst im Knochen die natürliche Fähigkeit zur Heilung unzureichend sein, besonders, wenn größere Mengen an Gewebe wiederhergestellt werden müssen. So tritt in etwa bei 10% aller Knochenbrüche eine verzögerte oder sogar eine Nicht-Heilung auf, welche klinische Behandlung erfordert.

Bone morphogenetic proteins (BMPs) sind Wachstumsfaktoren mit einem hohen osteoinduktiven Potential und sind zur klinischen Behandlung offener Tibia-Frakturen sowie Wirbelkörperfusionen zugelassen. Obwohl eine Behandlung mit BMPs den generellen Heilungsverlauf verbessert, sorgen die hohen Mengen die eingesetzt werden oft für Nebenwirkungen. Während allgemein angenommen wird, dass BMPs hauptsächlich durch die gerichtete Einwanderung und Differenzierung von Stammzellen wirken, ist nur wenig darüber bekannt inwieweit frühe Gewebeformationsprozesse beeinflusst werden.

Diese Arbeit befasste sich mit dem Prozess der Gewebeformation *in vitro* mittels eines makroporösen Kollagen Biomaterials sowie dem Einfluss von BMP Stimulation auf diese Prozesse. Es konnte gezeigt werden, dass Gewebeformation und Vorspannung stark von der Anwesenheit von Kollagenfasern abhängig waren. Dies bedeutet, dass gewebebildende Zellen schrittweise Kraft in vorgespannte Kollagenfasern übertragen und speichern was zu einer Vervielfachung der makroskopischen Gewebespannung führt. BMP Stimulation beschleunigte diesen Prozess, was zu einer erhöhten Gewebeversteifung führte, die jedoch durch einen Metalloproteinase-vermittelten Umbauprozess reduziert wurde. Biomaterialen mit unterschiedlicher Steifigkeit wurden zu guter Letzt als Modellsystem verwendet um den Einfluss einer veränderten mechanischen Umgebung auf die BMP Signalgebung zu untersuchen. Zellen wiesen eine erhöhte BMP-Antwort auf wenn sie in einem weichen Biomaterial kultiviert wurden (0.5kPa) verglichen mit steiferen

Umgebungen (>4kPa). Es zeigte sich, dass zelluläre Bewegungen in einer weichen Umgebung zu einer systemischen Verformung des zugrundeliegenden Materials führt, was auf eine Möglichkeit zellulärer mechanischer Kommunikation mittels Substratverformung hindeutet.

Zusammengefasst zeigt diese Arbeit bisher unbekannte Aspekte der Gewebeformation auf, sowie der Einfluss von BMP Stimulation auf diese Prozesse. Diese neuartigen Erkenntnisse unterstützen potentiell die Entwicklung zukünftiger Biomaterialien um sowohl die Limitationen gegenwärtiger Behandlungsoptionen bei der Behandlung großer Knochendefekte zu überwinden, als auch Sicherheit und Effizienz von BMPs in klinischen Anwendungen zu verbessern.

Content

List of figures

List of tables

1 Introduction

Until the early 1980s, the extracellular matrix (ECM) was sparsely considered as anything different as the “Styrofoam packing material” of tissue cells mainly fulfilling a passive scaffolding and shielding function. With the discovery of the family of integrin cell surface receptors [1] this view has dramatically changed and our current understanding pictures these proteins to be integrated into a dynamic and versatile machinery that not only serves as a transducer of mechanical signals but enables cells to actively explore their surrounding environment [2].

In fact, current research more and more focuses on the extracellular matrix as an active component that steers cellular functions by providing tissue-specific structure and adhesion sites, serving as a reservoir for ions, water, nutrients and growth factors but also featuring distinct geometrical and mechanical properties. In particular, the relevance of mechanical cues was demonstrated in a pioneering study by the group of Dennis Discher in 2006 showing that lineage commitment of mesenchymal stem- and progenitor cells can be influenced by the culture substrate stiffness [3]. With more than 6500 citations (December 2018) this work shaped the field of mechanobiology with a strong focus on the interaction of cells and tissues and further studies could demonstrate an influence of mechanical cues on diverse cellular functions in development and repair, homeostasis and disease [4–6].

Aside of the improved understanding, these findings substantially contributed to the fields of tissue engineering and regenerative medicine [7] to meet specific cellular requirements by an optimized and advanced biomaterial design in order to harness the endogenous regeneration capacity. Further improvements might help to overcome limitations of current treatment options for musculoskeletal defects and injuries but also in the fields of cancer research or neurodegenerative diseases [4,8].

1.1 Bone – the blueprint of regeneration?

Normal tissues usually maintain in an equilibrium of formation and degradation that is tightly balanced. Upon a traumatic injury, a provisional hematoma needs to be replaced by new tissue in concert with the original architecture in order to recreate full functionality - a process that is understood as regeneration. Some lower vertebrates exhibit the

remarkable ability to fully regenerate parts of their organs or even entire limbs [9,10]. This capacity is mostly lost in higher mammals during embryogenesis and most tissues experience a process, which is referred to as repair and mainly involves fibroblasts to deposit a collagen-rich extracellular matrix serving as a transitional “patch” but lacking the full functionality of the original tissue.

However, aside of the liver where parts can be removed and over time the organ regains its original mass and functionality, bone is the only tissue that can undergo a true regeneration process after injury. This mostly unique feature motivated intense investigations of the regenerative processes occurring during fracture healing with the hope that it might inspire approaches for other tissues and organs suffering rather from irreversible scarring [11].

Unlike many other tissues and organs, bone experiences a continuous and highly dynamic self-renewal in which bone becomes resorbed by osteoclasts and newly build by osteoblasts. Both processes are tightly coupled allowing the bone to meet its mechanical needs and become tougher where it is mechanically challenged. This principle was described by Julius Wolff in the 19th century and is referred to as Wolff’s law. Over the past decades numerous studies were able to demonstrate the molecular mechanisms behind this principle showing that the differentiation and activity of osteoblast and osteoclast precursor cells is depending on mechanical cues [12].

1.1.1 Phases of fracture healing

The unique multiphase processes occurring during fracture healing have been described in detail over the last decades and involve the spatiotemporal presence of multiple cell types such as adaptive and innate immune cells, fibroblasts, endothelial cells, osteoblasts, chondrocytes or their respective precursor cells (Figure 1-1).

The initial response after a bone fracture is characterized by a hematoma formation followed by the invasion of immune cells into the fracture gap. These involve the presence of innate immune cells such as macrophages [13] but also cells of the adaptive immune system which are involved in removing necrotic tissue, driving angiogenesis as well as stem cell differentiation [14,15]. The general inflammatory milieu is supported by the secretion of various pro-inflammatory cytokines such as TNF-α, IL-1β or IL-6 and successively is transferred into an anti-inflammatory phase characterized by the presence of

TGF-β, FGF-2 and BMPs [16]. Following the initial inflammatory response, tissue forming cells (fibroblasts, MSCs) are driven into the fracture gap by chemotactic morphogen gradients from different sources such as the bone marrow, but can also originate from the periosteum or surrounding soft tissue [17,18]. These cells participate in a primary tissue formation process that involves the secretion of transitory ECM proteins such as fibronectin but also fibrillar collagen. The latter allows a first mechanical stabilization and structural organization of the trauma region. In particular, the structural organization of the fibrillar collagen network deposited at early stages of healing was recently shown to precede and further guide bone mineralization processes [19].

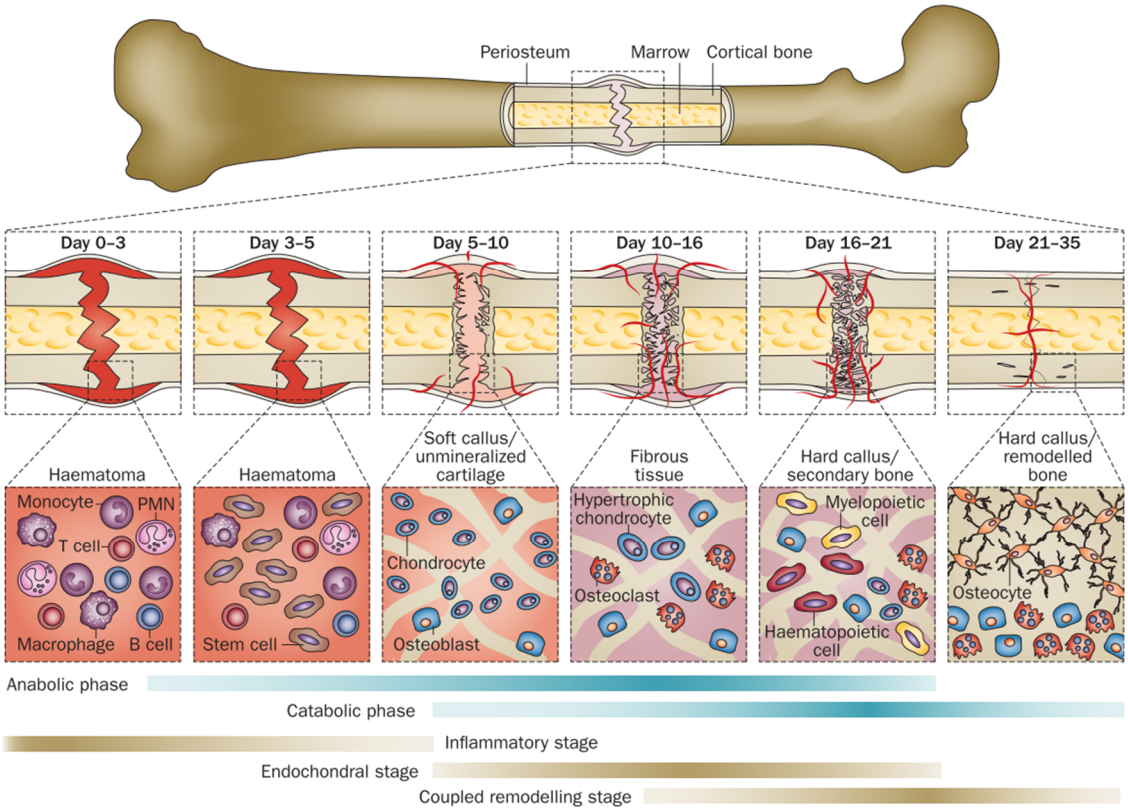

Figure 1-1: The phases of fracture healing. Figure reproduced with permission from Springer Nature [20].

Reconstitution of bone tissue can occur in two different modes. Intramembranous ossification is the process where new bone is directly created by osteoblasts calcifying the granulation tissue. In contrast, endochondral ossification depends on the generation and replacement of a cartilage template by chondrocytes that are driven intro hypertrophy. A preference either of intramembranous or endochondral ossification during healing depends on various parameters such as vessel ingrowth and resulting oxygen supply [19].

Furthermore, the spatiotemporal presence of distinct growth factors such as bone morphogenetic proteins (BMPs), Indian Hedgehog (IHH), Wnt and parathyroid hormone–related peptide (PTHrP) influences cellular proliferation, survival and differentiation during progenitor cell lineage commitment and chondrocyte hypertrophy [20]. Within a final remodeling phase the mineralized hard callus that is also referred to as “woven bone” is reorganized into cortical or trabecular lamellar bone featuring superior mechanical strength.

Although several influencing factors of bone regeneration have been described, the whole process is not fully understood yet. Since in principle all factors that are described to modulate bone regeneration are directly or indirectly interdependent, little focus has been spend on a potential crosstalk. However, several studies could demonstrate the synergistic effect of mechanical loading and BMP stimulation *in vitro* and *in vivo*, which underlines the strong regulatory potential but also the high complexity [21–23].

1.2 The ECM – from composition to function

The extracellular matrix is a composite collection of cell-secreted macromolecules, which resembles all non-cellular parts of living tissue. Originating in the evolution of multicellularity, the extracellular matrix has its main function in providing scaffold, stress shielding and support for adhering cells. Aside of this general concept, however, the ECM has multiple tissue-specific functions including sequestering, retaining and presenting of growth factors, serving as water and nutrient supply and providing mechanical and architectural cues to cells (Figure 1-2).

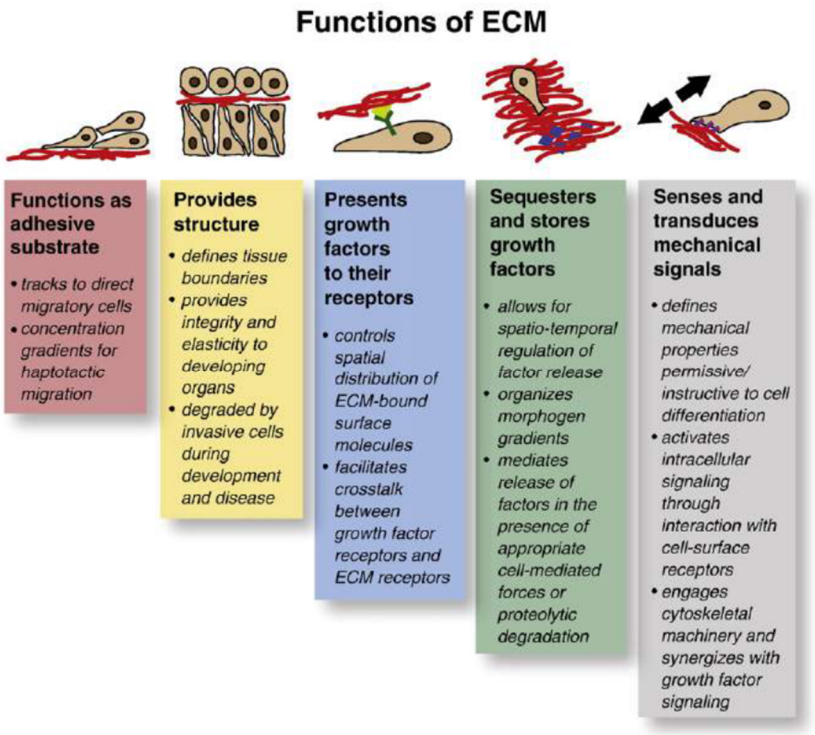

Figure 1-2: Summary of various extracellular matrix functions. Figure reproduced with permission from Springer Nature [5].

1.2.1 Classes of ECM proteins

The molecular composition of the ECM is an essential determinant of the specific tissue function. ECM molecules can be grouped into distinct families and classes based on their evolutionary origin or based on function [5,24]. In general, one can distinguish between collagens and microfibrillar proteins as fiber-forming molecules, proteoglycans and a rather heterogeneous group of non-collagenous glycoproteins. In addition, cells further secrete and regulate the activity of matrix-degrading enzymes.

Collagens – Collagen is the most abundant component of the extracellular matrix and is used by the cells to shape most of the structural and mechanical properties of the tissue. It comprises about a third of the total protein and up to three quarters of the dry weight in human skin [25] and mutations are often associated with severe hereditary connective tissue disorders [26,27]. At least 28 different types of collagen have been described which can be classified into four groups according to their location and function: the fibrillar collagens, network forming collagens, FACITs (fibril-associated collagens with interrupted helices), MACITs (membrane-associated collagens with interrupted helices) and MULTIPLEXINs (multiple triple-helix domains and interruptions) (Supplement 1).

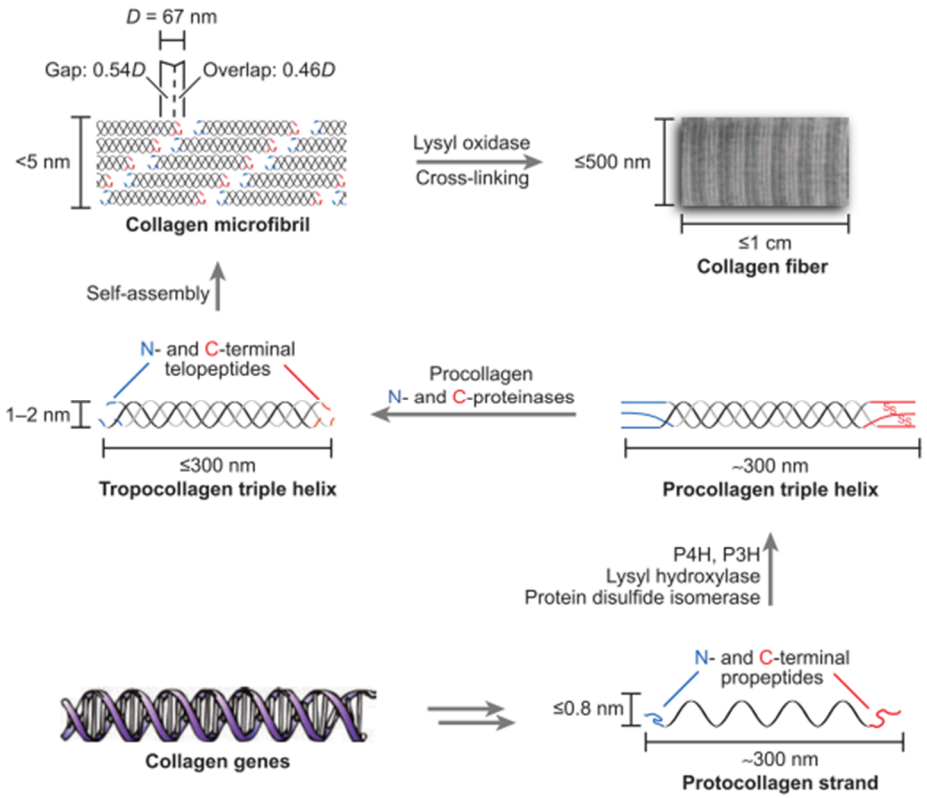

Figure 1-3: Synthetic route of collagen fibers. Figure reproduced with permission from Annual Reviews.[25]

Collagens are synthesized as large single-stranded molecules (Figure 1-3) that all follow the same repeat of a $X_{aa}Y_{aa}Gly$ sequence in which X_{aa} and Y_{aa} can be substituted by any amino acid, but with high abundance of proline and hydroxyproline [28]. This amino acid sequence allows the tight packing of three left-handed collagen single strands into a staggered right-handed triple helix. These intracellularly assembled procollagen molecules experience further extracellular cleavage of the N-terminal and C-terminal pro-peptides after which individual tropocollagen molecules self-assemble into staggered collagen fibrils and fibers. Lysyl oxidase-mediated covalent crosslinking of adjacent triple helices further enables macroscopic mechanical stability.

Fibrillar collagens usually follow this process, whereas all non-fibrillar collagens usually have an imperfection in their triple helix and, such as the FACITs, are adherent to the surface of collagen fibrils or form other kinds of collagen networks such as the basement membrane of blood vessels (collagen type IV).

Fibrillar components – Aside of collagen proteins, other ECM proteins are capable to form an ECM network of fibrillar character including elastin, fibronectin and laminins. Whereas collagen fibers are responsible for the load-bearing properties of the ECM and

provide tensile strength, elastin fibers provide resilience to tissues that experience continuous mechanical strain (e.g. skin, lung, ligaments, arteries). Elastin fibers are extremely stable and are mostly deposited during embryogenesis and neonatal stages of adolescence. Fragmentation and degradation of elastin fibers by elastases is a process that gradually increases with age and is considered as a hallmark of aging [29]. Fibronectin is a glycoprotein that features many different functions during embryogenesis, tissue repair and homeostasis [5] and becomes, aside of collagens, one of the most abundant and important ECM proteins. Fibronectin features a multidomain architecture that is involved in the interaction either with other ECM components (e.g. via Heparin of proteoglycans, collagen, Tenascin, fibrin) or cell adhesion via integrin receptors [30]. Due to its essential role in steering cell-matrix interactions via integrin binding, fibronectin is highly relevant for cellular migration, growth and differentiation.

Proteglycans – Proteoglycans are composite molecules consisting of a core protein (except hyaluronic acid) covalently linked to at least one glycosaminoglycan (GAG) polysaccharide chain. This relatively heterogeneous group of macromolecules can be classified either by its specific location (intracellular – membrane-bound – extracellular), by the core protein or by the respective sugar moiety [31,32]. A large group is the family of small leucine-rich proteoglycans (SLRPs) with more than 15 different PGs. GAG polysaccharide chains consist of repeating disaccharides and can appear as sulfated (chondroitin sulfate, heparan sulfate, keratan sulfate) or non-sulfated (hyaluronic acid) GAGs. PGs associate to collagens or other fibrillar components by distinct binding motifs. Due to their highly charged character, PGs have essential function in balancing the hydration level of tissues, store and supply ions, nutrients and growth factors and, as for example in cartilage, function as lubricant.

MMPs & TIMPs – The spatiotemporal control over the breakdown of ECM is essential during developmental morphogenesis, tissue homeostasis and regeneration. A large family of calcium-dependent endopeptidases, the so-called matrix metalloproteinases (MMPs) is thought to play an essential role in this process [33,34]. In humans, 23 different isoforms are present. MMPs are capable to cleave a variety of different ECM proteins at different specificities and efficacies and can be grouped according to their preferred substrate. One can distinguish between collagenases (MMP1/8/13), gelatinases (MMP2/9) and stromelysins that cleave many different proteins except for fibrillar collagen (MMP3/10/11).

1.2.2 The ECM in disease

The importance of a defined composition and proper structural assembly of the extracellular matrix is evident in situations, where dysregulations can be associated with malfunctions and disease. Some of the components such as fibronectin are so essential for a proper cell and tissue function that depletion leads to early embryonic lethality [35] or are associated with connective tissue disorders such as the Ehlers-Danlos syndrome or osteogenesis imperfecta [27].

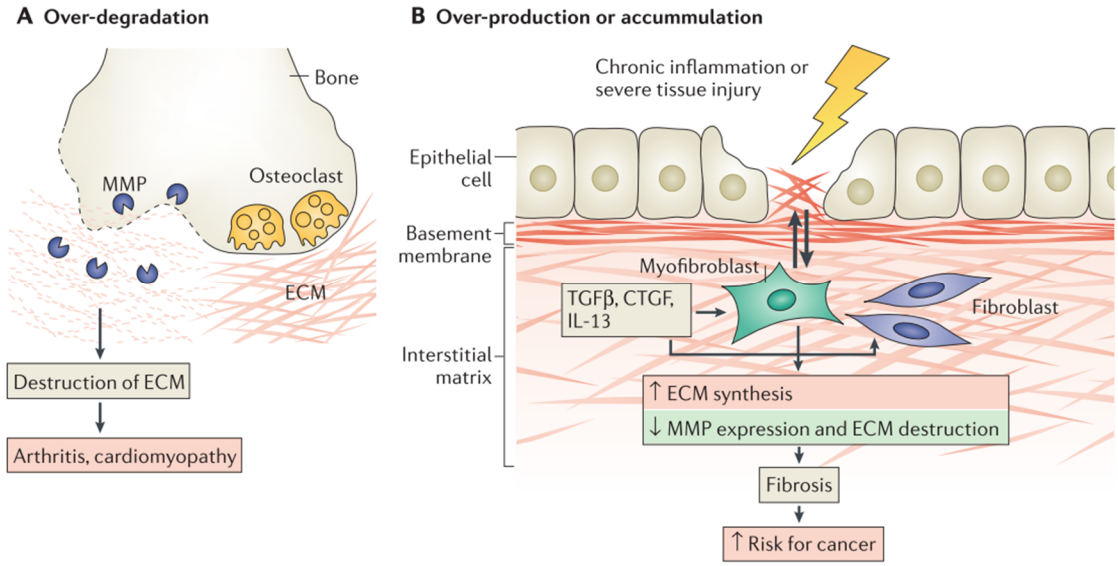

Figure 1-4: Altered ECM synthesis and remodeling is associated with pathological conditions. Figure reproduced with permission from Springer Nature [36].

Aside of genetic mutations causing pathological conditions, especially the dysregulation of ECM expression, posttranslational modification and turnover is linked to a plethora of disease phenotypes including osteoarthritis, fibrosis and cancer [36] (Figure 1-4). In several situations such as osteoarthritis or dilated cardiomyopathy [37] dysregulations are caused by an increase in the activity of MMPs and ADAMs. Opposing, chronic tissue injuries that are linked to an excessive immune response increase the risk of TGF-β-mediated fibrosis that leads to increased deposition of collagen I/III and downregulation of MMP activity. Such regulations often can lead to a vicious amplification as altered mechanical properties feed back into the regulation of ECM protein expression. In the context of fibrosis it was shown that a fibrotic ECM further stimulates the production of ECM by fibroblasts. This was even independent of the context from which the cells were isolated which highlights the strong priming function of the ECM on cellular processes [38]. Multiple and rather complex dysregulations can further be found in cancer where

the tumor stroma is often characterized by increased collagen I expression and crosslinking that leads to a stiffening which manifests the pathogenic phenotype [4] (“wounds that do not heal”).

Taken together, control over the precise spatiotemporal expression and proper assembly greatly determines many biological processes during development and homeostasis and guarantees a physiological tissue/organ function.

1.3 Cellular Mechanotransduction

Distinct properties of the ECM, e.g. composition, structure and stiffness, not only determine the functionality of a tissue but greatly affect cellular behavior during development, homeostasis, regeneration and disease. On the other hand, cells actively steer the ECM throughout these stages via synthesis and secretion of ECM proteins or their degrading enzymes. This tightly balanced relationship can only be maintained and controlled if cells are able to sense, convert and respond to extracellular mechanical cues – a process referred to as mechanotransduction.

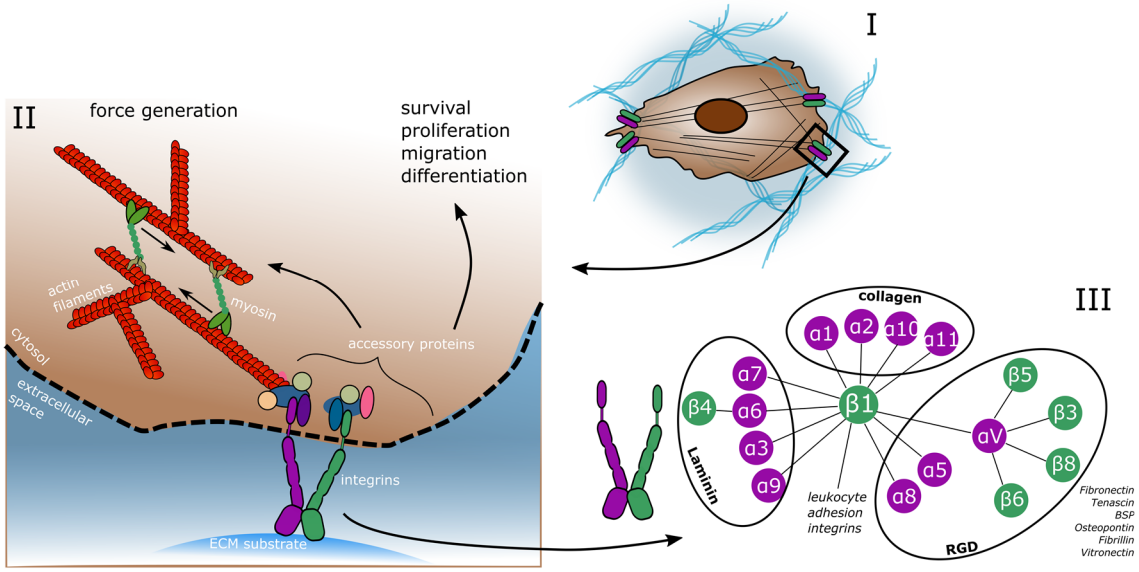

Figure 1-5: key components in cellular mechanotransduction. (I) cells are surrounded by extracellular matrix and adhere via integrins. (II) integrin proteins are intracellularly connected to a plethora of adapter proteins which mediate a mechanical link to the contractile acto-myosin complex or initiate intracellular signaling cascades. (III) integrins are heterodimeric complexes (α/β isoforms) and the distinct assembly determines their preference for a specific adhesion substrate or binding motif. Figure inspired by [39] *and* [40].

Activation & sensation: Although distinct mechanisms allow a passive mechanosensation, e.g. flattening of caveolae membrane invaginations due to fluid flow or osmotic

pressure [41], cells continuously probe their environment. An elaborate machinery is responsible that involves a class of single-pass transmembrane receptors – the so-called integrins, intracellular accessory proteins and the acto-myosin complex (Figure 1-5).

Integrins are the major adhesion receptors of the cell towards the extracellular matrix that also transduce signals across the cell membrane. Integrins resemble a whole family of cell adhesion receptors that comprises of 18 α- and 8 β-subunits [40]. Each receptor fulfills a distinct function and most integrin mutations or knockouts are embryonically lethal or result in severe disorders which underlines their essential, non-redundant function. Their assembly as heterodimers allows a strong diversity and determines the affinity towards an extracellular ligand [42]. Initially, integrin dimers occur in a resting state, or also called "bent" conformation that requires activation through unfolding to allow ligand binding. Key mediators of integrin activation are talin and kindlin which bind the short cytoplasmic tail of β-integrins via a PTB-domain [43]. Additionally, the generation of phosphatidylinositol (4,5)-bisphosphate (PIP_2) seems to play an important role in the initial activation of talin from its auto-inhibited head-tail conformation [44]. The conformational change in integrin dimers upon binding reveals an extracellular binding site and thus allows ECM binding. Upon recognition and binding of an extracellular ligand, integrins form clusters, the so-called focal adhesions. Focal adhesion assembly is critical for cell adhesion and the generation of intracellular signaling hubs which allow a conversion of mechanical signals into biochemical signaling cascades [45].

Conversion & Response: Activated integrins intracellularly bind to a variety of adapter proteins, which either connect to the actin cytoskeleton or serve as a hub for intracellular signaling cascades. In total, 156 different components with almost 700 interactions comprise the integrin adhesome that is formed upon integrin activation and focal adhesion maturation [46]. One of the key molecules that is recruited towards clustered integrin complexes is focal adhesion kinase (FAK). FAK interacts with paxillin and talin and mediates further signaling events including Rho GTPase activation and Src kinase recruitment.

Another key signaling hub is integrin-linked kinase (ILK) which acts as a central signaling platform (Figure 1-6). ILK directly interacts with β1-integrin, as well as with actin- and paxillin-binding proteins parvin. Its functions are evolutionary highly conserved and mutations cause embryonic lethality and increased activity patterns of ILK are reported for several types of cancer [47]. Through its kinase activity, ILK regulates the activity of

several important signaling proteins that are involved in migration, proliferation and survival such as AKT, GSK3β and myosin light chain. ILK activity itself is highly dependent on the presence of phosphatidylinositol (3,4,5)-trisphosphate (PIP_3). This phospholipid is a product of PI3K-mediated phosphorylation of PIP_2 and interacts with ILK via specific PH-domains [48].

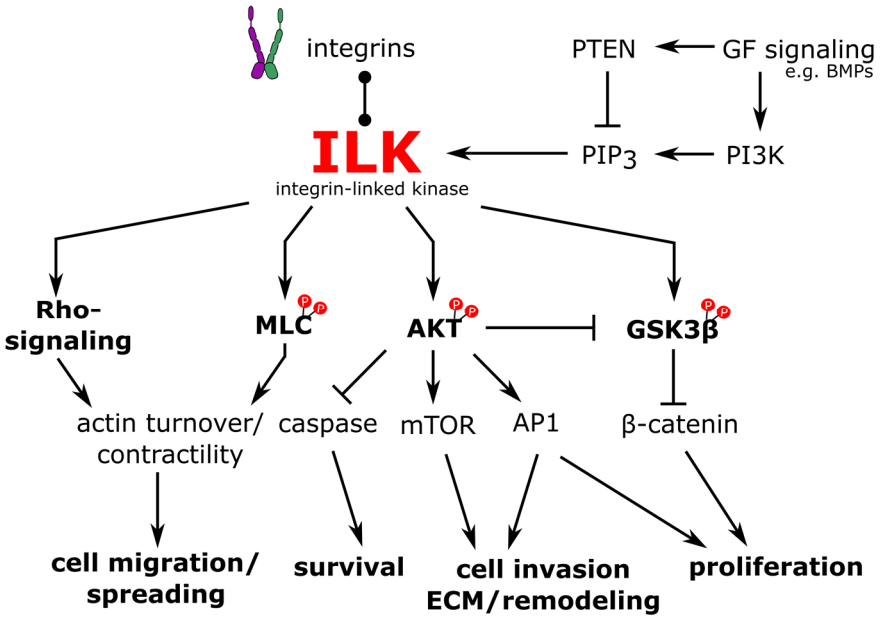

Figure 1-6: overview of down ILK-signaling. Integrin-linked kinase (ILK) is activated via binding of PIP_3 and, through its kinase activity, regulates the activity of several key signaling pathways such as Rho GTPases, AKT and GSK3β with consequences for cell migration, survival (apoptosis), invasion and proliferation. Figure inspired by [47].

Via this process, other signaling pathways can integrate and modulate ILK signaling since PI3K or the corresponding PIP_3 phosphatase PTEN can be regulated through growth factor stimulation. One example is the BMP pathway (see also section 1.4). Earlier, it was demonstrated that BMP receptors not only interact with integrins [49–51], but that BMP type II receptor interaction with a regulatory subunit of PI3K modulates PIP_3 production [52]. It shall be noted that ILK was chosen as an example to highlight both the versatility of effected process as well as the integration of other growth factor pathways. Other key molecules such as FAK and Src exhibit similar networks and are of highest relevance as well [53].

Resulting from focal adhesion assembly and intracellular downstream effector pathways, cells are able to sense and respond to extracellular cues. In turn, the mechanical link of the acto-myosin complex to the extracellular matrix allows cells to apply forces

to their environment which is a prerequisite for cellular motility as well as ECM tensioning and wound contraction and cell-cell communication. A constant sensing and responding potentially allows a collective and synchronized behavior of cells [54,55].

1.4 Bone Morphogenetic Proteins

BMPs originally have been described by Marshall Urist in the 1960s according to their ability to induce bone formation at non-skeletal sites [56]. Since then, a complete subfamily of more than 15 secreted ligands within the TGF-β superfamily has been discovered [57] with a plethora of regulatory functions during developmental morphogenesis, tissue homeostasis but also regeneration and disease [58–60]. In contrast to their original description, BMP ligands are known to regulate cellular processes in various tissues & organs including bone, cartilage [61,62], tendon [63,64], muscle [65], kidney [66], cardiovascular [67,68] and neuronal networks [69].

Due to their essential role throughout embryonic development and tissue homeostasis, BMPs are evolutionary highly conserved [70] and multiple diseases are associated with mutations either in BMP ligands, receptors or co-receptors [71].

With the receipt of FDA approval for BMP2 and BMP7 for use in spinal fusions and open tibial fractures BMP growth factors have gathered a significant clinical relevance [72], but moderate efficiencies in stimulating fracture repair [73] as well as adverse side effects[74] indicate that signaling mechanisms and regulatory cascades occurring under physiological conditions might not be fully understood.

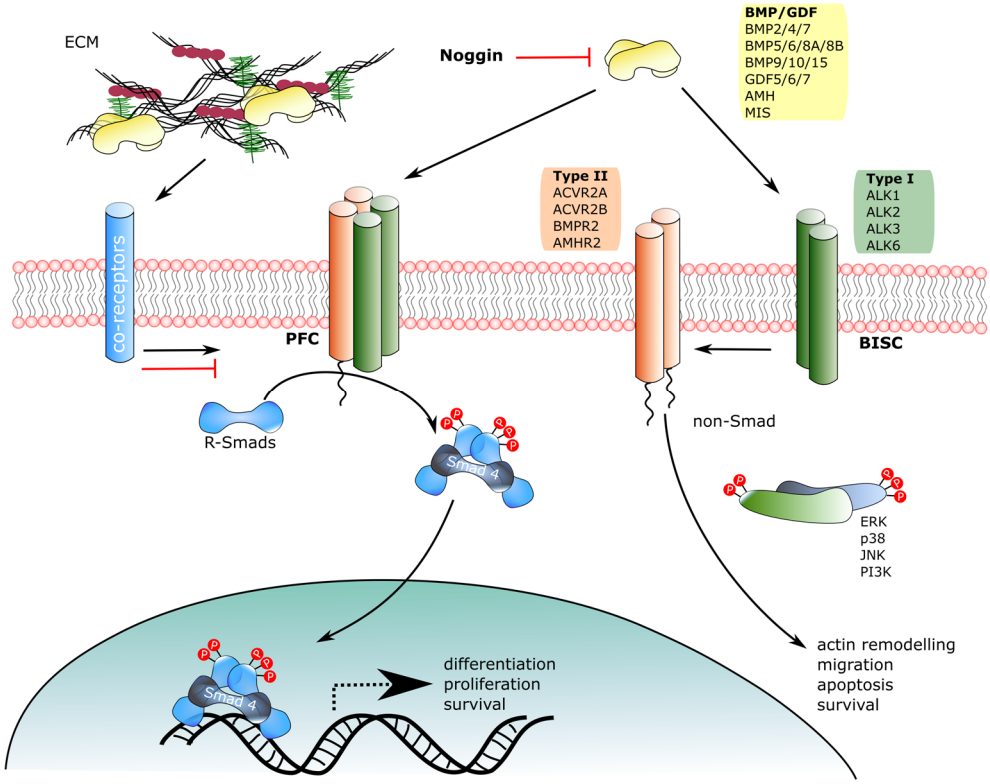

Figure 1-7: The BMP signaling pathway – Dimeric ligands bind to BMP receptor complexes which undergo activation by auto-phosphorylation. Intracellular Smad transcription factors are recruited to and phosphorylated by the activated receptor complex. Trimeric Smad signaling complexes translocate to the nucleus where they act as transcription factors. Non-canonical signaling occurs via different MAP kinases (e.g. ERK, p38, JNK) and Rho GTPases in order to regulate actin polymerization, migration and survival. Figure inspired by [58,75].

1.4.1 The BMP signaling cascade

BMP growth factors occur as homo- but also heterodimeric ligands and pathway activation requires binding to a heterotetrameric receptor complex consisting of two type I and two type II receptors. BMP receptors are single-spanning transmembrane serine/threonine kinases, which share the same principle architecture of a highly conserved extracellular ligand-binding domain, a α-helical transmembrane domain and an intracellular kinase domain. The type I receptors feature an additional motif termed glycine/serine-rich box (GS-box) which, upon ligand binding, becomes phosphorylated by the constitutively active type II receptor. At the mode of ligand-receptor oligomerization, a variety of about 15 different BMP/GDF ligands face a limited number of 4 type I and 4 type II receptors [59] (Figure 1-7) which show tissue-specific expression and different affinities to the ligands [57] and allows a diverse and context-specific response of the signaling cascade.

Aside of this ligand-receptor promiscuity, the mode of ligand-receptor oligomerization determines the specific activation of downstream intracellular cascades. BMPs can

bind to so-called preformed complexes (PFCs) of type I and type II receptors which results in the activation of canonical Smad signaling. Type II receptors can also be recruited to type I receptors to form a BMP-induced signaling complex (BISC) inducing non-Smad signaling responses [76].

The canonical signaling depends on the phosphorylation of Smad transcription factors (R-Smads) at the C-terminal site by BMP type I receptors, which enables the formation of a trimeric complex together with the common mediator Smad4 and subsequent nuclear translocation. Activated Smads there act as transcription factors by binding to Smad binding elements in the promoter region of target genes via their N-terminal domain [77,78].

In addition to the Smad pathway, activated BMP receptors can further signal through diverse cascades including mitogen-activated kinases (MAPK) p38 and JNK but also phosphatidylinositol 3-kinase (PI3K) which mediate non-transcriptional responses such as actin reorganization and directional migration according to growth factor gradients [52].

In order to allow a precise control over pathway activation and inactivation, depending on the context, various regulatory cascades orchestrate the BMP pathway at multiple levels. Those steering elements can comprise of BMP antagonists in the extracellular space obstructing ligands from binding to the receptors by masking receptor-binding epitopes [79]. Further regulations occur at the receptor level where various co-receptors or additional interacting receptors modulate signaling outcome [80–82]. Intracellular responses include the BMP-induced increase in inhibitory Smads 6 and 7 [83,84], which establishes a negative feedback loop as well as the MAPK and GSK3β-mediated Smad linker phosphorylation that targets Smad transcription factors for proteasomal degradation [85].

1.4.2 Integration into the biomechanical context

General remarks: So far, regulatory mechanisms of the signaling cascade have been described under defined but static 2D *in vitro* culture conditions. However, depending on the tissue in which they are residing in, cells experience different mechanical stimuli such as hydrostatic pressure, fluid flow, tensile or compressive forces and substrate architecture, stiffness, elasticity and deformation. Such mechanical signals usually are tissue-specific and may vary in their magnitude, direction, frequency and duration.

Specifically in the context of bone development, homeostasis and repair, mechanical cues are known to be a crucial regulator (see also section 1.1) and it is well-known that the mechanical context directs stem cell lineage commitment [3,86] as well as general cellular functions such as proliferation [87], migration [88] and apoptosis [89] which ultimately impacts on bone formation [90]. Additionally, also BMPs have been described to regulate cellular functions and to stimulate bone formation by enhancing stem cell differentiation [91]. This observation motivated the use of recombinant BMPs in spinal fusions and open tibial fractures [72,92,93]. Emerging studies using *in vitro* [23] but also *in vivo* [21,22] approaches further point to regulatory crosstalk mechanisms between active mechanical stimuli and the BMP signaling cascade. Aside of active mechanical triggers, indications are found that also the stiffness of the underlying substratum of the cell impacts not only BMP signaling outcome [49], but in general growth factors of the TGF-β [94–98] and other growth factor superfamilies [99–101]. Although crosstalk between the BMP pathway and mechano-responsive modulators can occur at any level of the cascade, the relevance of the ECM and integrins shall be highlighted in the following:

The ECM: As BMPs are shown to be affected by the mechanical environment, they in turn also shape and modulate the mechanical environment by regulating the expression of ECM and ECM-remodeling enzymes (Figure 1-8). This mutual regulation establishes a tissue-specific and highly dynamic system in which growth factors determine the mechanical properties and composition that in turn modulates again growth factor function either by sequestering ligands, cell adhesion or the signaling cascade itself.

An important component of the ECM that greatly determines its mechanical properties is collagen and individual BMP ligands have been shown to regulate the expression of different types of collagen. Most regulatory features were described in the context of cartilage formation and chondrogenic differentiation of MSCs where BMPs stimulate the expression of collagen type II [62,102–105] and type X, but also of GAGs such as aggrecan [62]. Other collagens were also found to be regulated with partially controversial but in general stimulatory outcome [103,106]. One study could further show the crucial role of collagen type IV on sequestering of BMPs during developmental processes using *drosophila* embryos [107].

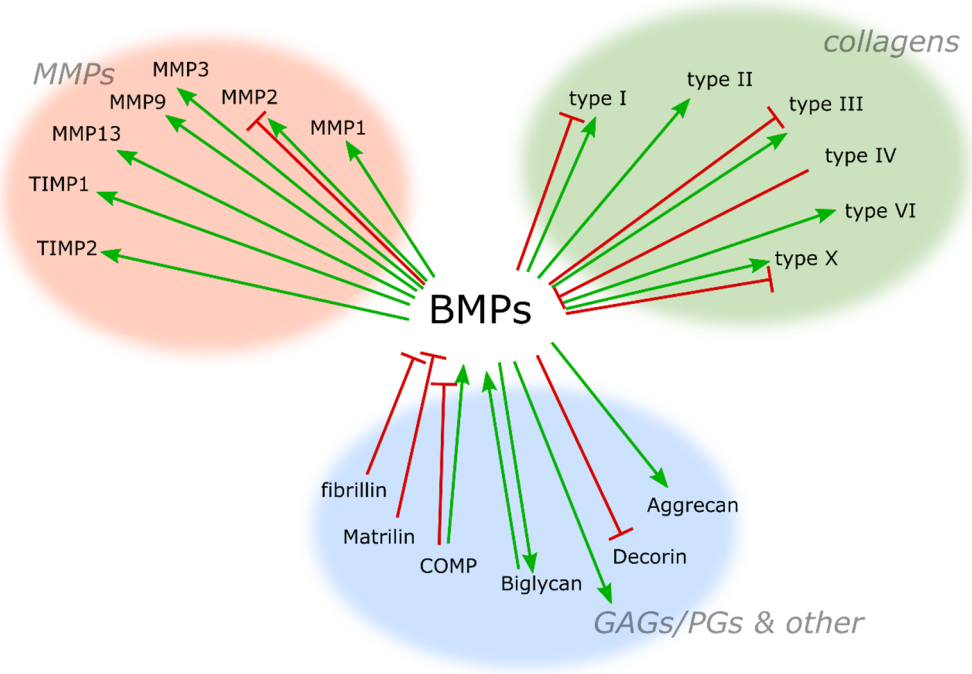

Figure 1-8: summary of regulatory features of BMPs on ECM protein expression and vice versa. Differential regulations for individual proteins originate from variability in ligands and cellular context. Based on [49,61–63,66,102–127].

Aside of collagen, accessory proteins which provide a tissue-specific furniture such as proteoglycans and glycoproteins reveal a stronger interdependency. While several of those proteins are also regulated by BMP stimulation [102,105] multiple ECM components show either stimulatory [61,108,113,118] or inhibitory [109,122,127] effects on BMP signaling which is mostly due to sequestering or presenting of ligands or ligand antagonists [114] towards their corresponding cell surface receptors.

Furthermore, BMPs are shown to be highly involved in the regulation of ECM-degrading enzymes (MMPs) and their antagonists (TIMPs). Stimulation is often associated with a dramatic increase in MMP activity that is linked to metastasis and cell invasion [106,116,120].

Integrins: As already indicated in section 1.3, growth factor signaling pathways such as the BMP pathway integrate into cellular mechanotransduction. Both co-localization as well as direct interaction was reported between BMP type I/II receptors and several different integrins [128]. In addition, various accessory proteins of the mechanotransduction machinery, e.g. LIMK, Src & PI3K, interact with the long cytoplasmic tail of the BMP type II receptor that by itself resembles a versatile signaling hub. These interactions were proven to affect BMP signaling behavior and differentiation of cells [51,129].

Although the particular crosstalk dynamics are poorly described, recent *in vivo* work could demonstrate the strong potential of extrinsic mechanics as modulator of BMP healing outcome [21,22].

1.5 Clinical challenges & limitations in fracture repair

Despite the general ability of bone to fully regenerate without the formation of scar tissue fully regaining its initial structure and functionality, a certain percentage (>10%) of all bone fractures result in delayed healing or even non-unions [130]. The individual healing outcome is influenced by multiple factors including age, gender, weight but also location, size and stability of the fracture gap. In particular large bone defects resemble a challenging situation since large quantities of tissue need to be restored that usually exceeds the natural self-healing ability of bone.

Although several regenerative therapy strategies are available [7], the gold standard is the use of autologous material next to or in combination with BMPs [131]. However, either treatment option faces distinct limitations and drawbacks. In the case of autologous bone grafting, depending on the size of the defect, the amount of material that can be harvested is limited and can be accompanied by donor side morbidity. Allogeneic graft material resembles an alternative source which does not require additional surgery procedure for the patient and is available in different configurations. Yet, allogeneic material exhibits reduced osteoinductive potential and are subject to immune rejection reactions [132].

Aside of various bone graft substitute materials that are commercially available, BMPs are used to enhance the healing outcome. Both, BMP2 and BMP7 received approval for clinical applications and are frequently used in the treatment of non-unions, open tibial fractures, spinal fusions and critical sized bone defects [133]. Due to supra-physiological doses applied during surgery, various adverse side effects have been reported such as ectopic bone formation, callus swelling as a result of increased inflammatory response and infection [74]. Despite the described side effects and expensive production, hBMPs significantly helped to improve the healing outcome and show shorter surgery time and patient hospitalization compared to the use of autograft material. Furthermore, the risk or need for a second intervention was also found to be reduced [134].

Consequently, until promising treatment strategies such as biomaterial-based approaches (osteoinductive or osteoconductive biomaterials, bone substitutes, etc.) bone tissue engineering, growth factors other than BMPs or gene therapy prove to be superior not only in terms of healing outcome but also cost-effectiveness, the current strategies will maintain their status as standard treatment options.

1.6 Motivation & Aim

Since most tissues exhibit only very limited endogenous regeneration capacities, novel regenerative therapy approaches are needed to improve the overall poor healing outcome after injury. However, even in the case of bone healing which exhibits an intrinsic self-regeneration capacity, the endogenous potential is limited which leads to delayed healing or non-unions. Although the use of BMPs is established as a standard treatment option for large bone defects, limitations in the healing outcome and adverse side effects motivate further research on the mechano-dependency of BMP function in order to increase safety and efficacy.

Most of the effect of BMP treatment is attributed to its osteoinductive potential. Although callus formation and mineralization usually occur several weeks after surgery, BMP loaded onto a carrier exhibits a burst release kinetics from its carrier over few days post implantation [22,135]. This indicates that the majority of clinically applied BMP function potentially affects early healing events such as cell invasion of the injured region and granulation tissue formation.

It is therefore a highly intriguing hypothesis that BMPs steer early tissue formation events during healing, especially as the structural relevance of soft tissue patterns for guiding bone formation was shown recently [19]. Consequently, BMPs potentially affect ECM synthesis, deposition and/or organization in a way that the resulting properties are favorable for bone formation – in other words: BMPs might be involved in a early feed forward stimulation of ECM formation with relevance for bone regeneration. More specifically, these ECM properties are not exclusively affecting cellular function through its mechanical properties, e.g. stiffness-dependent differentiation [3] A feed forward mechanism could establish in which the resulting ECM exhibits properties which are favorable for BMP secretion or signaling itself. ECM-modulated endogenous BMP secretion by tissue-resident cells (callus formation, mineralization) might be potent in driving osteogenic differentiation of progenitor cells at later stages. Although this concept of an induction of early ECM formation by a protein stimulus such as BMP would not be expected to function exclusively or isolated from other factors, yet it would provide novel opportunities for regenerative therapy approaches, e.g. via mimicry of ECM properties that favor endogenous growth factor signaling. Indications for the role of the ECM in controlling tissue fate were recently found in the context of cancer development, where

decellularized malignant tissue increased the malignant potential of breast cancer cells [136].

The hypothesis underlying this thesis was that BMP stimulation influences ECM formation in a way that the resulting ECM properties in turn favor BMP signaling. To address this hypothesis, the work program of this thesis was split into three consecutive parts (see Figure 1-9):

At first, the process of tissue formation was investigated in a 3D-environment without the addition of BMP. Although several processes such as the deposition and tensioning of fibronectin were described earlier [137,138], detailed insights into the cellular blueprint for tissue formation remain elusive. For this, tissue formation was studied *in vitro* using a macroporous collagen scaffold which provides a model system for soft tissue formation and patterning. Second, early tissue formation events were studied under supplementation of BMP2 during culture *in vitro*. As summarized in Figure 1-8, various studies reported on the influence of BMP stimulation on ECM proteins, which was mostly based on gene expression alone. Since it was highlighted in a recent study *in vivo* that BMP affects the contractility of cells [22], a particular focus was put on macroscopic contraction and stiffening. Consecutively, a decellularization protocol was established in order to harvest conditioned ECM. In a third step, cellular signaling response was evaluated on decellularized matrices in order to demonstrate if a matrix grown under BMP stimulation provides implemented cues that are beneficial for BMP secretion (positive feedback loop) and signaling.

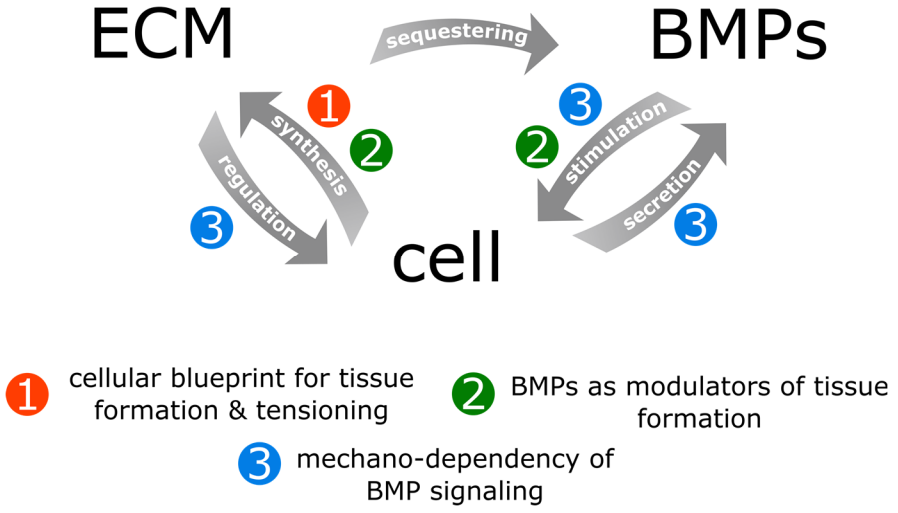

Figure 1-9: work program of the thesis. Grey arrows indicate the connection between the components. Colored spheres and numbers refer to the individual parts of the thesis.

Together, the research aspects addressed in the three parts shall contribute to a principle understanding of how BMPs are involved in tissue formation and regeneration. The findings are regarded to be of benefit for the development of new regenerative therapy approaches such as an advanced biomaterial design or enable a more directed and efficient use of current treatment options.

2 Materials

2.1 Chemicals, compounds & consumables

All basic chemicals, if not otherwise specified, were purchased from Sigma Aldrich, Carl Roth or Merck. Equipment and consumables such as Eppendorf tubes and tips were purchased from Eppendorf, Corning or Hartenstein.

2.2 Devices

Table 2-1: list of devices

device	specification	model	Manufacturer
Autoclave	Pot	5L steam pot	Fissler
	plate	1051	Severin
Cell counter		Casy Modell TT	Casy
Centrifuge	Tubes, cooling	Heraeus Fresco 17	Thermo Fischer
	Cells	Rotofix 32	Hettich
Clean Bench		Herasafe	Heraeus
		Safe2020	Thermo Fischer
Cryotome		CM1950	Leica
Freezer	-20°C	Liebherr premium	Liebherr
	-80°C	UF 755G	Dometic
Fridge	4°C	Profiline	Liebherr
Heating plate/stirrer		-	VWR
Incubator		-	Binder
Microscope	Confocal	SP5	Leica
	Cell culture, bright-field	-	Leica
Microplate reader		Infinite pro 2000	Tecan
PCR cycler	qPCR	iQ5	Bio-Rad
	RT-PCR	Mastercycler gradient	Eppendorf
Peristaltic pump	Perfusion decellularization	Econo pump	Bio-Rad
pH meter		-	Inolab

device	specification	model	Manufacturer
Pipette		Reference	Eppendorf
Power supply	Western blotting	Power Pac HC	Bio-Rad
scale		Scout pro 400g	Ohaus
Shaking device		Vortex genie 2	Scientific industries
Thermomixer		Thermomixer comfort	Eppendorf
Spectrophotometer		ND-1000	Thermo Fischer
Ultrasound bath		Elmasonic P	Elma
Vacuum pump		AC1 PH-MTR Serie 71	Pfeiffer Vacuum
Water bath		-	Memmert
Western Blotting	Western Blot	XCell II™	Thermo Fischer
	Imaging system	Odyssey	Li-Cor
	SDS-PAGE	XCell Sure-Lock™ Mini-Cell	Thermo Fischer

2.3 Buffers

The pH of all solutions was adjusted at room temperature using a pH-sensor and 1N HCl or 2N NaOH solution. If detergents were present, the pH was adjusted prior to addition of them. If no pH was specified, no measurement was performed. If applicable, solutions were sterile filtered (0.2µm pore size) or autoclaved to obtain sterile solutions for cell culture applications. If not otherwise specified, volumes were equilibrated using double distilled ultrapure water (AMPUWA).

Table 2-2: list of custom-made buffers & exemplary calculations

component	company	ordering	Concentration [- / vol.%]	exemplary calculation
gelatin solution				
gelatin	Weishard Inter-national	-	5 wt.%	25g
sucrose	Calbiochem	573113	5 wt.%	25g
DPBS	Thermo Fischer	14190-094	1x	500ml
collagenase buffer (pH 7.4) – 100ml				
Tris-HCl	Sigma Aldrich	T3253	100mM	1.57g
NaN_3	Sigma Aldrich	52002-25g	0.05mg/ml	500µl of 10wt.% sol.

component	company	ordering	Concentration [- / vol.%]	exemplary calculation
$CaCl_2$	Sigma Aldrich	C5670-100G	5mM	5ml of 0.1M sol.
4% PFA (200ml)				
Paraformaldehyde	Merck Millipore	1.04005.1000	4 wt.%	8g
PBS (10x)	Biochrom AG	L1835	10x	20ml
Ammonium chloride solution				
NH_4Cl	Merck Millipore	1.01145.0500	25mM	0.134g
DPBS	Thermo Fischer	14190-094	1x	100ml
ECM extraction buffer I (pH 7.5) – 100ml				
CHAPS	Carl Roth	1479.3	4 wt.%	4g
Tris Base	Sigma Aldrich	T6066	50mM	0.6g
KCl	Carl Roth	P017.2	50mM	0.37g
Glycerol	Merck Millipore	1.04093.1000	20 wt.%	20g
ECM extraction buffer II – 100ml				
$MgCl_2$	Carl Roth	KK36.2	5mM	5ml of 0.1M sol.
Urea	Merck Millipore	138.487	6.5M	39g
Thiourea	Carl Roth	HN37.1	2M	15.2g
Western Blot Transfer buffer (1x)* – 250ml				
Glycin	Carl Roth	0079.2	192mM	25ml of 10x stock
Tris base	Sigma Aldrich	T6066	25mM	
Methanol	Carl Roth	0082.3	20 vol.%	50ml
TBS-T† (1x)/Western Blotting, pH 7.6 – 1l				
NaCl	Merck Millipore	567440-1KG	136mM	8g
Tris	Merck Millipore	108.382	20mM	2.42g
Tween-20	Sigma Aldrich	P1379-100ml	0.1%	1ml
TBS-T† (1x)/Immunohistochemistry, pH 8.2 – 1l				
Tris HCl	Sigma Aldrich	T3253	50mM	6.6g
Tris	Merck Millipore	108.382		0.9g
NaCl	Merck Millipore	567440-1KG	150mM	8.78g
Triton X-100	Sigma Aldrich	T8787-100ml	0.025-0.2%	250µl (0.025%)

* A 10x stock was prepared w/o MeOH. A necessary amount of 1x solution w. MeOH was prepared fresh prior to usage

† The addition of detergent and its concentration may vary

2.4 Kits & reagents

All kits and reagents were prepared and used according to the manufacturer's instructions, if not otherwise specified.

Table 2-3: list of miscellaneous kits, substances & consumables

component	ordering N°	manufacturer	storage
10% SDS solution	15553027	Thermo Fischer	RT
10% Triton X-100 solution	93443	Sigma Aldrich	RT
4x protein loading buffer	928-40004	Li-Cor	RT
Bovine Serum Albumin	8076.2	Carl Roth	4°C
cOmplete™, Mini Protease Inhibitor	4693124001	Roche	4°C
Crude collagenase I	17100017	Thermo Fischer	4°C|-20°C
CyQUANT™ Cell Proliferation Assay Kit	C7026	Thermo Fischer	-20°C
DNase I grade II	10104159001	Roche	4°C|-20°C
IRDye® 680RD Goat anti-Mouse IgG	925-68070	Li-Cor	-20°C|4°C
IRDye® 800CW Goat anti-Rabbit IgG	925-32211	Li-Cor	-20°C|4°C
Luciferase assay system	E1500	Promega	-20°C
Nitrocellulose membrane	10600002	GE healthcare	RT
NuPAGE™ 4-12% Bis-Tris Protein Gels	NP0336BOX	Thermo Fischer	4°C
NuPAGE™ MES SDS Running Buffer	NP0002	Thermo Fischer	RT
NuPAGE™ MOPS SDS Running Buffer	NP0001	Thermo Fischer	RT
PhosSTOP™ phosphatase inhibitor	4906845001	Roche	4°C
Pierce™ BCA Protein Assay Kit	23225	Thermo Fischer	RT
RIPA lysis buffer	9806	Cell Signaling	-20°C

Crude collagenase I was dissolved in collagenase buffer and frozen at a concentration of 100U/ml at -20°C. DNase I was dissolved in DPBS with calcium and magnesium at a concentration of 3500U/ml and frozen in aliquots at -20°C. RIPA cell lysis buffer was diluted to 1x with DPBS and supplemented with protease and phosphatase inhibitors.

Aliquots were frozen at -20°C. Western blotting secondary antibodies were dissolved at a concentration of 1mg/ml in double distilled water and aliquots were frozen at -20°C.

2.5 Histology & Imaging

2.5.1 General histology equipment

Table 2-4: list of diverse and general consumables used for histology

component	ordering N°	manufacturer	storage
Alizarin Red S	A5533	Sigma Aldrich	RT
Alkaline-Phosphatase-Standard-Kit	AK-5000	Vector Laboratories	4°C
Antibody diluent	S3022	Dako	4°C
Bovine Serum Albumin	A7906-100g	Sigma Aldrich	4°C | -20°C
Cetylpyridiniumchloride	C0732	Sigma Aldrich	RT
Cover slips	01-2446	Langenbrinck	RT
Fluoromount-G®	0100-01	Southern Biotech	4°C
Mayer's Hämalaun solution	1092490500	Merck Millipore	RT
Microscope slides	08.100 00	Marienfeld	RT
Normal donkey serum	017-000-1212	Jackson Immunoresearch	-20°C | 4°C
Normal goat serum	S-1000	Vector Laboratories	4°C
Normal horse serum	S-2000	Vector Laboratories	4°C
Saponin	47036	Sigma Aldrich	4°C
Scalpels	5518067	Aesculap AG	RT
Tissue-Tek® Cryomold	4566	Sakura Finetek	RT
Tissue-Tek® O.C.T.™ Compound	4583	Sakura Finetek	RT

2.5.2 Primary antibodies

Table 2-5: list of primary antibodies

Target	ordering N°	manufacturer	clonality	Source	storage
Collagen type II	1-CO071-02	Quartett	polyclonal	mouse	-20°C
Fibronectin	ab23750	Abcam	Polyclonal IgG	Rabbit	Aliquots -20°C
GAPDH	2118S	Cell Signaling	14C10 monoclonal IgG	Rabbit	-20°C
Histone H3	14269S	Cell Signaling	1B1B2 monoclonal IgG3	Mouse	-20°C
pMLC	3675S	Cell Signaling	Monoclonal IgG1	Mouse	-20°C
pPaxilin	2541S	Cell Signaling	Polyclonal IgG	Rabbit	-20°C
pSmad 1/5/9	13820S	Cell Signaling	D5B10 monoclonal IgG	Rabbit	-20°C

2.5.3 Secondary antibodies

Table 2-6: list of secondary antibodies

Target	ordering N°	manufacturer	specification	Source	storage
Anti-mouse IgG	405309	Biolegend	Cy3-conjugated	Goat	4°C
Anti-mouse IgG	A11001	Thermo Fischer	Alexa Fluor 488-conjugated	Goat	4°C
Anti-mouse IgG	AK-5000	Vector laboratories	Biotinylated	Horse	4°C
Anti-rabbit IgG	A21206	Thermo Fischer	Alexa Fluor 488-conjugated	Donkey	4°C
Anti-rabbit IgG	711-165-152	Jackson Immunoresearch	Cy3-conjugated	Donkey	-20°C

2.5.4 Other dyes

Table 2-7: list of small molecule dyes used in immunohistochemistry

component	ordering N°	manufacturer	storage [stock|in use]

Alexa Fluor™ 488 Phalloidin	A12379	Thermo Fischer	6.6µM in MeOH stored at -20°C
Alexa Fluor™ 633 Phalloidin	A22284	Thermo Fischer	6.6µM in MeOH stored at -20°C
DAPI (4',6-Diamidino-2-Phenylindole, Dihydrochloride)	D1306	Thermo Fischer	5mg/ml stock in PBS stored in aliquots at -20°C
DRAQ5 (5mM solution)	424101	Biolegend	4°C

2.5.5 Traction Force Microscopy

This section specifically refers to all materials needed for the preparation of TFM gels and coatings that are ready to use for cell seeding.

component	ordering N^{o}	manufaturer	storage [stock|in use]
2% Bisacrylamide	161-0142	Bio-Rad	4°C
25% Glutaraldehyde	G5882	Sigma Aldrich	4°C
40% Acrylamide	161-0140	Bio-Rad	4°C
APS	A3678	Sigma Aldrich	RT
APTMS	281778	Sigma Aldrich	RT
Cover slips	01-2240/1	R. Langenbrinck	RT
DMSO (anhydrous)	276855	Sigma Aldrich	RT
Fibronectin	341635	EMD Millipore	-20°C
FluoSpheres™ 0.1µm	F8800	Thermo Fischer	4°C
Microscope slides	08.100 00	Marienfeld	RT
Rain-X	26014	Rain-X	RT
Sulfo-SANPAH	22589	Thermo Fischer	-80°C
TEMED	161-0800	Bio-Rad	RT

A 10wt.% solution of APS was prepared prior to use and was stored at 4°C for < 1 week. Sulfo-SANPAH was dissolved at 25mg/ml in anhydrous DMSO and snap frozen in liquid nitrogen at 40µl aliquots. Fibronectin solution was aliquoted for single thaw/use and stored at -20°C

2.6 PCR

2.6.1 Kits & reagents

Table 2-8: list of kits & reagents used for RNA isolation, reverse transcription and qPCR

component	ordering N°	manufaturer	storage [stock|in use]
Ethanol EMPROVE®	1009861000	Merck Milipore	RT
iQ™ SYBR® Green Super-mix	170-8882	Bio-rad	-20°C
iScript™ cDNA Synthesis Kit	170-8891	Bio-rad	-20°C
Nuclease-free H_2O	AM9937	Thermo Fischer	RT
PureLink® DNase	12185010	Thermo Fischer	-20°C
PureLink® RNA Mini Kit	12183018A	Thermo Fischer	RT

2.6.2 Primer

Target	gene name	sequence [FWD/REV]	ENSEMBL ID
hypoxanthine phospho-ribo-syl-transferase 1	HPRT	TATGGACAGGACTGAACGTC TGATGTAATCCAGCAGGTCA	ENSG00000165704
Inhibitor of DNA binding 1	Id1	GCTGCTCTACGACATGAACG CCAACTGAAGGTCCCTGATG	ENSG00000125968
Inhibitor of DNA binding 2	Id2	GTGGCTGAATAAGCGGTGTT TGTCCTCCTTGTGAAATGGTT	ENSG00000115738
Matrix metallo-proteinase 1	MMP1	ACATGAGTCTTTGCCGGAGG ATCCCTTGCCTATCCAGGGT	ENSG00000196611
Matrix metallo-proteinase 13	MMP13	TTGAGCTGGACTCATTGTCG TCTCGGAGCCTCTCAGTCAT	ENSG00000137745
Bone morphoge-netic protein 4	BMP4	CCACGAAGAACATCTGGA-GAAC ATACGGTGGAAGCCCCTTT	ENSG00000125378
Bone morphoge-netic protein 6	BMP6	GCAGACCTTGGTTCAC-CTTATG AGAATGTGTGTCCCCAGCA	ENSG00000153162
Noggin	NOG	GCCAGCACTATCTCCACATCC GGGTGTTCGATGAGGTCCAC	ENSG00000183691

Target	gene name	sequence [FWD/REV]	ENSEMBL ID
Smad family member 1	Smad1	CAACAG AGTGAAAC-CATCCACCAACACAGGA-GATGTTCAGGC	ENSG00000170365
Smad family member 5	Smad5	GGATGAGTTTT-GTCAAGGGTTG ACAGAAGA-TATGGGGTTCAGAGG	ENSG00000113658
bone morphogenetic protein receptor type 1A	BMPR1A	TTCGATGGCTGGTTTTGCTC ACGACGTCTGCTTGAGATGC	ENSG00000107779
bone morphogenetic protein receptor type 1B	BMPR1B	CCTGGAGAATCCCTGAGAGAC AGTCCTTTGGACCAGCAGAG	ENSG00000138696
Bone morphogenetic protein receptor type 2	BMPR2	GTTGGAGCTGATTGGCCGAG TTTACAGCAACTGGACGCTC	ENSG00000204217

2.7 Cell culture

2.7.1 Cells

C2C12-BREluc – C2C12 stably transfected with a BRE-luciferase reporter[139] were received from the lab of Petra Knaus (Institut für Chemie und Biochemie, Freie Universtität Berlin, Germany).

hFOBs – human fetal osteoblasts were purchased from ATCC® (LGC Standards GmbH, Mercatorstr. 51, 46485 Wesel, Germany).

hdFs – primary human dermal fibroblasts were isolated from human skin biopsy samples by tissue culture plastic adhesion. All used patients were between 11 and 35 years old.

hMSCs – primary human mesenchymal stromal cells were provided by the core unit cell harvesting of the BCRT (Simon Reinke, Augustenburger Platz 1, 13353 Berlin, Charité Berlin, Germany) and isolated from human bone marrow of patients with an age of >55 years.

2.7.2 Cell culture media, reagents & supplements

Table 2-9: list of media, supplements, solution & buffers used for standard cell culture

component	ordering N°	manufaturer	storage [stock|in use]	
10x Trypsin/EDTA	59418C-10ml	Biochrom GmbH	-80°C/-20°C	4°C
DMEM (high glucose)	41965-039	Thermo Fischer	4°C	
DMEM (low glucose)	D5546	Biochrom GmbH	4°C	
DMEM/F12	11320-082	Thermo Fischer	4°C	
DPBS (w Ca^{2+}/Mg^{2+})	14040-091	Thermo Fischer	4°C	
DPBS (w/o Ca^{2+}/Mg^{2+})	14190-094	Thermo Fischer	RT	
FBS superior	S0615	Biochrom GmbH	-80°C	4°C
Geneticin disulphate (G418)-solution	CP11.3	Carl Roth	4°C	
GlutaMAX™	35050-038	Thermo Fischer	4°C	
Non-essential amino acids	K0293	Biochrom GmbH	4°C	
Nutridoma-SP	11011375001	Roche	4°C	
Penicillin/Streptomycin 10.000 U/ml / 10 mg/ml	A2213	Biochrom GmbH	-80°C/-20°C	4°C

2.7.3 Growth factors & additives

Stock solution of all growth factors and additives summarized in Table 2-10 were produced under sterile conditions or were sterile filtered prior to use. Appropriate volume aliquots of stock solutions were created.

Table 2-10: list of growth factors and additives used in cell culture

component	ordering N°	manufaturer	dissolved in	concentration of stock	storage [stock|in use]	
Dexamethasone	D2915	Sigma Aldrich	ddH_2O	1mM	-20°C	4°C
L-Ascorbic acid 2-phosphate	A8960	Sigma Aldrich	DMEM | H_2O	100mM | 50mM	-20°C	4°C
rhBMP2	-	Thomas Müller‡	1mM HCl	1mg/ml	-80°C	4°C

‡ Lehrstuhl für Molekulare Pflanzenphysiologie und Biophysik, Julius-Maximilians-Universität Würzburg

component	ordering N°	manufaturer	dissolved in	concen-tration of stock	storage [stock|in use]	
β-Glycerol-phosphate	G9422	Sigma Al-drich	ddH_2O	200mM	-20°C	4°C

2.7.4 Drugs and other substances

Table 2-11: list of small molecule inhibitors, drugs, substances and other

component	ordering N°	manufaturer	dissolved in	concen-tration of stock	storage [stock|in use]	
Alamar Blue	DAL1100	Thermo Fischer	-	11x	-80°C	-20°C
CellTracker™ Green CMFDA Dye	C2925	Thermo Fischer	DMSO (an-hydrous)	1mM	-20°C	-

2.8 Biomaterials

Macroporous collagen scaffolds “Optimaix” were purchased from Matricel GmbH (Kaiserstraße 100, 52134 Herzogenrath, Germany) and were fabricated from purified collagen from porcine skin by a directional freeze-drying process [140]. Scaffold sponges were delivered sterile and single-packed in a 30x40x3mm format (width/length/height). Sealed packages were stored at room temperature and in the dark, while sponges in use were stored at 4°C.

3 Methods

For most of the methods described here, standard operating procedures were established to guarantee quality and reproducibility of experiments which can be provided upon request.

3.1 Molecular biological methods

3.1.1 RNA isolation

Cellular mRNA was isolated from 2D using the PureLink® RNA Mini Kit (Thermo Fischer) in combination with PureLink® DNase according to the manufacturer's instructions. Isolation from 3D was performed with slight modifications to the original protocol which shall be described here in brief:

Samples were lysed at the required time point extracting excessive culture medium by pulling samples over a sterile filter paper and re-soaking samples with placing them inside prepared Eppendorf tubes containing 500µl of 1x lysis buffer supplemented with 1 vol.% of 2-mercaptoethanol. Tubes were vortexed and frozen at least overnight at -80°C to enhance the lysis efficacy. Next, samples were thawed and the scaffolds were centrifuged at 2000 x g for 2 minutes through a 10µl pipetting tip loaded with a pierced bead serving as a cartridge to yield the total lysate and to retain the scaffold. All further steps were conducted according to the manufacturer's protocol.

In order to boost the isolation efficacy and yield, RNA was isolated by eluting twice and with nuclease-free water heated to 70°C. The RNA concentration was measured using a NanoDrop spectrophotometer. Samples were finally stored at -80°C.

3.1.2 cDNA synthesis

Reverse transcription of isolated RNA into complementary DNA was performed using the iScript™ cDNA Synthesis Kit (Bio-Rad) according to the manufacturer's instructions. With one reaction 500ng of RNA were reverse transcribed. The reaction was performed inside a Mastercycler® gradient (Eppendorf).

3.1.3 qPCR

Quantitative PCR was performed with an iQ™ 5 Real-Time PCR Detection System (Bio-Rad) and iQ™ SYBR® Green Supermix (Bio-Rad). The reaction setup was done according to the following protocol:

1x iQ™ SYBR® Green Supermix (50%)
5ng cDNA
500nM Primer

The reaction was performed according to the protocol described in Table 3-1. Collected PCR data were analyzed according to the $\Delta\Delta C^T$ method to derive mean normalized expression (MNE) values and fold changes relative to a control sample [141]. The efficacy of primers was calculated by creating a standard curve as described previously [142].

Table 3-1: qPCR cycler protocol

	step	time [minutes]	temperature [°C]
1x	initiation	3:00	95
40x	denaturation	0:30	95
	annealing	0:30	60
	elongation	0:30	72[§]
1x	denaturation	1:00	95
1x	melt curve	0:10	55-95 (0.5 incr.)[§]

3.1.4 CyQUANT™ assay

Quantification of the DNA content of scaffold samples was performed using the CyQUANT™ Cell Proliferation Assay Kit (Thermo Fischer) with making slight modifications to the manufacturer's instructions. Scaffolds were cultured for the desired time point and treated under the respective conditions. If native samples were harvested, the were washed with PBS at 37°C consecutively as phenol red from cell culture media interferes with the detection.

Samples were frozen at -80°C and shattered under liquid nitrogen conditions using custom made silicone pots and steel pestles. The sample powder was mixed with 800µl

[§] Measurement of fluorescent signal

of 1x lysis buffer used from the kit, vortexed and centrifuged at 5000 x g for 2 minutes in a tabletop centrifuge. 250µl of the supernatant were transferred into a new tube and mixed in a 1:1 ratio with 2x of GR dye (1:200 dilution of 400x stock, dissolved in lysis buffer). 200µl were transferred to a 96well plate and samples were measured in duplicates. A standard curve was prepared in parallel according to the manufacturer's instructions and used for quantification of the DNA concentration from fluorescent values. The fluorescence was quantified at 480nm excitation and 520nm emission using a microplate reader (Tecan). Calculated DNA concentration were calculated back to total DNA amount per sample.

3.2 Protein biochemical methods

3.2.1 Cell lysis & sample processing

For the extraction of cellular proteins (e.g. Smad phosphorylation), the RIPA buffer protocol was used while for the harvesting of total ECM lysates an adapted ECM extraction protocol was used as described recently[143].

RIPA-buffer: Cells were treated as required and washed once with 200µl of cold PBS by dragging samples over a filter paper to aspirate the medium. PBS wash buffer was removed in the same manner and scaffolds were transferred into an Eppendorf tube loaded with 100µl of 1x RIPA buffer, vortexed thoroughly and incubated on ice for 5 minutes. Samples were sonicated for 30 seconds inside an ultrasound bath and the scaffold was transferred into a 10µl pipetting tip loaded with a pierced bead serving as a cartridge. Finally, samples were centrifuged at 2000 x g for 2 minutes (4°C) to dry the scaffold and to harvest the total lysate and were stored at -20°C.

ECM-extraction buffer: Samples were frozen at -80°C and shattered under liquid nitrogen conditions as described in section 3.1.4. 200µl of ECM-extraction buffer I were added to the cryo-powder, vortexed and sonicated for approx. 2 minutes at 3°C inside an ultrasound bath. Next, 100µl of ECM-extraction buffer II were added and the samples were vortexed again. Finally, the insoluble debris was pelleted by centrifugation at 5000 x g for 2 minutes. The supernatant was further used for gel electrophoresis and stored at -20°C.

3.2.2 Gel electrophoresis

Protein lysates were separated on a polyacrylamide gel using the NuPAGE® electrophoresis system (Thermo Fischer) according to the manufacturer's instructions. In brief: lysates were mixed for 4x LDS loading buffer (Li-Cor) and heated to 85°C for 3-5 minutes to denature proteins. Mixtures were chilled on ice again, vortexed and spun briefly before loading onto NuPAGE™ 4-12% Bis-Tris Protein Gels mounted into XCell SureLock™ Mini-Cell container (both Thermo Fischer). Electrophoresis was performed in 1x MES running buffer at 180V constant for 50-80 minutes until desired separation was achieved. Gels were removed from the caskets and further used as described in section 3.2.3.

3.2.3 Western blotting & detection

Proteins separated by polyacrylamide gel electrophoresis were transferred onto nitrocellulose membranes using the XCell II™ Blot Module (Thermo Fischer) mounted into the XCell SureLock™ Mini-Cell. The inner chamber was filled with 1x of transfer buffer and run at 30V constant for 1 hour.

Afterwards, nitrocellulose membranes were washed once briefly in TBS and cut as required. Individual stripes were blocked using 5%BSA/TBS as blocking reagent for 1 hour under gentle agitation at room temperature. Individual membranes were further incubated with the primary antibody at 4°C overnight according the individual manufacturer instructions. The next day, membranes were washed three times for 10 minutes in TBS-T and incubated with secondary antibody (Li-Cor) diluted 1:15 000 - 1:20 000 in 3% BSA/TBS-T for 2 hours at room temperature. Membranes were finally washed three times for 10 minutes with TBS-T and subjected to signal detection and quantification.

Signals from antibody-labelled nitrocellulose membranes were quantified using the Li-Cor Odyssey® imaging system (Li-Cor Biosciences) by scanning with 42µm spatial resolution and appropriate signal amplification to prevent oversaturated signals. Detected bands were quantified by manual contouring of a rectangular ROI around the signal of interest and the raw intensity was measured. Signals of intracellular proteins or phosphorylated proteins were normalized to GAPDH or β-actin as housekeeping genes.

3.2.4 Collagenase incubation

Collagenase treatment for the specific degradation of cell-derived ECM inside 3D scaffolds after decellularization was performed using crude collagenase I (Thermo Fischer) as described before[144]. In brief: crude collagenase I was dissolved in collagenase buffer (see section 2.3) and samples were treated at 37°C for 24 hours in 1ml of collagenase solution (≤ 100U/ml).

3.3 Cell biological methods

3.3.1 Cell culture

All handling of living cell cultures was performed under sterile conditions under a clean fume hood. The surface was disinfected by the consecutive application of 2% aqueous Incidin (ECOLAB Healthcare) solution, Descosept (Dr. Schumacher GmbH) and 70% Ethanol. All necessary equipment such as racks, pipettes, tubes and bottles were disinfected with 70% Ethanol solution prior to use. Additional tools such as Eppendorf tubes and tweezers were autoclaved using an autoclave pot.

3.3.1.1 Thawing, & cultivation of cells

Cells were thawed by immersing and agitating the respective cryo-vial inside a water bath conditioned to 37°C temperature. The suspension was immediately transferred to a prepared cell culture flask containing pre-warmed expansion media of the respective cell type. The next day, the medium was replaced by fresh medium in order to remove DMSO freezing agent.

C2C12-BREluc – cells were cultivated in DMEM (low glucose, Sigma Aldrich) supplemented with 10 vol.% Fetal Bovine Serum (FBS, Biochrom AG), 1 vol.% GlutaMAX™ (Thermo Fischer) and 1 vol.% Geneticin (G418, 0.5 mg/ml, Carl Roth) at 37°C with 5% CO_2 in a humidified incubator. The cells were passaged every 2-3 days with reaching ~70% confluency and were further expanded in a fresh tissue culture flask at a density of approx. 1100 cells/cm^2 (200 000 cells/T175 flask). All experiments were performed between passage 9 and 15.

hFOBs – cells were cultivated in DMEM/F12 (Thermo Fischer) supplemented with 10 vol.% FBS, 1 vol.% Pencillin/Streptomycin (P/S, Biochrom AG) and 0.6 vol.% G418

(0.3 mg/ml) at 34°C with 5% CO_2 in a humidified incubator. hFOBs were passaged every 3-4 days with reaching ~80% confluency and were further expanded in a 1:4 ratio of harvested cells with an approx. density of 2800 cells/cm^2. Cells were used between passage 6 and 13.

hdFs – primary fibroblasts were cultivated in DMEM (high glucose, Thermo Fischer) suuplemented with 10 vol.% FBS, 1 vol.% P/S and 1 vol.% non-essential amino acids (NEA, Biochrom AG) at 37°C with 5% CO_2 in a humidified incubator. Cells were passaged with reaching full confluency and were further expanded at a density of approx. 3300 cells/cm^2 (1x10^6/T300 flask). Cells were used between passage 4 and 9.

hMSCs – primary MSCs were cultivated DMEM (low glucose, Sigma Aldrich) supplemented with 10 vol.% Fetal Bovine Serum (FBS, Biochrom AG), 1 vol.% GlutaMAX™ (Thermo Fischer) and 1 vol.% Penicillin/Streptomycin (P/S, Biochrom AG) at 37°C with 5% CO_2 in a humidified incubator. With reaching ~90% confluency, cells were passaged and further expanded at a density of approx. 3300 cells/cm^2 (1x10^6/T300 flask). Cells were used between at passages 3 and 4.

Table 3-2: summary of medium composition for cell culture

Medium	C2C12-BREluc	hFOBs	hdFs	hMSCs
DMEM (high glucose)			✓	
DMEM (low glucose)	✓			✓
DMEM/F12		✓		
Supplement				
FBS	10 vol.%	10 vol.%	10 vol.%	10 vol.%
P/S		1 vol. %	1 vol. %	1 vol. %
NEA			1 vol. %	
GlutaMAX™	1 vol. %			1 vol. %
G418	1 vol. %	0.6 vol.%		

3.3.1.2 Passaging & freezing

All cells were passaged by trypsinization using a 1x Trypsin/EDTA solution (Biochrom AG) at 37°C following two times consecutive washing with 1x phosphate buffered saline (PBS, Thermo Fischer). The time of incubation varied between 2-3 minutes depending

on the adhesiveness of the cells and was monitored under a cell culture bright field microscope. The reaction was stopped with the corresponding expansion medium.

Table 3-3: overview of respective volumes during culture & passaging for different culture formats

Medium vol.	culture	PBS wash	1x Trypsin/EDTA	stop vol.
T300	60 ml	25 ml	4[**]/5[††] ml	15[††]/16[**] ml
T175	35 ml	10 ml	2[**]/2.5[††] ml	7.5[††]/8[**] ml
T75	15 ml	5 ml	1 ml	4 ml

The cell suspension was put through a cell strainer to remove or separate aggregated cells and cells were pelleted by centrifugation using a tabletop centrifuge at 375 x g for 6 minutes[††] or 325 x g for 8 minutes[**]. In parallel, the cell concentration was quantified using the CASY ™ cell counter (Model TT, Roche) by diluting 70µl of the respective cell suspension in 7ml of CASY®ton (1:101 dilution factor) and with threshold parameters summarized in Table 3-4. The concentration of viable cells was calculated based on the evaluation range with correction for aggregation and the percental viability from the ratio of counts [evaluation range] and counts [reference range].

Table 3-4: CASY™ cell counting parameters

cells	debris [µm]	reference range [µm]	evaluation range [µm]
C2C12	< 7.0	7.0 – 70	11.5 – 70
hFOBs	< 6.5	6.5 – 100	10 – 100
hdFs	< 8.25	8.25 – 70	13.25 – 70
hMSCs	< 8.5	8.5 – 100	16.5 – 100

For cryo-conservation, the supernatant of the pellet was removed and cells were resuspended with expansion medium at a concentration of $2x10^6$ cells/ml and chilled to 4°C on ice. In parallel, a mixture of the respective expansion medium supplemented with 20% FBS and 20% DMSO (anhydrous, Sigma Aldrich). 500µl of the cell suspension was transferred to a cryo-tube and mixed in a 1:1 ratio with the DMSO mixture. Tubes were transferred to a -80°C freezer overnight and finally stored in the gas phase of a liquid nitrogen container. The freezing protocol was applicable to all used cell types.

[**] hMSCs, hFOBs, C2C12-BREluc
[††] hdFs

3.3.1.3 Scaffold seeding

Seeding of macroporous collagen scaffolds was performed by dip-in uptake of cells from a concentrated suspension (see Table 3-5). Therefore, cylindrical samples were prepared from sheets (30x40x3mm [WxLxH]) using a biopsy punch (5mm Ø) before uptake of the suspension. Cells were then allowed to adhere for 60 minutes. Finally, non-adhering cells were removed by 2x consecutive washing in a reservoir containing fresh expansion medium and placed into a new 12-well plate on top of PEEK meshes.

Table 3-5: summary of cell concentrations for scaffold seeding, epxeriment type & culture time

cells	suspension conc.	experiment type	culture time
C2C12	2D experiments only, luciferase reporter assay		
hdFs	7500 cells/µl	Histology/Imaging, Mass spectrometry, q-RT-PCR, Decellularization, mech. Testing	≤ 3 weeks
hFOBs	5000 cells/µl	Histology/Imaging, Western blotting, q-RT-PCR	≤ 2 days
hMSCs	5000 cells/µl, 50 000 cells/µl‡‡	Histology/Imaging, q-RT-PCR, 3D migration, chondrogenic differentiation	≤ 3 weeks

3.3.1.4 3D migration

To investigate the directed 3D migration of hMSC into collagen scaffolds, initially a cell suspension (2000cells/µl) as described was created. A custom-made silicone ring of 6mm ID was placed into a 12well plate and 104µl (208 000 cells) was pipetted into the ring and placed at 37°C for 1h to create confluent layer of cells (~740 000 cells/cm²). The silicone ring was removed and the cell layer was washed twice with DPBS. The scaffold was carefully placed onto the cell layer and 800µl of growth medium were added for o/n incubation and adhesion. The next day, the scaffold was removed from the layer and transferred into a well of DMEM (high glucose) supplemented with 1 vol.% Nutridoma, 1 vol.% P/S and 1 vol.% NEA. Cells were cultured for 3 days and then fixed and processed according to chapters 3.3.2.1 - 3.3.2.3 for nuclei staining. Tile scans of stained sections were recorded and the median migration of cells relative to the starting position (scaffold surface) was calculated in ImageJ.

‡‡ For chondrogenic differentiation assay

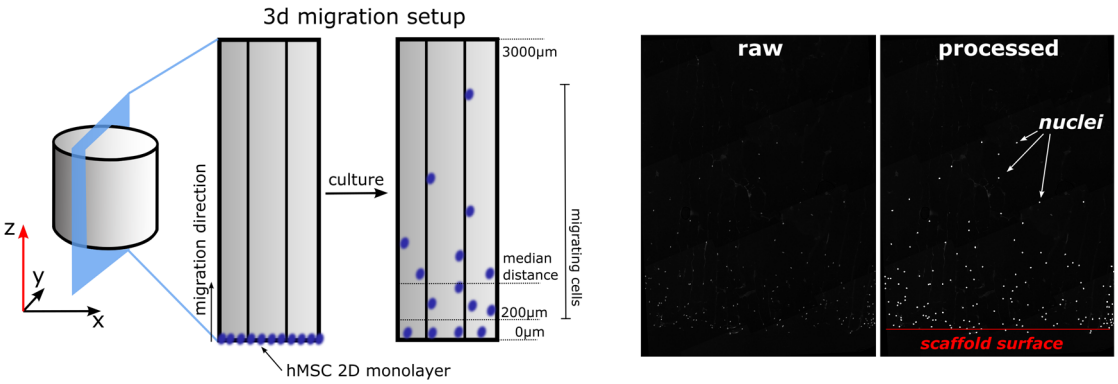

Figure 3-1: Overview of the 3D migration setup.

3.3.1.5 ECM formation (hdFs)

To enable cells to produce a fibrillar collagen matrix[145], ascorbic acid was added as a supplement to the culture medium at a concentration of 1.36 mM [146]. In order to reduce proliferation of cells but also to allow growth factor stimulation (i.e. BMP2, TGF-β1), the FBS content was reduced to 2 vol.% while P/S and NEA concentrations were kept at 1 vol.%. The medium was exchanged and replaced by a fresh mixture at 3,7,10,14 and 17 if cultured for up to 3 weeks. Scaffold constructs enriched with cellular ECM are henceforth termed as *in vitro*-grown micro-tissues (IVMTs)

In addition, growth factor stimulation could be combined by the addition of rhBMP2 at a concentration of 500ng/ml or TGF-β1 at a concentration of 10ng/ml.

3.3.1.6 Decellularization

For removal of cellular components, detergent-based decellularization was performed with the aid of DNase I (Roche) at various concentrations and incubation times. An overview about different decellularization strategies and the respective disrupting agents can be found elsewhere[147–149].

2D – confluent ECM-rich monolayers of cells were decellularized by a protocol adopted from Prewitz and colleagues[150]. 2D cultures were washed once with PBS prior to treatment with a 0.5% Triton X-100/20mM ammonium hydroxide solution for 5 minutes at 37°C. The ECM layers were washed three times with PBS before seeded with primary hMSCs for performing osteogenic differentiation.

3D [agitation] – scaffolds were cultured according to chapter 3.3.1.4. and transferred into a new 12-well plate and treated according to the protocol described in Table 3-6. All

steps were conducted under sterile conditions and at room temperature, if not otherwise stated.

Table 3-6: summary of standard agitation-based decellularization protocol

step	solution	time
detergent	2.5ml 1% TritonX-100/0.1% SDS in ddH_2O	2 x 24 hours
wash	3ml of PBS (with Ca^{2+}/Mg^{2+})	3 x 20 minutes
DNase	2ml of DNase (350U/ml) dissolved in PBS (with Ca^{2+}/Mg^{2+})	24 hours
wash	3ml of PBS (without Ca^{2+}/$Mg^{2+)}$	3 x 20 minutes

3D [perfusion] – scaffolds were cultured according to chapter 3.3.1.4. and transferred to an incubation chamber a custom-made perfusion system connected to a peristaltic pump. Each chamber holds space for one sample and consists of a lower and an upper silicone striated plug and a cylindrical glass tube. The modular concept allows to connect individual chambers either in parallel or in line at will and is connected to a large reservoir via silicone tubing (0.8mm Ø-ID). Individual units can be mounted by clamping on a plastic (POM) rack linked to a base plate.

A peristaltic pump enabled active perfusion at a speed of 1.7ml/min. The volumes for the individual steps of the protocol were calculated according to:

$$V\ (total\ volume) = 10ml + n \cdot x$$

With n as the amount of samples and x as variable to be set to 2ml (for DNase), 3ml (detergent, deionized water) or 4ml (wash step). After each step the reservoir was changed but as solution of the previous step remains in the system for a certain time frame, a pre-out volume was defined to be discarded to a waste bottle via a T-valve switch. The volume and time depended on the amount of reactors and was calculated according to:

$$V^{pre} = 2 + n$$

The time of pre-outing a former solution from the system could be calculated by dividing the volume V^{pre} by the flow rate. An exemplary protocol for 3 reactors is shown in Table 3-7.

Table 3-7: exemplary short protocol for a perfusion-based decellularization of 3 samples

step	solution	time	volume
ddH_2O	deionized water + 1x cOmplete™ protease inhibitor	90 min	19ml [760µl of 25x protease inh. Stock]
	pre-out	3:30 min	6ml
detergent	0.05% SDS	30 min	19ml [95µl of 10% SDS stock 1:200]
	pre-out	3:30 min	6ml
wash	PBS (with Ca^{2+}/Mg^{2+})	2x15 min	22ml
	pre-out	3:30 min	6ml
DNase	DNase (350U/ml) dissolved in PBS (with Ca^{2+}/Mg^{2+})	5h	16ml
	pre-out	3:30 min	6ml
detergent	0.025% SDS	20 min	19ml [47µl of 10% SDS stock 1:400]
	pre-out	3:30 min	6ml
wash	PBS	2x15min	22ml

3.3.1.7 Luciferase reporter gene assay

Luciferase reporter gene assay was carried out according to the protocol from Herrera and Inman[139]. In brief, C2C12 BRE-luc reporter cells were seeded at a density of 13 100 cells/cm^2 (25 000 cells/24well plate in 400µl) with expansion medium and cultured overnight. The next day, cells were washed once with PBS (500µl) and starved for 8 hours in DMEM (low glucose) supplemented with 1% GlutaMAX™ (300µl). Further, a volume of 50µl of either defined BMP2 concentration serving as standard or a sample to test was added to the cells and incubated for further 16 hours.

After that, the cells were washed once with PBS, lysed using 100µl of 1x lysis buffer (Promega) and agitated for 15 minutes at 400rpm on top of a thermo-mixer. 20µl of each sample were transferred to 96 well plate and 20µl of Firefly luciferase substrate was added directly prior to measurement of luminescent signal using a plate reader (Tecan).

3.3.1.8 BMP stimulation

After scaffold seeding cells were cultured overnight (hdFs) or for 2 days (hMSCs, hFOBs) with normal expansion medium prior to stimulation. At the day of stimulation, scaffolds were washed once with starvation medium and incubated for 3 hours in order to decrease unspecific background signaling due to the presence of growth factors in FBS.

The remaining concentration of FBS inside the medium depended on the time of stimulation (Table 3-8) ranging from 0% (≤ 2 hours) to 2% (≥ 1 day). Other supplements were kept at the same concentration according to Table 3-2.

Table 3-8: FBS concentrations present in stimulation media depending on stimulation time

time of incubation	cell type	FBS concentration	assay
≤ 2 hours	hFOBs, hMSCs	0%	Smad phosphorylation (western blotting)
2 – 6 hours	hFOBs	0.5%	gene expression
≤ 24 hours	hFOBs	1%	gene expression
≥ 2 days	hMSCs, hdFs	2%	gene expression, ECM formation

For stimulation, a 30x working solution of the final concentration was created either by diluting BMP2 stock (1mg/ml) in PBS (western blotting) or stimulation medium (gene expression, ECM formation). As BMP signaling is highly mechanosensitive, short time stimulation (≤ 6hours) was performed inside the incubator with as little movement as possible of the samples.

3.3.2 Histology

3.3.2.1 Sample fixation, processing & cryo-cutting

PFA fixation – samples were fixed by placing them into a PBS-buffer 4%-paraformaldehyde (PFA) solution for at least 5 hours at room temperature. The reaction was quenched by a 25mM ammonium chloride/PBS solution for 1 hour at room temperature under gentle agitation.

Ethanol fixation – a 70% e-thanol solution was chilled to -20°C and samples were washed at least once with PBS or other applicable wash buffers. Fixation was performed inside plastic staining tubes by the dropwise addition of 1ml ice cold ethanol under gentle agitation on top of a vortex shaker and finally incubated >30 minutes[§§] at -20°C. Scaffolds were finally washed at least three times with PBS at room temperature.

[§§] Open porous samples (e.g. BrdU assay) are fixed fast within 30 minutes, while dense, ECM-rich scaffolds require a time frame of at least 2-3 hours at -20°C

Methanol fixation – a 100% methanol solution was chilled to -20°C and samples were washed at least once with PBS or other applicable wash buffers. Fixation was performed inside plastic staining tubes by the dropwise addition of 1ml ice cold ethanol under gentle agitation on top of a vortex shaker and finally incubated >2 hours[§§] at -20°C. Scaffolds were finally washed at least three times with PBS at room temperature.

Scaffolds were transferred to a 5% gelatin/sucrose solution and incubated overnight at 37°C. The next day, scaffolds were transferred with gelatin solution to a custom-made cutting mold and were allowed to gelatinize at 4°C for 30-60 minutes. Samples were cut in halves using a scalpel and the gelatin was washed out by incubation at 37°C in PBS with repetitive exchange of buffer after 1-2 hours.

In order to provide an even plane for imaging or to provide sections, scaffolds were processed by embedding scaffold halves into tissue-tek by snap-freezing on an aluminium block placed in liquid nitrogen and performing sectioning using a cryotome at -20°C. For histology (3D migration, chondrogenic differentiation), sections at 20/12µm thickness, respectively, were transferred onto microscope slides and air-dried prior to further processing. If stored unprocessed for a longer time, sections were frozen at -80°C.

3.3.2.2 Immunohistochemistry

Sections of 3D migration were dried and stained for DAPI according to Supplement 2

at a dilution of 1:1000 of the dye. Samples were preserved by covering with cover slips and Fluoromount-G solution. Slides were air dried overnight at RT prior to imaging.

3.3.2.3 Immunofluorescent labeling

Samples were labelled either with epitope-specific immunoglobulins, fluorescently labelled small molecule probes or with a combination of both. An overview of different pre-treatment, blocking and dilution conditions can be found in Table 3-9. If not otherwise stated, all steps were conducted in a 24well plate format at room temperature and under gentle agitation. To avoid photo bleaching, all steps with fluorophores present were performed in the dark.

Table 3-9: summary of IF staining protocol conditions

Step	time	condition
Wash	1-3x10min	0.025% TBS-T
Permeabilization	10min	0.1-0.2% TBS-T
Wash	5min	TBS
Pre-block	10min	1% BSA/TBS
Block	30min	1% BSA/5% normal serum/TBS
Primary antibody	4°C o/n	Diluted in antibody diluent
Wash	3x5min	0.025% TBS-T
Secondary antibody	2h	Diluted in 1% BSA/5% normal serum/TBS
Wash	3x5min	0.025% TBS-T
DNA stain	5-60min	DAPI (in PBS) or Draq5 (in TBS)
Wash	3x10min	TBS
Storage	4°C	PBS/TBS

Staining of actin via Alexa Fluor-coupled phallotoxins was combined with secondary antibodies. If Phallotoxin staining was performed alone, permeabilization and blocking was not conducted and the dye was diluted in TBS. In addition, DNA stains, if performed separately, directly were conducted in TBS or PBS, respectively. The dilutions of the respective antibodies and dyes may vary. Exemplary staining protocols for fibronectin staining or actin/Nuclei staining may be referred to in Supplement 2.

3.3.3 Imaging

3.3.3.1 Confocal Microscopy

Confocal images were obtained using a Leica SP5 confocal microscope equipped with a Mai Tai HP multiphoton laser and a 25x (overview and ECM images) or 63x (zoom in focal adhesion images) water immersion objective. Second harmonic generation imaging [151] was used to visualize the collagen scaffold and newly formed cell-derived fibrillar collagen inside scaffold pores at 910nm wavelength and detection at 450-460nm. Signals were detected using non descanned detectors (NDD) and internal photomultiplier detector. For quantification of signals, laser power as well as detection parameters were kept constant for all experiments. The standard setup for imaging was set with a 1024x1024

(approx. 1.65 pixel-to-micron ratio for 25x objective) pixel spatial resolution and 4µm z-resolution.

3.3.3.2 Image analysis

Images usually were analyzed according to the workflow described in Figure 3-2. Recorded z-stacks were transferred either into maximum projections (brightest point per pixel in stack) or a sum of slices (sum of signals per pixel over stack) for analysis.

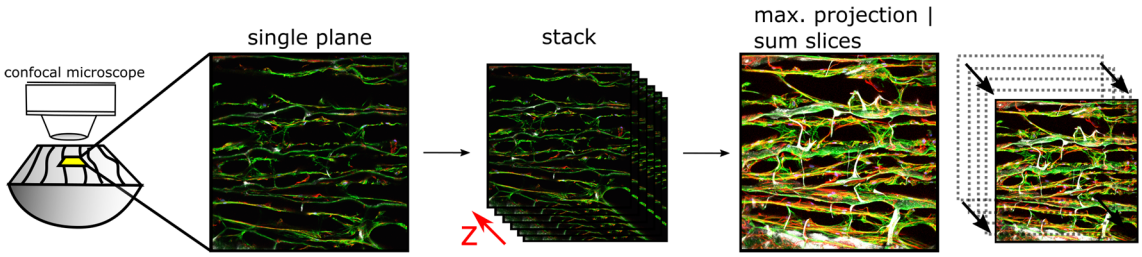

Figure 3-2: summary of the image acquisition and analysis workflow.

Signal density, orientation & anisotropy: Fibrillar collagen signal was analyzed for density by sum slices of recorded stacks and manual contouring of scaffold pores. A background subtracted histogram was summed up and divided by the ROI volume to obtain the signal density. Orientation distribution of signals (fibronectin, actin, fibrillar collagen) was performed in a maximum projection using the OrientationJ ImageJ plugin [152]. The angle of images was corrected prior to measurement according to the pore direction to obtain values relative to the scaffold axis. Signal anisotropy was calculated using the FibrilTool ImageJ plugin [153].

Scaffold architecture: To determine the wall thickness, high resolution scans were taken at 63x magnification and the images were analyzed on single planes using the BoneJ ImageJ plugin [154]. The pore spanning distance was calculated by manual measurement of multiple pores from at least two different sheets of the same batch. The density of stabilizing beam elements was calculated by manual counting within a view field and normalization to the image volume.

Focal adhesion analysis: size and amount of focal adhesions per cell was calculated from phospho-paxillin staining imaged at high resolution using a custom-made ImageJ macro. In brief: Images were binarized for the pPax channel and selected for the cell outline. Count and size was further determined by particle tracking. Particles were categorized according to size and normalized to the total number of particles per cell.

3.3.3.3 Live-cell imaging

Time-lapse live-cell imaging was performed using the Leica SP5 confocal microscope as described in combination with a custom-made incubation chamber mounted on top of the microscope together with carbon dioxide gassing. Prior to that, cells were stained inside seeded scaffolds using cell tracker green at a dilution of 1:1000 in 0% FBS containing medium for 1h at 37°C. Cells were washed once with 0.5% FBS containing medium and scaffolds were transferred into a custom made chamber made from stainless steel that included an observation window at the bottom and pins to fix the scaffold position. Several positions were marked and images were recorded at 512x512 (approx. 0.83 pixel-to-micron ratio) with 4µm z spatial resolution at a time interval of 30 minutes.

Analysis of cellular migration was performed in 3D, while lateral wall displacement was performed using a maximum projection of SHG signals. Images were binarized and tracking of movement was performed using the TrackMate ImageJ plugin [155].

3.3.3.4 Traction force microscopy

Traction force microscopy was performed according to a protocol described by Plotnikov and colleagues [156]. It is based on the casting of a thin polyacrylamide gel covalently linked to an activated glass surface in which fluorescent beads are embedded. The gel is coated with fibronectin to allow cell adhesion and spreading and bead displacement due to cellular traction forces is recorded under a confocal microscope.

Coverslip activation – borosilicate coverslips (22x40x0.15mm) were cleaned successively by sonication in an ultrasound bath at 60°C for 30 minutes in various different solutions: 0.1% SDS, deionized water, 70% ethanol, 100% ethanol. Coverslips were cleaned in batch mode and stored in a closed jar in 100% ethanol until use. Four coverslips were activated at once by placing them clean and dry in a glass petri dish with 0.5ml of 50% APTMS solution incubated for 10 minutes. Next, approx. 30ml of ddH_2O were added and incubated on an orbital shaker for another 30 minutes. Coverslips were rinsed several times with ddH_2O, transferred to another petri dish and incubated with 0.5% glutaraldehyde solution for 30 minutes under agitation. Finally, coverslips were rinsed again several times with ddH_2O and dried in a vacuum desiccator. In parallel, microscope slide (preferably cleaned with ddH_2O and 100% ethanol before) were prepared with a hydrophobic surface by wiping them with a RainX-soaked fuzz-free tissue. The

solution was allowed to dry for 1-2 minutes and microscope slides were extensively washed with ddH_2O and 100% ethanol and dried in a vacuum desiccator as well.

Polyacrylamide gel casting – depending on the desired stiffness of the gel, 40% acrylamide and bis-acrylamide solutions were mixed at different ratios. Working solutions can be prepared in advance and stored at 4°C for up to a year. A summary can be found in Table 3-10. The effective substrate stiffness was measured by nano-indentation and used for the calculations of strain energy.

Table 3-10: Composition of acrylamide working solutions and final mixtures. Adopted from Plotnikov et al.[156].

shear modulus G [kPa]	2.3	4.1	8.6	16.3	30	55
Young's modulus E [kPa]	6.9	12.3	25.8	48.9	90	165
working solution [5ml total, 4°C storage]						
40% acrylamide [ml]	3.75	2.34	2.34	3.00	3.00	2.25
2% bis-acrylamide [ml]	0.75	0.94	1.88	0.75	1.4	2.25
ddH_2O [ml]	0.5	1.72	0.78	1.25	0.6	0.5
final mixture						
working solution [µl]	125	200	200	250	250	333
0.1µm fluorescent beads [µl]	20	20	20	20	20	20
10% APS [µl]	2.5	2.5	2.5	2.5	2.5	2.5
TEMED [µl]	0.75	0.75	0.75	0.75	0.75	0.75
ddH_2O [µl]	352	277	277	227	227	158
total	579	579	579	579	579	593

The mixture of working solution, beads and ddH_2O was prepared, mixed and degassed under vacuum for 30 minutes to remove oxygen and air bubbles. APS and TEMED were added, the solution was gently mixed and a drop was pipetted on top of a hydrophobic microscopy slide. Activated coverslips were placed on top so that the solution could equally spread and the gel was allowed to polymerize for approx. 30 minutes. The coverslip was carefully detached using a scalpel and thoroughly washed in ddH2O. The thickness can be calculated according to:

$$V\ [\mu l] = 0.88 \cdot h\ [\mu m]$$

Fibronectin functionalization – PAA-gels were liberated from excess water by carful soaking with a fuzz-free tissue. An aliquot of Sulfo-SANPAH (40µl) was thawed and

mixed with 960µl of ddH_2O. 0.5ml of this mixture was applied on top of a gel and exposed to 10mW/cm^2 for 150s long wavelength (365nm) UV-light. Excess solution was decanted, the gels were washed once in ddH_2O, dried and placed on top of a 50µl drop of fibronectin solution (1mg/ml in PBS) inside a petri dish lined with parafilm. The gels were incubated for 4h at room temperature. Finally, gels were washed several times in PBS and stored at 4°C until use.

Assessment of PAA-gel properties – In order to ensure that the PAA gels were homogeneous regarding surface functionalization and mechanical properties, they were characterized by confocal imaging for fibronectin/collagen staining (coating-dependent) as well as by Nanoindentation using the Piuma system (Optics11).

Cell seeding & Image aquisition – PAA-gels were seeded with hdFs at a density 2000 cells/cm^2 (< 30% confluency) and cultured overnight at 37°C. The next day, cells were labelled with 10µM CellTracker™ Green (Thermo Fischer) for at least 50 minutes until green fluorescence was visible. The coverslip was mounted into a custom-made perfusion chamber made from stainless steel (Figure 3-3).

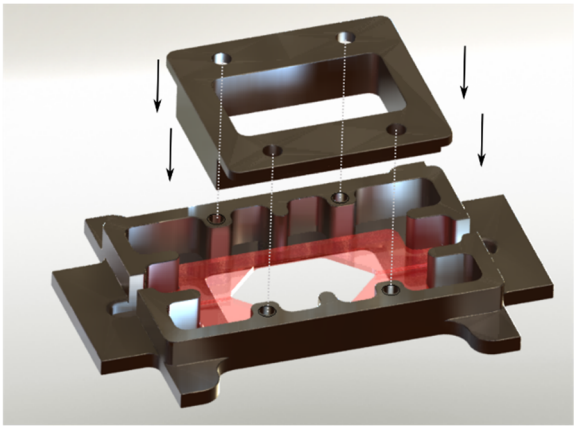

Figure 3-3: CAD model of perfusion chamber. Upper holder is used to fix lower coverslip containing cells, a silicone sealing providing inlet and drainage and sealing and an upper coverslip.

Images were acquired under a confocal microscope equipped with a 63x objective and a z-spacing of 0.5µm to record multiple planes at each position including the cells and fluorescent beads. Positions with adherent cells were spotted by green fluorescence of the cells. After recording of the first stack, cells were removed by trypsinization and the same positions were recorded again.

Data analysis – Calculation of cellular forces was performed according to a protocol described by Martiel and colleagues [157] using the provided ImageJ macros and plugins. The overall workflow is summarized in (Figure 3-4). In brief: Recorded stacks were

transferred into image pairs consisting of one image prior and one after trypsinization. One slice out of each stack was selected for analysis and image pairs were corrected first for lateral displacement by template matching. Next, ImageJ plugins for Particle Image Velocimetry and Fourier Transform Traction Cytometry [158] were used to generate displacement and force magnitude/vector maps. Based on the cell outline derived from cell tracker green signals, a ROI was selected in which total force magnitude and total strain energy values were calculated.

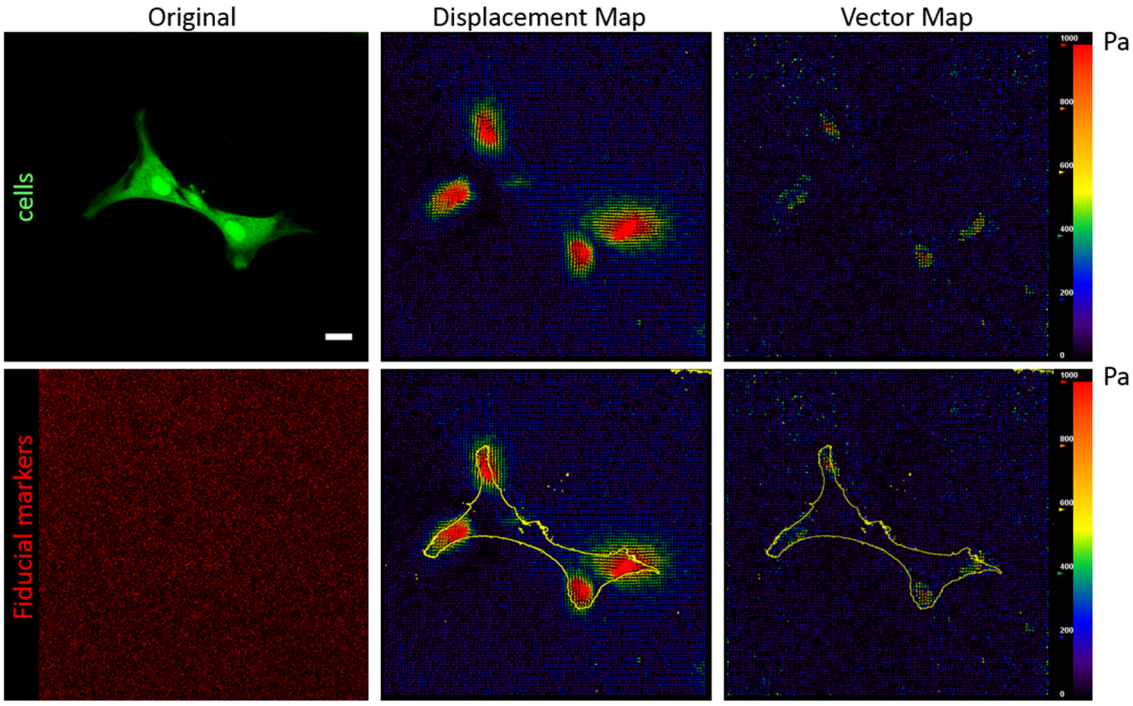

Figure 3-4: TFM data analysis. Confocal images showing green fluorescent cells and red fiducial markers. Bead displacement of image pairs is transferred into a displacement map and further into a vector map of force fields. Scale bar 20µm.

3.4 Biomechanical methods

3.4.1 Mono-axial compression testing

For characterization of the mechanical bulk properties of collagen scaffolds, mono-axial compression testing was performed using the BOSE ElectroForce Mechanical Test Instruments TestBench system combined with a Model 31 Low load cell (Honeywell Corp.). Compression was performed in PBS solution using a custom-made chamber with a lower and an upper plunger and a peek mesh to guarantee homogenous force distribution.

Three consecutive cycles of compression at 0.05mm/s compression speed to 0.3 and 0.6 mm displacement were performed including a dwell of 30 seconds at 0, 0.3 and 0.6 mm displacement.

Load/displacement curves were recorded and transferred into stress(σ)/strain(ε) curves according to:

$$\sigma = \frac{m \cdot g}{A}$$

with gravity acceleration g = 9.81 m/s^2 and:

$$\varepsilon = \frac{l}{\Delta l}$$

The elastic modulus as a measure of the stiffness of the tested materials was derived from the slope of the linear region of stress/strain curves according to:

$$\sigma(\varepsilon) = E \cdot \varepsilon$$

3.4.2 Contraction analysis for scaffold-based cell culture assays

Calculation of changes in the outer shape of scaffold samples was done by scanning (1200 dpi) at the respective time point and in the respective culture medium using a digital scanner (Epson Perfection V200) both in top and side view. Scaffold cross-sectional area was quantified from top view by manual contouring and the scaffold height from side view by calculating the mean distance between top and bottom (Figure 3-5).

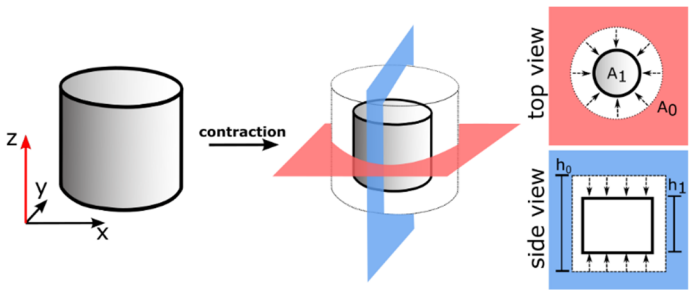

$$\varepsilon^m_{top}(\%) = \frac{A_0 - A_m}{A_0} \cdot 100$$

$$\varepsilon^m_{side}(\%) = \frac{h_0 - h_m}{h_0} \cdot 100$$

Figure 3-5: schematic presentation of scaffold contraction analysis & its calculation

In order to correct for the squared behavior of the top contraction, values were corrected according to:

$$\varepsilon^m_{x|y}(\%) = \left(1 - \sqrt{1 - (\frac{\varepsilon^m_{top}(\%)}{100}}\right) \cdot 100$$

The total volume contraction was calculated according to:

$$\varepsilon_{total}^{m}(\%) = (1 - \frac{\varepsilon_{top}^{m}(\%)}{100}) \cdot (1 - \frac{\varepsilon_{side}^{m}(\%)}{100}) \cdot 100$$

3.5 Data analysis, presentation & statistics

All data presented in a graphical format in this work have been built using the OriginPro 2015G (OriginLab Corporation) software. Bar charts, dot plots, line plots are presented as mean values with standard deviation. Box plots are presented as boxes with 25% and 75% quantile as lower and upper limits. The mean is shown as square and the median as horizontal line. Vertical lines with marked ends indicate upper and lower Whisker and diagonal crosses minimum and maximum values.

Statistical analysis was performed using a two-sided Mann-Whitney U test with Bonferroni correction for comparison of multiple groups according to $p^* = p \cdot n$. A p-value < 0.05 was considered as statistically significant and the different significance levels are indicated according to: # $p < 0.1$, * $p < 0.05$; ** $p < 0.01$; *** $p < 0.001$.

4 Results

Upon injury, the healing process of a bone fracture but in principle also of any kind of tissue starts from a coagulated blood clot – the so-called hematoma. The hematoma is a very soft and unstructured environment. Musculoskeletal tissues in particular feature a highly aligned architecture and all tissues exhibit a basal level of tension – even at rest. So during healing not only the tissue-specific ECM signature needs to be rebuild, but also its original structure and tensional state. Fibroblasts and myo-fibroblasts play an important role in the formation of early tissue structures subsequent to migrating into the site of injury. Fibroblasts feature a high abundance in connective tissue and can be isolated from various tissues including skin, muscle, heart and lung. Although their relevance for wound healing is widely appreciated [159], only limited information is available how ECM deposition and tissue tensioning are linked.

4.1 Investigating the cellular blueprint for tissue formation & patterning

In the first part, the process of tissue formation and tensioning was studied with a particular focus on the interdependency of these processes on extracellular matrix deposition. Various *in vitro* systems have been developed to study tissue formation. The probably most simple and widely used approach is based on the incorporation of cells into a collagen gel [160,161]. Although they are easy to handle and can be combined with deflecting micro-posts for quantification of cell forces [162], visualization of newly deposited ECM, especially collagen, is difficult since signals from hydrogel and cell-secreted ECM are superimposed.

4.1.1 Collagen scaffolds as wound healing model system

Therefore, it was chosen to work with macroporous collagen scaffolds that were fabricated from purified porcine collagen by a directional freezing and freeze-drying process [140]. Cylindrical samples were prepared from material sheets of 3mm height using a biopsy punch (5mm Ø) and the scaffold architecture could be visualized for the two cylinder axis using scanning electron microscopy (Figure 4-1, **a**). The images revealed a high porosity and a strong alignment of channel-like pores in the axial direction. The

material featured a mean pore spanning distance of 101±30µm and relatively thin wall of 2.3±0.9µm. The stiffness was further validated using mono-axial compression tests which demonstrated a higher stiffness when compressing along the pores (axial compr. E=4.1kPa) compared to compression perpendicular to the pores (radial compr. E=1.1kPa) (Figure 4-1, **b**).

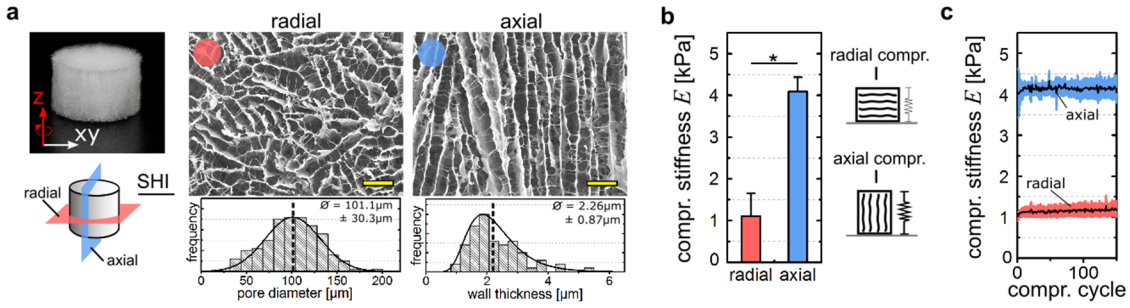

Figure 4-1: macroporous scaffolds from porcine collagen with highly aligned pores. ***(a)*** *image of a cylindrical scaffold prepared using a 5mm biopsy punch. Center and right: SEM images illustrate the pore architecture revealing highly aligned pores along the cylinder axis. Histograms indicate distribute of pore diameter and wall thickness. Scale bar 200µm.* ***(b)*** *Compressive stiffness E for the two pore directions (radial, red and axial, blue).* ***(c)*** *Repetitive compression over 150 cycles showing maintenance of mechanical properties over time. Figure modified from* [163].

In order to verify a stable and elastic behavior over time, scaffolds were compressed repetitively over 150 cycles (Figure 4-1, **c**). The scaffold maintained its mechanical properties during repetitive loading/un-loading. Due to this defined and stable elastic behavior, the scaffold was regarded as an *in situ* force sensor with a high porosity to allow cell spreading and ECM deposition.

Primary human dermal fibroblasts (hdFs) were seeded into the scaffold by immersing them in a concentrated cell suspension. This led to a homogenous distribution of cells throughout the material after seeding that was maintained during culture (Figure 4-2).

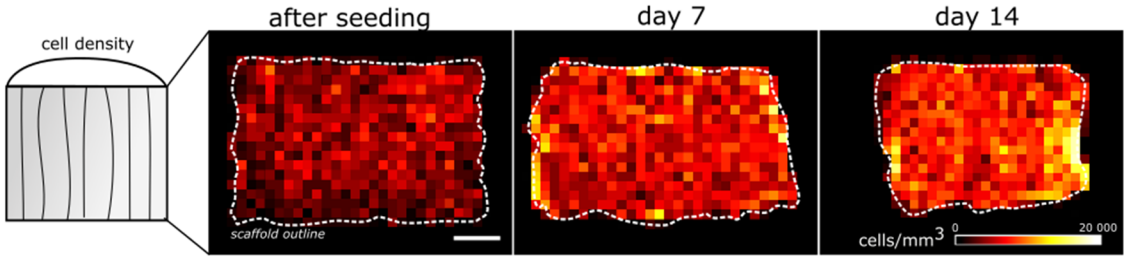

Figure 4-2: distribution of cells within the collagen scaffold. Confocal imaging of whole samples for cell nuclei was converted into heat maps of cell density. The scaffold outline is represented as white dashed line. Scale bar 1mm. Figure modified from [163].

Tissue formation was studied in detail by confocal imaging of fibronectin-stained samples cultured 3, 7 or 14 days together with visualization of fibrillar collagen by SHI (Figure 4-3). The images indicate an initial localization of cells and early ECM to the collagen walls. Wall-interconnecting struts were used for bridging and initiation of pore filling in a centripetal manner (Figure 4-3, **a**). Over time, the scaffold pores were completely filled with cells and cell-derived ECM and pore filling also resulted in an increase in collagen density (Figure 4-3, **c**). Although preferential alignment along the pores was visible after 3 days, this was further intensified until the cell, but also ECM network was highly aligned (Figure 4-3, **b and d**). These observations indicate that cells collectively sense and adopt to the macroscopic structural properties of the cell carrier. This is further supported by the observation that cell-ECM network orientation was structurally influenced by the occurrence of wall-interconnecting struts at early time points, but mostly independent at later stages (Figure 4-3, **a - yellow arrows**).

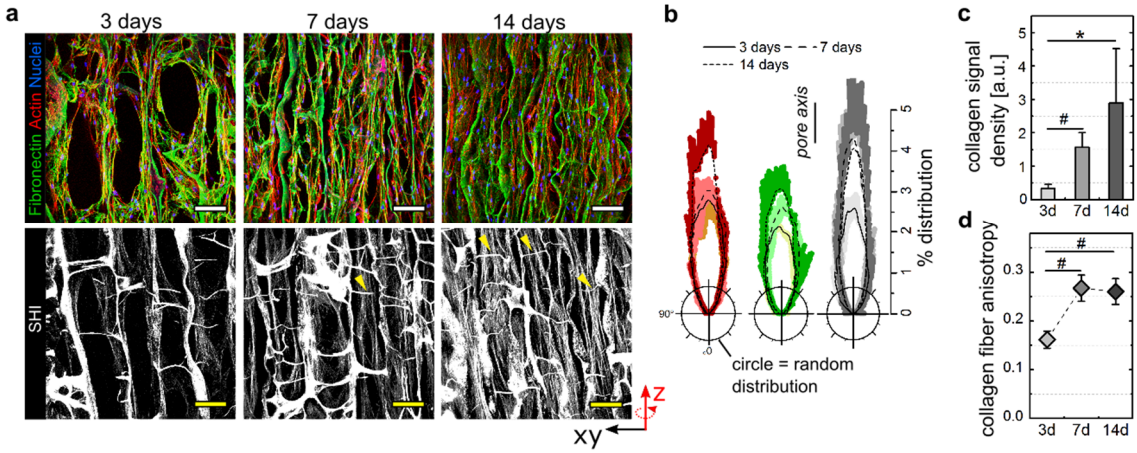

Figure 4-3: fibroblasts deposit new ECM inside collagen scaffold. ***(a)*** *Confocal images of cell-seeded scaffolds 3, 7 or 14 days after culture. Samples were stained either for fibronectin (green), actin (red) or cell nuclei (blue). Fibrillar collagen signal was detected by SHG (white). Yellow arrows indicate wall-interconnecting struts. Scale bar 100µm.* ***(b)*** *orientation analysis of actin, fibronectin or fibrillar collagen signal. The mean is presented as black line with colored belt as S.D.* ***(c)*** *Quantification of fibrillar collagen density inside scaffold pores.* ***(d)*** *Quantification of fiber anisotropy of fibrillar collagen network. Figure modified from* [163].

In summary, it was demonstrated that fibroblasts undergo a self-organization process that lead to a high alignment of cells and cell-deposited fibronectin and collagen fibers following the biomaterial architecture.

4.1.2 Scaffold contraction depends on collagen deposition

In line with previous studies that reported on the macroscopic contraction and force generation *in vitro*, a time-dependent contraction of the biomaterial was observed (Figure

4-4, **a-c**). Although very weak at 3 days, a continuous contraction was observed until 14 days of culture. Since the biomaterial differed in stiffness for axial and radial directions, contraction was recorded for both and found to be significantly higher after 7 and 14 days for the radial compared to the axial direction (Figure 4-4, **b and c**). However, this observation was contradictory to observations from confocal imaging, as cells were found to be highly aligned along the pores. By converting scaffold contraction into a mechanically quantitative measure of scaffold strain energy *U*, it could be demonstrated that significantly more force is acting in axial direction of the scaffolds compared to radial (Figure 4-4, **d**).

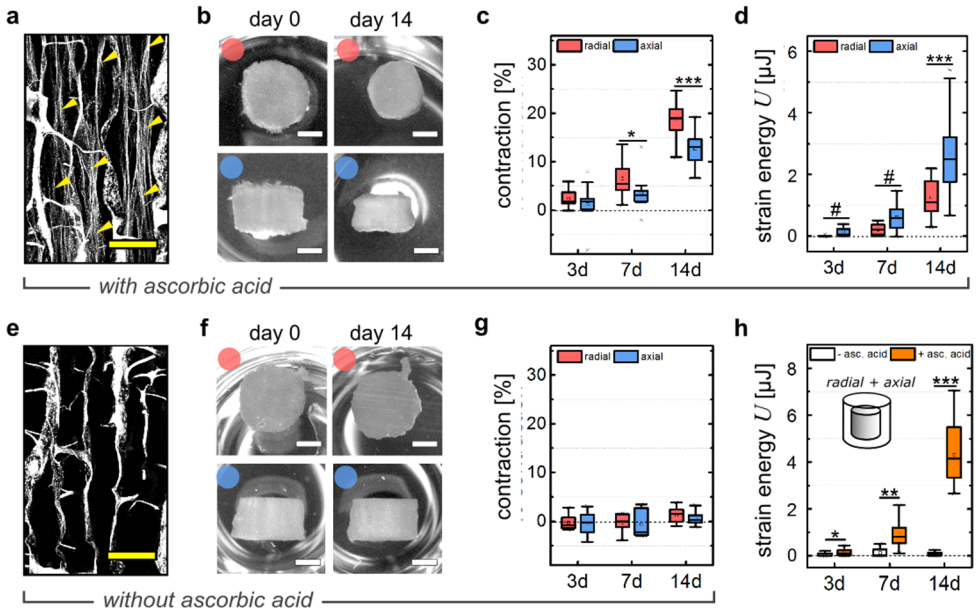

Figure 4-4: scaffold contraction depends on the presence of collagen fibers. ***(a)*** *SHI after 14 days of culture. Yellow arrows indicate cell-derived collagen fibers. Scale bar 100µm.* ***(b)*** *representative images of scaffolds in radial and axial direction after seeding and 14 days of culture. Scale bar 1mm.* ***(c)*** *Quantification of scaffold contraction over time.* ***(d)*** *Calculated strain energies for axial and radial direction based on contraction and the corresponding compressive stiffness (see Figure 4-1).* ***(e)*** *SHI after 14 days without asc. acid supplementation. Scale bar 100µm.* ***(f)*** *Representative images of scaffolds in radial and axial direction after seeding and 14 days cultured without ascorbic acid. Scale bar 1mm.* ***(g)*** *Quantification of scaffold contraction over time without asc. Acid supplementation.* ***(h)*** *Comparison of scaffold strain energy (axial + radial combined) of samples cultured either with or without ascorbic acid supplementation. Figure reproduced from* [163].

Until now, collagen formation and contraction were observed as parallel occurring processes without investigation of a potential inter-dependency. However, efficient contraction particularly in axial direction was only observed after 7 days, where also a long-range collagen network was visible. Assuming that collagen deposition is necessary for scaffold contraction, cells would not be able to macroscopically deform the material without a fibrillar collagen network. To test this, collagen fibrillogenesis was prohibited by

eliminating ascorbic acid supplementation that resulted in a complete lack of collagen fibers after 14 days (Figure 4-4, **e**). Most intriguingly, a complete lack of scaffold contraction was observed for both scaffold directions and all analyzed time points (Figure 4-4, **f-h**). This was a first indication that collagen deposition and contraction are interdependent rather than consecutive processes.

In order to exclude that a lack of ascorbic acid supplementation unspecifically affected cellular proliferation or soft tissue (=fibronectin) deposition, cell number and fibronectin deposition were visualized by confocal imaging showing no difference (Figure 4-5).

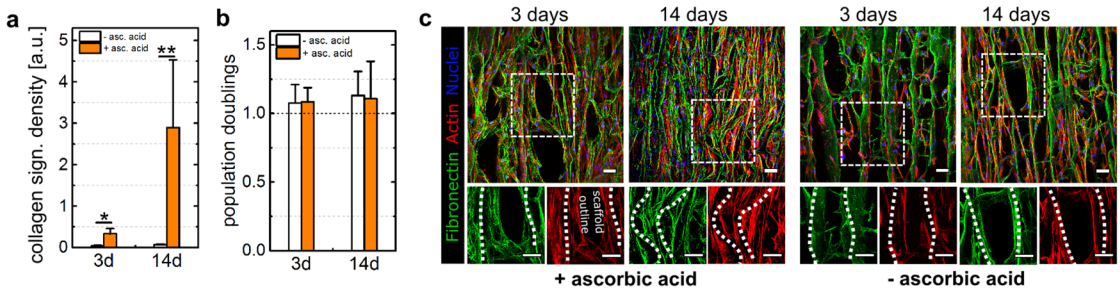

Figure 4-5: Ascorbic acid depletion does not affect cell spreading, proliferation or fibronectin deposition. ***(a)*** *Quantification of SHI signals.* ***(b)*** *Quantification of cell proliferation expressed as population doublings. Values are based on total cell number per sample and an estimated density of 7500 cells/µl directly after seeding.* ***(c)*** *Confocal images of samples stained for fibronectin (green), actin (red) or cell nuclei (blue). Scale bar 50µm. Figure reproduced from* [163].

4.1.3 Cells gradually transfer forces into a fibrillar collagen network

In the previous section, indications were found for a potential inter-dependency of collagen deposition and macroscopic tensioning/contraction. If the tensional state hereby depends on the presence of active cell forces to keep their environment under tension, the amount of contraction would strongly depend on the quantity of single cell forces. Since previous studies point to gradual a transfer of tension from cell forces to the extracellular matrix [137,164], it was speculated that this might occur in the presented wound healing model as well. Consequently, the quantity of macroscopic tension would rather depend on the amount of deposited ECM than on single cell forces and would scale with ECM density.

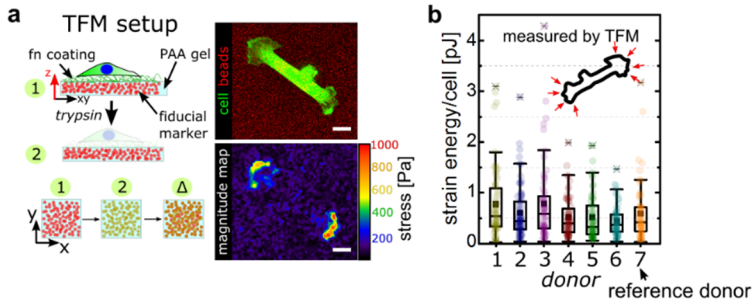

Figure 4-6: measurement of single cell forces by traction force microscopy. ***(a)*** *Schematic representation of the TFM measurement that is based on the incorporation of fiducial markers into an elastic polyacrylamide gel of defined stiffness.* ***(b)*** *Quantification of single cell forces for 7 primary fibroblast donors. Figure modified from* [163].

To test this, primary fibroblasts were isolated from 7 different human donors and subjected to traction force microscopy in order to quantify the individual single cell forces (Figure 4-6). Surprisingly, only small differences were detected between the individual donors as mean values of single strain energy ranged from 0.44 (D6) to o.76 pJ/cell (D1) compared to the intrinsic variability between individual cells of the same donor (Figure 4-6, **b**). Most strikingly, when cultivating the individual donors inside the biomaterial for 14 days under ascorbic acid supplementation, up to a 10-fold difference in macroscopic contraction (D1, D3) was observed that correlated with the quantified collagen density but not with their single cell forces (Figure 4-7).

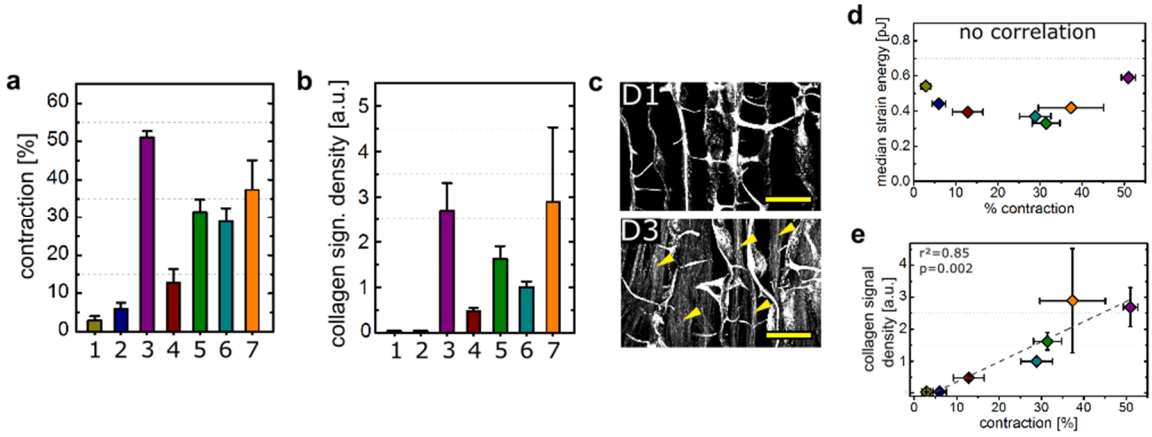

Figure 4-7: scaffold contraction depends on collagen density. ***(a)*** *Quantification of total scaffold contraction (axial + radial contribution).* ***(b)*** *Quantification of fibrillar collagen signal inside scaffold pores.* ***(c)*** *Representative SHG images of donor 1 (D1) and 3 (D3) after 14 days of culture. Yellow arrows indicate cell-derived fibrillar collagen. Scale bar 100µm.* ***(d)*** *Correlation of single cell forces and scaffold contraction.* ***(e)*** *Correlation of collagen density and scaffold contraction. Figure modified from* [163].

In order to estimate the contribution of a single cell to the macroscopic tensioning, contraction was converted into values of scaffold strain and normalized to the total amount of cells present in the sample (Figure 4-8, **a**). The obtained values were further

correlated to the quantity of single cell forces measured by TFM in order to obtain a single cell force amplification factor A_F (Figure 4-8, **b**). Interestingly, this factor varied between 0.5 (D1) and 46 (D3) as mean values. When correlating the derived force amplification factor A_F with the fibrillar collagen density, a linear trend could be observed further emphasizing the strong relevance of fibrillar collagen deposition for the generation of macroscopic tension (Figure 4-8, **c**).

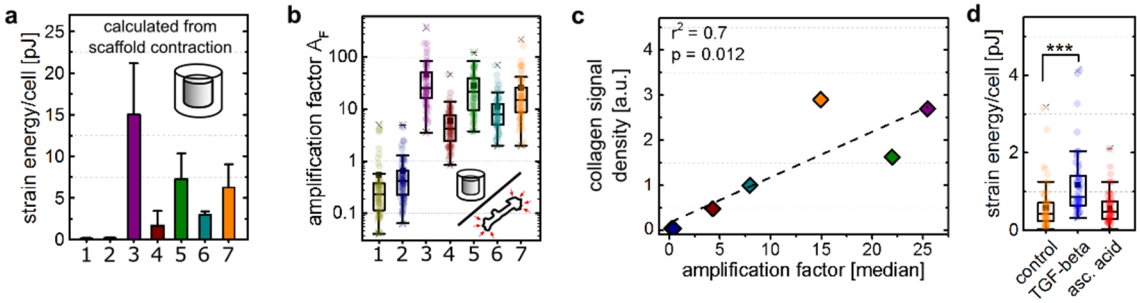

Figure 4-8: single cell force amplification depends on collagen density. ***(a)*** *Single cell strain energy per cell calculated from scaffold contraction and the amount of cells per sample* ***(b)*** *Single cell force amplification factor A_F derived from the ratio of strain energy per cell in the scaffold and measured by TFM.* ***(c)*** *Correlation of collagen density and force amplification factor.* ***(d)*** *single cell strain energy measured by TFM for donor 7 pre-stimulated either with 10ng/ml TGF-β or 50µM asc. acid. Figure modified from* [163].

It has to be mentioned that the derived factor A_F should be regarded as a simplified estimation purely based on scaffold deformation that neglects several factors. A key factor might be the limited ability to predict or measure actual cell forces in 3D which might intrinsically strongly vary from 2D values. Also the long culture environment, the contraction and collagen deposition might drive myo-fibroblast differentiation predominantly in highly contractile samples. In order to estimate the potential error, cells were stimulated with TGF-β1 (10ng/ml) to induce myo-fibroblast differentiation. An increase in single cell forces could be detected that was about 2-fold in the mean value ($U_{control}$ = 0.59pJ/cell, $U_{TGF\text{-}\beta}$ = 1.17pJ/cell). Conclusively, although different cellular response between donors could not be excluded, the difference in force amplification was found to be up to 100-fold (A_F mean values).

Taken together, tissue tension and contraction were found to strongly depend on the cell's ability to deposit a dense fibrillar collagen network rather than on the ability of cells to generate high cell forces. The linear correlation also points to a gradual process according to a previously proposed "slip and ratchet" model [159].

4.1.4 Relevance of collagen for tissue tension during wound healing

As mentioned before, an injury initially results in hematoma formation. The hematoma is assumed to be very soft [165,166], but detailed information about mechanical and structural properties are missing. This, however, would be of high relevance as it provides information about the environment in which tissue formation and would healing is initiated. Therefore, human fracture hematoma harvested either from proximal humerus or closed acetabulum fractures* were characterized mechanically and via histology (Figure 4-9).

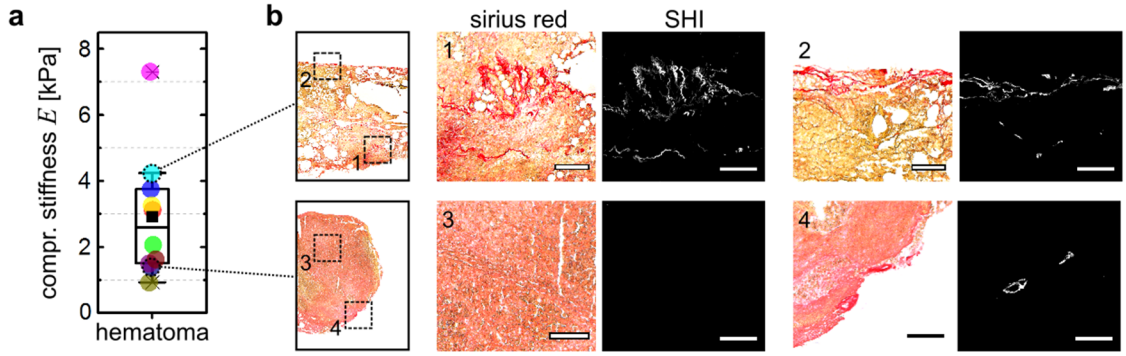

Figure 4-9: characterization of human fracture hematoma. (a) Mechanical characterization by mono-axial compression testing of in total 10 different hematoma samples. (b) Histological evaluation by Sirius Red staining and SHI. Scale bar 200µm. Figure modified from [163].

The hematoma samples exhibited a stiffness of 2.9±1.9 kPa and histological evaluation revealed that the samples were rich in soft ECM components but only with sporadically occurring collagen fibers.

This indicates that tissue formation by invading cells and thus contraction takes place in a soft and mostly collagen-free environment. Consequently, a sufficiently soft environment potentially does not require the aid of collagen fibers to be contracted. To test this, the biomaterial solid collagen content was modified (A - 1.1%, B - 1.5%, C - 3.0%) to obtain 3 scaffolds that vary in stiffness but share the same principle architecture as validated by SEM and structural analysis (Figure 4-10, **a-c**). The biomaterial varied in their stiffness, particularly in axial direction, ranging from 1.7kPa (scaffold A) up to 34kPa (scaffold C) next to the existing material (4.1kPa, scaffold B) which covers a range of stiffness from the measured hematoma up to mature granulation tissue (Figure 4-10,

* Hematoma samples were provided by Simon Reinke, BCRT cell harvesting core unit. Patients gave their written consent. Mechanical tests were performed by Evi Lippens and Dag Wulsten, Julius Wolff Institute.

d) [167]. Cells were equally forming a highly aligned cell-ECM network after 14 days of culture (Figure 4-10, **e**).

For scaffold contraction, the analysis was restricted to axial direction since alignment of cells and ECM was along this axis and scaffold stiffness varied mostly in this dimension. It was observed that scaffold contraction gradually decreased with increasing scaffold stiffness until only very little deformation was recorded for scaffold C (34kPa) (Figure 4-10, **f**). Furthermore, samples were also cultured either with or without ascorbic acid supplementation. Without supplementation and in line with the findings already described before (Figure 4-4), no contraction was observed for scaffolds B and C. Strikingly, a pronounced contraction was visible in the softest scaffold (scaffold A) after 14 days even without the presence of collagen fibers (Figure 4-10, **f and g**). Since the stiffness was also in the range of hematoma stiffness, it can be assumed that collagen fibers are dispensable for initial contraction and tensioning at early stages of healing but become essential to maintain this process when the hematoma matures and becomes stiffer. Furthermore, without providing additional stimuli, the process seems to reach limitations in ranges of mature granulation tissue (20-30kPa).

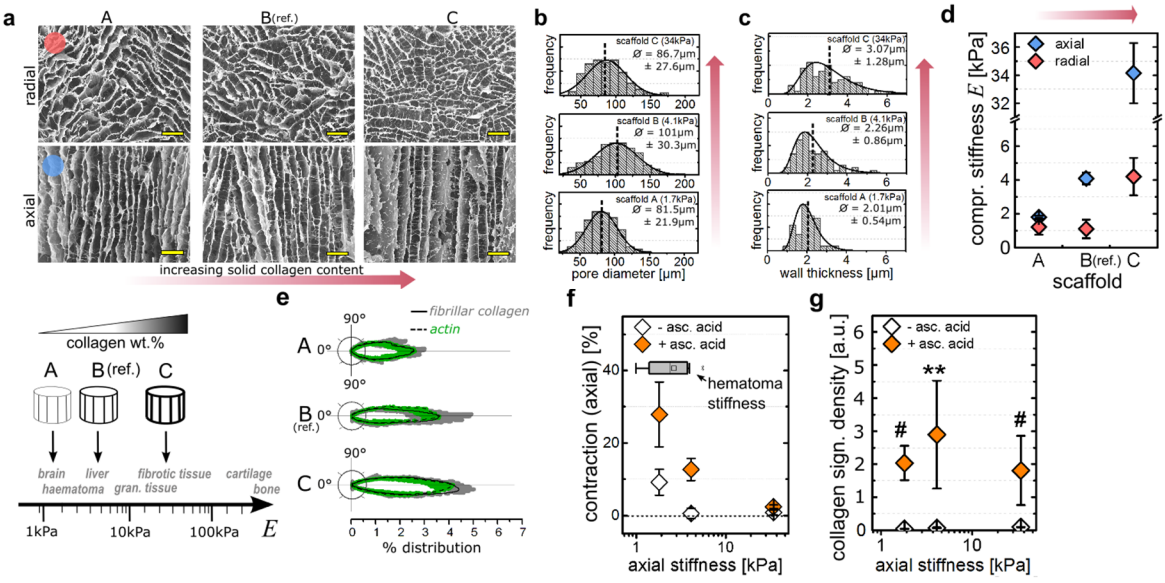

Figure 4-10: tissue straining depends on scaffold stiffness. ***(a)*** *SEM images of scaffolds A, B and C which differ in their solid collagen content. Scale bar 250µm* ***(b)*** *Distribution of pore diameter.* ***(c)*** *Distribution of wall thickness.* ***(d)*** *Compressive stiffness of scaffolds A, B and C both for axial and radial directions.* ***(e)*** *Orientation analysis of cellular actin signal (green) and collagen network (grey) after 14 days of culture.* ***(f)*** *Quantification of axial contraction after 14 days of culture. Box plot indicating the range of hematoma stiffness.* ***(g)*** *Fibrillar collagen density after 14 days of culture. Figure modified from* [163].

4.1.5 Cellular forces are permanently stored inside pre-tensioned collagen fibers

The data presented so far could demonstrate a strong dependency of macroscopic contraction and tensioning on collagen fiber deposition. This implies a gradual conversion and transfer of cell forces into fiber elements which leads to the described multiplication. Consequently, the tensional state of the tissue is strongly depending on cellular forces at early stages but should be mostly independent at later stages once a dense collagen network has formed. To test this, a decellularization protocol was established. Decellularization is a widely applied method to remove cellular components and a wide variety of protocols is available for 2D and 3D applications [149,150]. An optimized protocol was used based on the consecutive application of a mixture of 1% Triton X-100/0.1% SDS and DNase (Figure 4-11). While decellularization resulted in an efficient removal of cellular components (proteins and DNA) and soft tissue proteins such as fibronectin, no or little influence of the procedure was observed on collagen network density and structural integrity (fiber orientation and anisotropy).

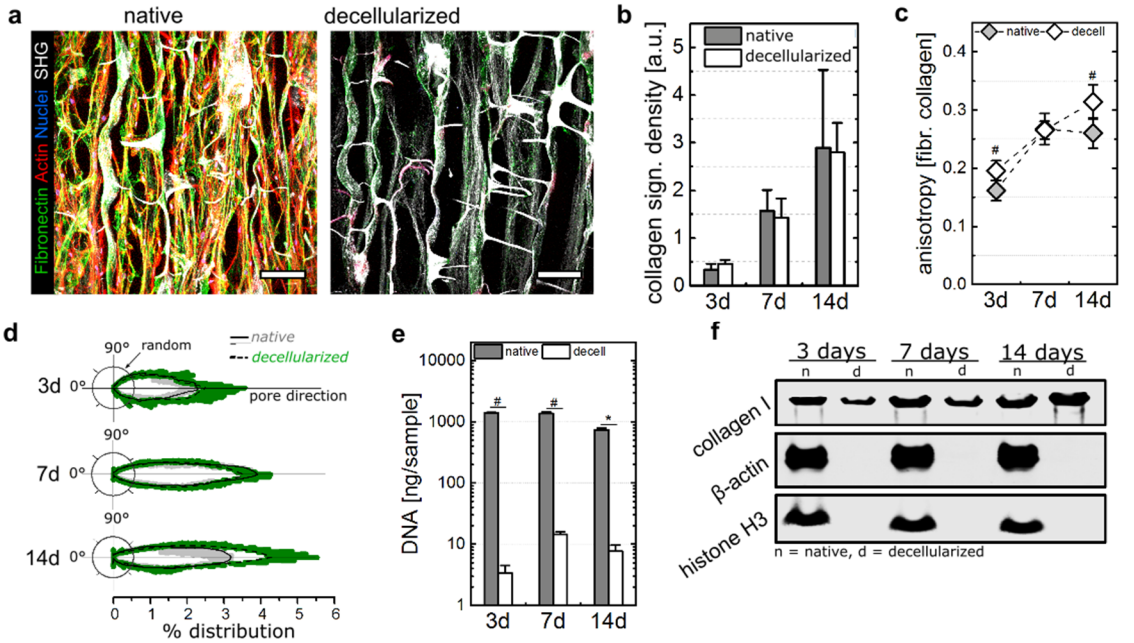

Figure 4-11: fibrillar collgen is preserved during tissue decellularization. ***(a)*** *Confocal images of samples before (native) and after decellularization stained for fibronectin (green), actin (red) and cell nuclei (blue). Collagen signal generated from SHG. Scale bar 100µm.* ***(b)*** *Quantification of fibrillar collagen density before and after decellularization.* ***(c)*** *Quantification of collagen fiber anisotropy before and after decellularization.* ***(d)*** *Collagen fiber distribution before and after decellularization.* ***(e)*** *Quantification of DNA content per sample before and after decellularization.* ***(f)*** *Western blotting of whole tissue lysates before and after decellularization detected for collagen I, β-actin and histone H3. Figure reproduced from* [163].

The data presented in Figure 4-11 indicated that most of cellular components were removed by the applied decellularization protocol, while mostly collagenous ECM proteins were preserved. To further validate this, mass spectrometry was performed* (Figure 4-12, **a and b**). With a strong abundance (>80%) of collagenous proteins (dominantly collagens type VI and I) amongst all detected peptides, the data obtained by histology could be verified.

Following decellularization, the residual contraction was quantified (Figure 4-12, **c**). While for early time points (3 and 7 days) no residual contraction was visible, a remaining contraction could be detected in samples cultured for 14 days. When transforming contraction values into scaffold strain as done before, it could be shown that the residual force was higher in axial direction which was also the direction of collagen fibers (Figure 4-12, **d**). This clearly supports the initial hypothesis that at early stages the tensional state is highly depending on active cell forces while through collagen deposition cellular contraction becomes dispensable for tissue tension.

To finally prove that indeed the collagen fiber network was responsible for residual contraction post decellularization, samples were treated with an optimized concentration of crude collagenase I that completely degraded the cell-derived network but without impairment of the scaffolds' mechanical properties (Figure 4-12, **e and f**). Treatment induced a complete release of the scaffold to its original shape which provides a first *in vitro* evidence that indeed cellular forces are stored inside a tensioned collagen network.

* MS measurements were carried out in collaboration with Oliver Klein and Grit Nebrich, BCRT core unit „tissue typing".

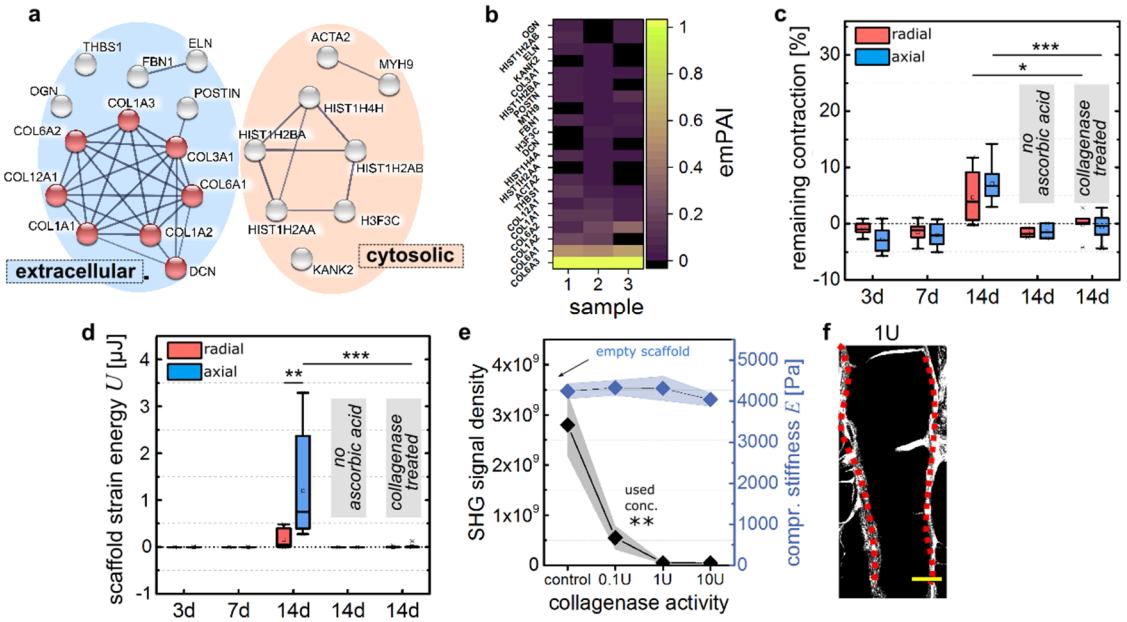

Figure 4-12: removal of collagen release tissue tensional state. ***(a)*** *Functional enrichment analysis of proteins detected by mass spectrometry. Red spheres highlight collagen trimer gene ontology term (GO: 0005581).* ***(b)*** *Heat map of emPAI (exponentially modified abundance index) for detected peptides.* ***(c)*** *Quantification of remaining contraction after decellularization.* ***(d)*** *Calculation of residual scaffold strain energy after decellularization.* ***(e)*** *Analysis of collagen density of cultured samples and macroscopic compressive stiffness of empty scaffolds treated with different concentrations of crude collagenase I for 24H at 37°C.* ***(f)*** *representative SHG image of 14d grown and decellularized samples treated with 1U of crude collagenase for 24h. Scale bar 50µm. Figure modified from* [163].

4.1.6 Collagen network tension facilitates directional migration of stem cells

In the previous section it was shown that collagen fibers are an essential component for generating and maintaining intra-tissue tension. As *in vivo* bone healing scenario is characterized by consecutive processes, the deposition and tensioning process resembles an early event and potentially precedes secondary processes such as mineralization during bone regeneration [19]. From this *in vivo* observation it was hypothesized that tensioned collagen fibers might exhibit beneficial effects, e.g. for the consecutive invasion of progenitor cells. This was assessed by analyzing the directional migration of primary human MSCs into decellularized (14d culture time point) samples from a confluent monolayer (see also Figure 3-1). Empty scaffolds served as a reference control. It could be observed that the directional migration into the material was significantly enhanced with the presence of tensioned collagen fibers (Figure 4-13). However, this does not necessarily imply actual faster migration. It rather could be the result of enhanced anisotropy of decellularized ECM compared to the empty scaffold that leads to a more directional movement of

cells (“contact guidance”). This is supported by histological evaluation of cells adhering to cell-derived collagen bundles that exhibit a highly aligned, spindle-like shape (Figure 4-13, **b**).

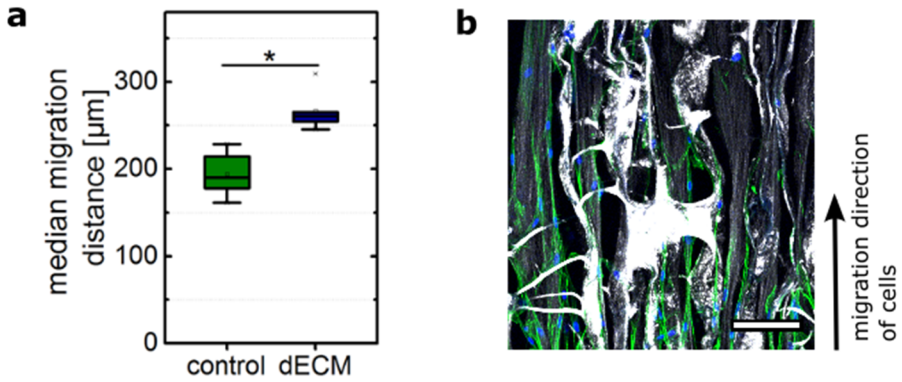

Figure 4-13: tensioned collagen fibrils enhance directional migration. ***(a)*** *Quantification of median migration distance of primary hMSC invading the material from a confluent mono-layer.* ***(b)*** *Confocal image of cells migrating on dECM (decellularized ECM) into the scaffold. Cellular components were stained in green (actin) and blue (nuclei). Fibrillar collagen shown in white recorded by SHI. Scale bar 100µm.*

In summary, it could be shown that collagen fibers resemble an essential element for the generation and maintenance of tissue tension during wound healing that has a guiding function for successive processes such as consecutive cell invasion.

4.2 Determining the effect of BMP stimulation on tissue formation

Until here the process of tissue formation has been studied under "neutral" conditions lacking additional mechanical or biochemical triggers. Since it was hypothesized that BMPs affect early tissue formation events, e.g. through secretion of collagens and proteases (see Figure 1-8), tissue formation was observed under stimulation of BMP2.

4.2.1 Influence of BMP2 stimulation on tissue formation

The responsiveness of primary fibroblasts seeded onto macroporous collagen scaffolds to BMP stimulation was validated by gene expression analysis (Figure 4-14). For both, Id1 and Id2, an induction shortly after stimulation (6h) was observed. While in particular for Id2 the responsiveness declined over time, after 14 days of culture a strong induction was observed that, by its fold change, even exceeded initial stimulation. This is even more remarkable as medium exchange with fresh BMP2 was performed every 3-4 days of culture and consequently for the latest analyzed time point (14 days) supplementation with new BMP2 was performed 4 days before analysis during which a significant loss in activity can be expected.

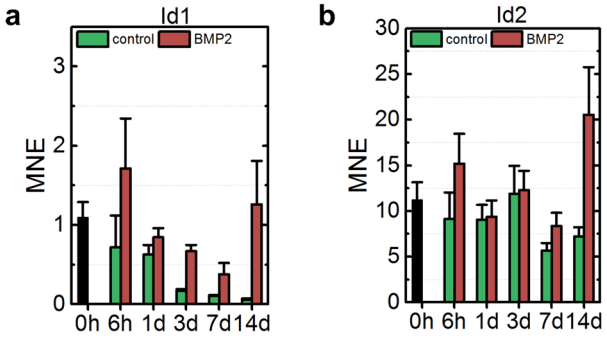

*Figure 4-14: primary fibroblasts show BMP responsiveness in 3D. Gene expression analysis (here presented as mean normalized expression, MNE) of Id1 (**a**) and Id2 (**b**) BMP target genes at various time points after stimulation.*

After validation of an overall responsiveness of hdFs to BMP2 stimulation, tissue contraction was monitored (Figure 4-15). Strikingly, a significant increase in scaffold volume contraction of BMP2-stimulated compared control samples was observed for all analyzed time points (Figure 4-15, **a**). Since it was already demonstrated that the amount of contraction depends on fibrillar collagen deposition, fiber network density was quantified inside scaffold pores after 1,2 and 3 weeks of culture. While at day 7 the density was even lower for BMP2-stimulated compared to control samples, collagen density was found to

be increased after 14 days (Figure 4-15, **b and c**). After 3 weeks, collagen density was comparable for both groups. While this shows that tissue densification was still occurring in control samples between 2 and 3 weeks, the small differences between the BMP2-stimulated samples at these two time points indicated that they might have reached an equilibrium. This is further emphasized by correlation of collagen density and contraction in accordance with data shown before (Figure 4-8, reproduced as grey symbols and line in Figure 4-15, **d**). Whereas control samples exhibited a linear trend over time (green line), BMP2-treated samples showed a pronounced contraction relative to the observed collagen density at day 7. Until day 14, especially collagen density increases tremendously with further contraction but with only very limited changes from day 14 to day 21 in both parameters (Figure 4-15, **d**).

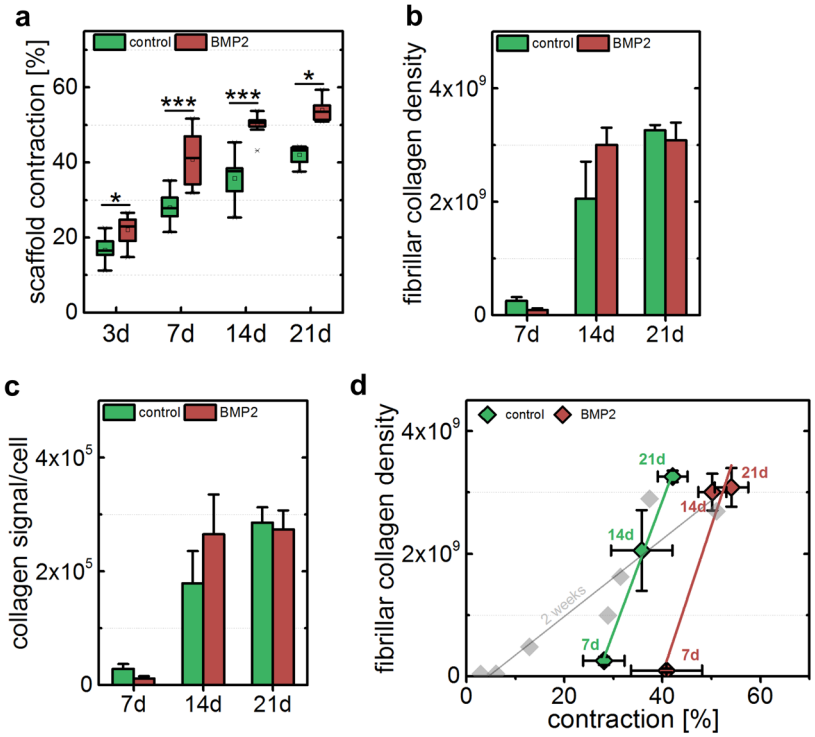

*Figure 4-15: BMP stimulation enhances tissue contraction. **(a)** Quantification of scaffold contraction under BMP2 stimulation. **(b)** Quantification of fibrillar collagen density. **(c)** Quantification of fibrillar collagen density per cell. **(d)** Correlation of collagen density and contraction. Grey boxes indicate data points after 14 days of culture for different donors and correlation from Figure 4-7.*

Taken together, BMP2 stimulation affected both contraction and collagen density in a dynamic, time-dependent manner. Since collagen density was enhanced after 2, but comparable after 3 weeks of culture, tissue formations seems to be facilitated due to BMP2 stimulation. The fact that contraction was enhanced at lower collagen density after 1 week might be explained by a potential regulation of cellular forces in line with recent *in vivo* observations [22].

4.2.2 BMP2 stimulation induces ECM remodeling via MMPs

To further characterize the effect of BMP stimulation on the mechanical properties of the growing tissue, mono-axial compression testing was performed after 1, 2 and 3 weeks of culture to characterize the compressive stiffness. Since compression was performed in the direction of the scaffold pores that compresses the sample, it cannot be expected that newly formed collagen mainly contributes by its load bearing capacity (= tensile strength) but indirectly by the occupied space and occurring deformation during compression. It was therefore expected that the stiffness depends mostly on the cross-sectional area (=densification through contraction) but also on ECM deposition (=stiffening due to material deposition). Indeed, a gradual stiffening process was observed for control samples that featured a linear correlation over time both with scaffold contraction and collagen density (Figure 4-16). Furthermore a significantly enhanced value for tissue stiffness upon BMP2 stimulation was recorded after 2 weeks. Correlation of Young's Modulus both with contraction and collagen density demonstrated a linear dependency (Figure 4-16, **b and c**). Most surprisingly, macroscopic stiffness was significantly reduced at 3 weeks compared to 2 week time point BMP2-stimulated samples. This resulted in a "breakout" of the BMP2-stimulated 3 week time point from the linear trend, particular for correlation of Young's Modulus and collagen density.

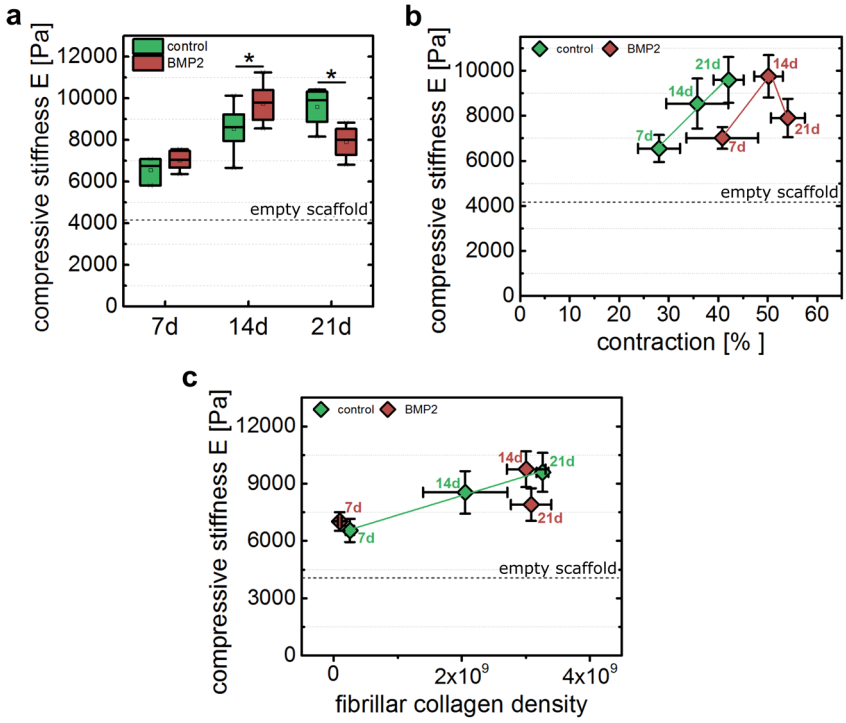

Figure 4-16: BMP2 stimulation modulates tissue stiffening. ***(a)*** *Mechanical characterization of tissue formation by mono-axial compression testing over time.* ***(b)*** *Correlation of calculated values of compressive stiffness and scaffold contraction.* ***(c)*** *Correlation of calculated values for compressive stiffness and collagen density.*

Although collagen density was stable for BMP2-treated samples between 2 and 3 weeks, a macroscopic softening indicated the induction of remodeling processes after 2 weeks. Key proteins involved in ECM remodeling and reported to be influenced by BMP stimulation are matrix metalloproteinases (see also Figure 1-8). Initially, the gene expression profile of 2 distinct collagenases was validated (Figure 4-17, **a and b**). While no differences were detected in the expression of MMP1 at the differet time points, MMP13 revealed a dynamic increase in expression over time as a consequence of BMP2 stimulation. Since MMPs are expressed and secreted as latent pro-peptides that require enzymatic cleavage, the activity of MMPs was further analyzed by zymography of conditioned medium harvested after 14 days (Figure 4-17, **c**). In concert with expression data, an increase in metalloproteinase activity could be detected. However, it could not be validated whether MMP13 itself exhibited an increased activity or if other MMPs became activated. In summary, it could be demonstrated that BMP stimulation facilitates tissue formation processes of collagen deposition and contraction and in addition, when tissues matured to a distinct density, BMP induced a dynamic remodeling process that was associated with macroscopic softening.

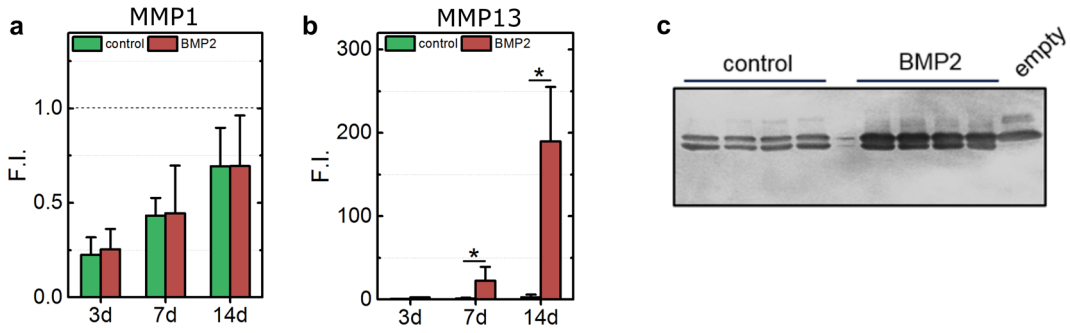

Figure 4-17: BMP2 stimulation affects MMP expression and activity. ***(a, b)*** *Gene expression levels of MMP1 and MMP13. Values are normalized to samples harvested prior to BMP2 stimulation* ***(c)*** *Zymographic analysis of conditioned media harvested after 2 weeks of culture.*

4.2.3 ECM formed under BMP2 stimulation affects stem cell differentiation

In the previous chapters, a beneficial effect of BMP2 stimulation on tissue formation, particularly by modulating collagen fibril-controlled contraction and ECM turnover was found. How this modulation might affect cellular behavior of invading cells was unclear until this point. It was therefore hypothesized that BMPs potentially affect differentiation of stem cells in an indirect manner through the instructive features of the extracellular matrix deposited at early stages of healing. In order to do so, "naïve" stem cells need to be seeded into the cell-derived extracellular matrix after removal of tissue forming cells by decellularization. In section 4.1.5 a protocol was shown that efficiently removes all cellular and soft ECM components. Since it was unknown if the cell-instructive features were of structural (fiber organization/alignment), mechanical (tension, contractile state) or biochemical (ECM composition) origin or a combination of all, the decellularization protocol was further optimized. A perfusion system was developed to allow simultaneous and reproducible decellularization of multiple samples (Figure 4-18). The active perfusion of samples in contrast to gentle agitation further enabled a reduction of incubation time and thus a more gentle procedure.

The optimized protocol was initially validated by (immuno)fluorescence histology for key cellular components representing the cytosol (actin cytoskeleton) and nucleus (histone and DNA) in combination with confocal imaging. It was clearly visible that the optimized protocol led to an efficient removal of actin and DNA but not of histone nuclear proteins that were found to be distributed across the ECM and even nuclear structure partially preserved (Figure 4-18, **b**). However, fibronectin soft ECM was not affected

either in structure or signal intensity indicating the improved retention of other ECM components than fibrillar collagen.

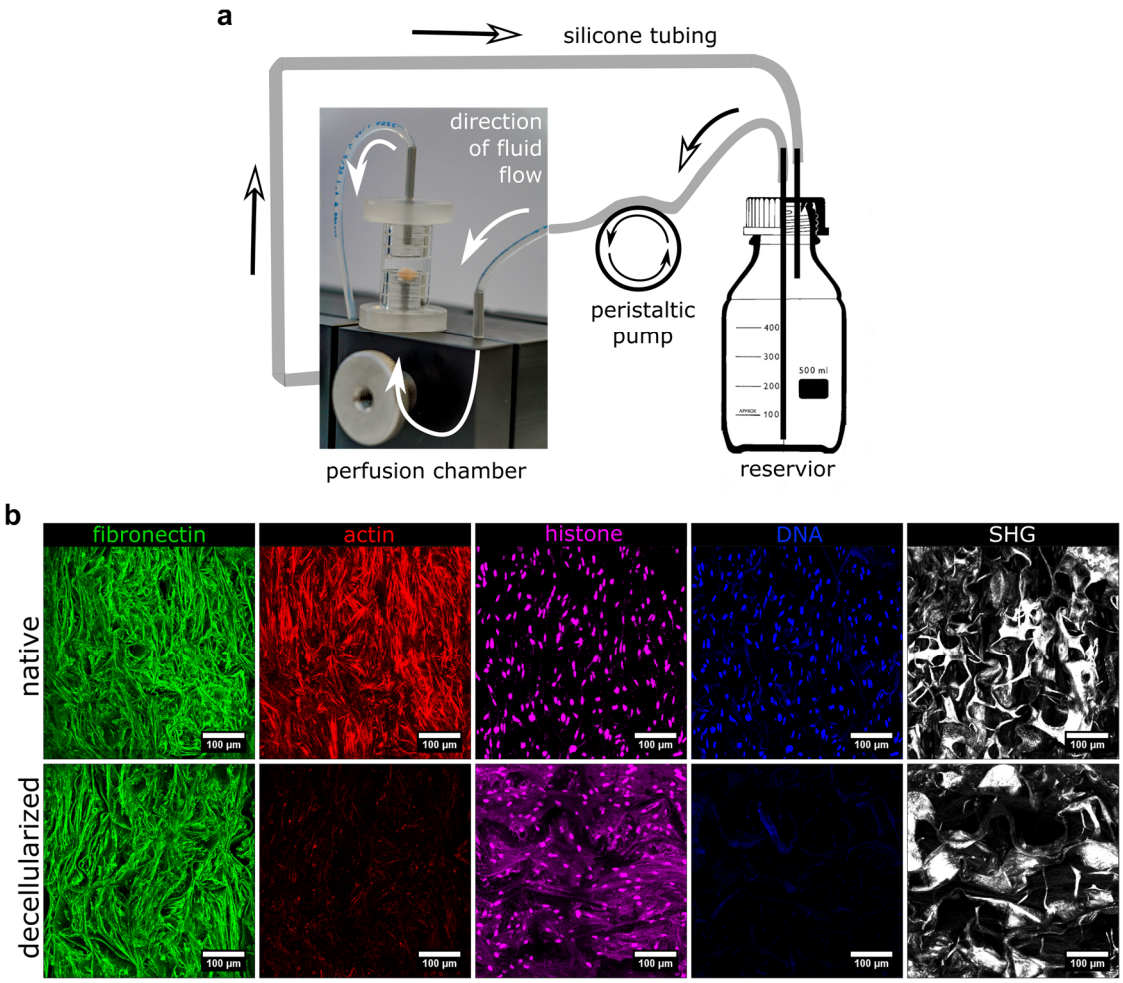

Figure 4-18: Perfusion system for biomaterial & tissue decellularization. (a) A perfusion chamber that holds the sample is connected to a reservoir via a peristaltic pump and silicone tubing. Individual reactors can be combined in a series connection mode. (b) Confocal images of scaffold cultured for 7 days to allow ECM formation either before (native) or after (decellularized) perfusion-based decellularization. Samples were stained for fibronectin (green), actin (red), histone (magenta), DNA (blue) and fibrillar collagen was visualized by SHG. Scale bar 100µm.

The biochemical composition was further assessed by mass spectrometry (Figure 4-19). Comparison of the protein interaction maps of the existing and the optimized perfusion-based protocol could further show that the diversity of retained ECM proteins was increased, particularly soft ECM components such as fibrillin, fibronectin and proteoglycans (e.g. biglycan & decorin). However, similar observations were made for cytosolic proteins where a plethora of different proteins could be detected. Although the pure detection does not resemble a quantitative measure of actual protein content within the sample, it clearly illustrates the strong association of cytosolic and extracellular proteins.

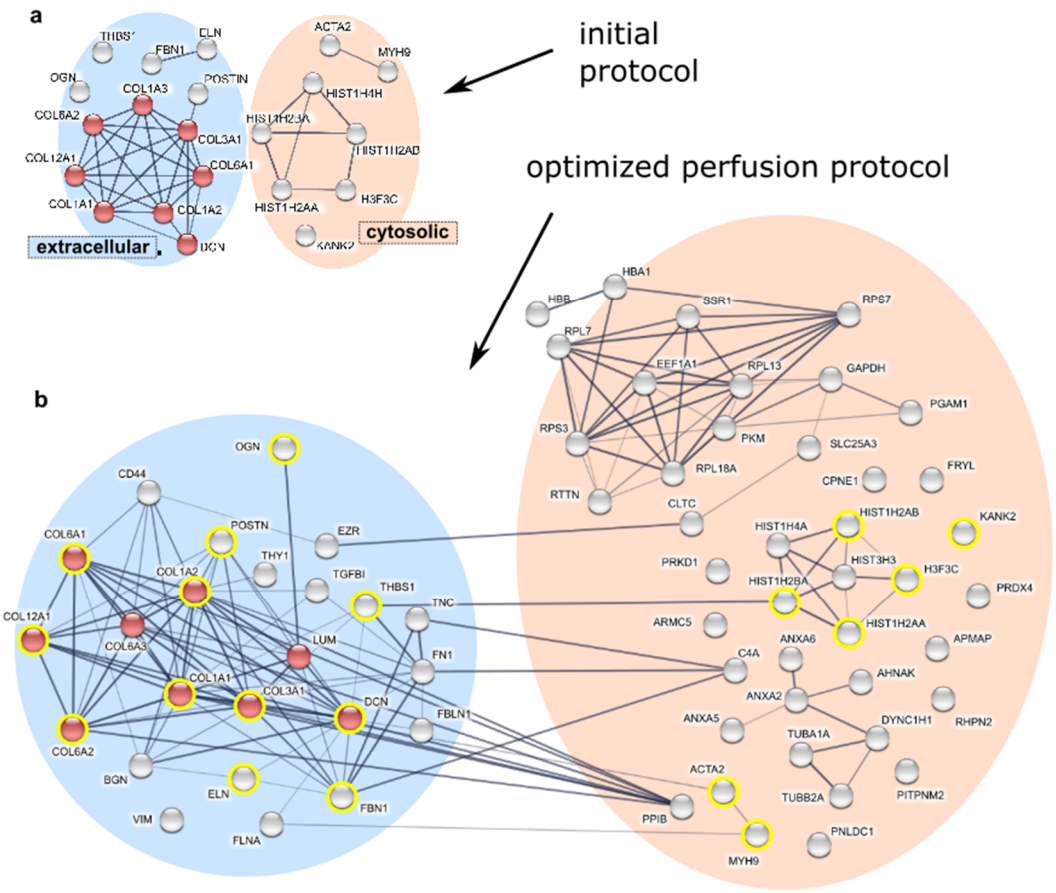

Figure 4-19: Comparison of decellularization protocols by MS. ***(a)*** *Protein interaction map obtained by agitation based decellularization over several days. Reproduced from* [163]. ***(b)*** *Protein interaction map obtained from perfusion-based gentle decellularization. Cytosolic (orange) and extracellular (blue) proteins are grouped into separate spheres. Yellow circles indicate proteins detected already in the initial procedure.*

Re-cellularization was initially tested both with hMSCs and hdFs by active perfusion of decellularized scaffolds obtained by the old protocol of agitation over several days in 1% Triton X-100/0.1% SDS. Different concentrations of the cell suspension as well as different time points of decellularization were tested (Figure 4-20). However, non-uniform cell distribution was observed with a strong dependency on the amount and concentration of cells as well as on the density of the dECM itself. Only for 3 days, a rather homogenous cell distribution could be achieved. It was assumed that the cell-derived ECM acts as a strainer that retains cells. This leads to a blocking of pores as retained cells further reduce the space available for perfusion. However, a reliable and reproducible repopulation independent of dECM density could not be achieved. A homogeneous density, however, is a prerequisite for differentiation of stem cells as differences in cell density and cell-cell contacts influence differentiation [168]. Since differences in tissue density (collagen/contraction) were observed between unstimulated and BMP2-stimulated

samples, aggregation of cells inside the dECM might vary after re-seeding for the two conditions. Consequently, the direct influence of a dECM on cellular function via re-seeding of decellularized scaffolds could not be analyzed.

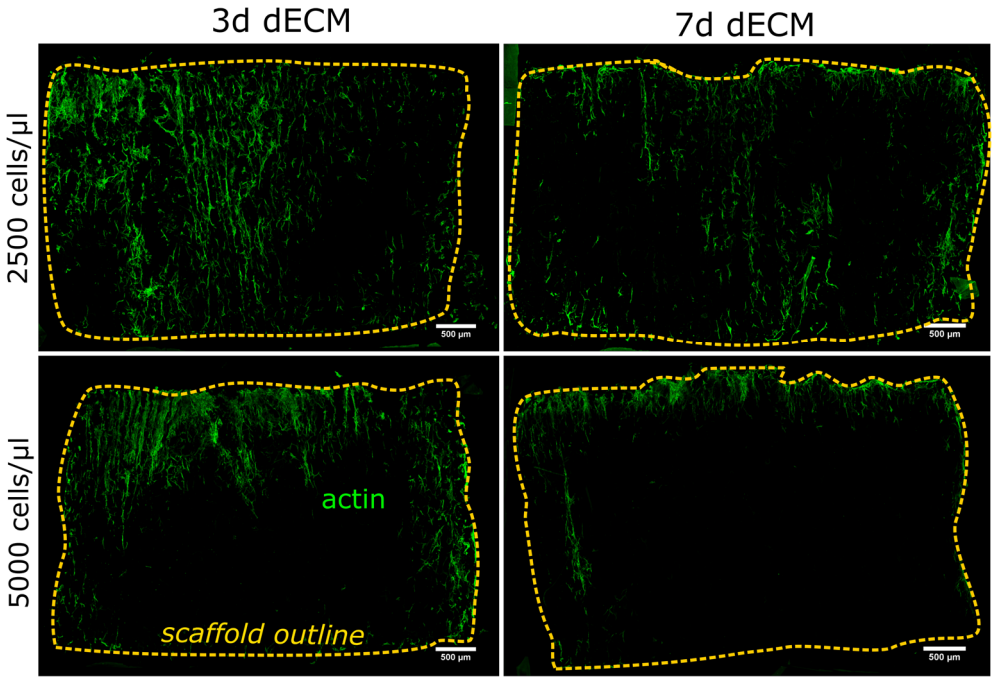

Figure 4-20: Re-cellularization by active perfusion with a concentrated cell suspension. Confocal images of fibroblasts re-seeded into scaffolds by active perfusion at a concentration of 2500 or 5000 cells/µl (500 000 cells in total). Decellularized scaffolds were obtained by detergent decellularization after 3 or 7 days of culture prior to re-seeding. Cells were stained for actin (green). Scaffold outline is indicated as yellow dashed line. Scale bar 500µm.

Since a direct assessment of the cellular response towards ECM grown inside the scaffolds was not possible, it was decided to separate the respective factors (structural, tensional, biochemical) which might influence cellular behavior. As it was reported previously, decellularized ECMs can be used to generate a hydrogel after pepsin digestion of the decellularized ECM [169,170]. Doing so, the distinct ECM peptide signature can be harvested while eliminating tensional and structural features. The protocol was adopted by digesting decellularized and freeze-dried matrices grown for 2 weeks in order to harvest a dECM peptide signature. However, the amount of protein that can be obtained by such a pure *in vitro* approach was found to be insufficient to create a hydrogel without additional collagen (data not shown). Hence, the dECM digest was used to coat tissue culture plastic at a concentration of 50µg/cm² and primary hMSCs were seeded into coated wells and subjected to osteogenic differentiation using osteogenic differentiation medium [171,172]. The degree of matrix mineralization was verified by Alizarin Red

staining after 2 weeks of treatment. As a coating control, one group was subjected to a pure collagen coating (rat tail collagen solution) at the same protein concentration.

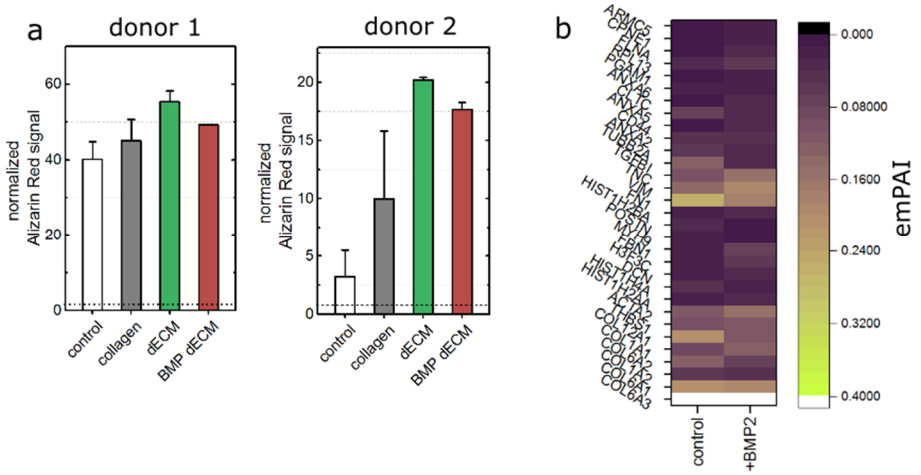

Figure 4-21: Decellularized ECM influences osteogenic differentiation of stem cells. ***(a)*** *normalized alizarin red signal after 2 weeks of osteogenic differentiation of 2 primary hMSC donors on tissue culture plastic (control), collagen-coated (collagen) or decellularized ECM-coated plates (dECM – grown for 14d without BMP2, BMP dECM – grown for 14d under 500ng/ml BMP2). Dashed line indicates signal obtained with cultivation in normal expansion medium.* ***(b)*** *Heat map of relative abundance (emPAI) of proteins detected by MS after decellularization.*

The quantification revealed that the two analyzed donors were able to produce a mineralized matrix and that the collagen coating exhibited a beneficial effect relative to pure osteogenic medium (Figure 4-21, **a**).

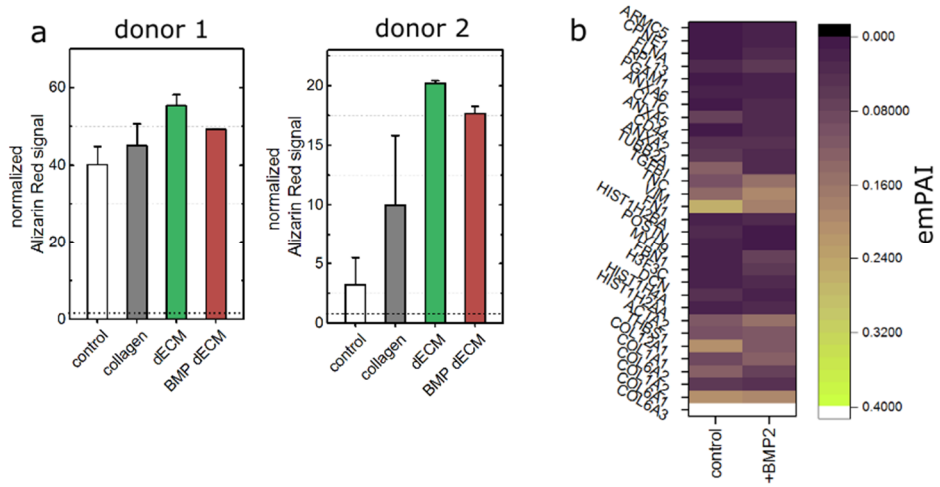

Intriguingly, using decellularized ECM for coating further increased this beneficial effect compared to collagen-coated groups. Most strikingly, a reduction in the Alizarin Red signal could be observed for osteogenic differentiation performed on matrices grown under BMP2 stimulation. Although the intensity of obtained signals varied between the

two analyzed donors, indicating that cell density and donor-specific potential greatly influence the outcome, the trend was constant. Since the digestion of decellularized ECM deletes any structural and mechanical information, the factor that influence cell behavior during differentiation was expected to be encoded in the protein signature. Indications that BMP2 stimulation during ECM formation leads to differences in the ECM composition could be obtained from further MS analysis where differences in the relative abundance of proteins, e.g. fibronectin, collagen type XII, tenascin-C, could be detected (Figure 4-21, **b**). From this observation it can be concluded that not only a decellularized ECM can be used for substrate coating influencing cellular behavior, but that the BMP stimulus that the cells received during ECM formation seemed also to be imprinted into the biochemical composition of the extracellular matrix.

Taken together, it was shown that BMP stimulation influences fibroblast behavior during ECM formation in a 3D environment by modulating tissue contraction and ECM degradation with consequences for its mechanical properties. The ECM formed by fibroblasts in vitro was further demonstrated to influence osteogenic differentiation of hMSC in 2D indicating that in addition to altered mechanical properties also the biochemical composition (e.g. ECM protein abundance, growth factor secretion) is changed. Consequently, the results demonstrate that BMP stimulation potentially also influences collagen deposition and tissue tensioning and further modulates cell behavior through distinct cues that reside encoded inside the extracellular matrix.

4.3 Analyzing the impact of extracellular mechanical cues on BMP signaling

The data obtained so far demonstrated that BMPs potentially influence early tissue formation processes independent of osteogenic differentiation. Further the research performed in this thesis showed that the extracellular matrix, by its biochemical composition, is capable to modulate the osteogenic differentiation potential of stem cells. A key question that remained unanswered was how alterations in the mechanical properties due to BMP stimulation in turn might tune the cellular response to BMPs. In other words: Does BMP stimulation lead to the production of a matrix that is compliant to BMP signaling? As repopulation of decellularized scaffolds was found to be impeded by a low reproducibility, a direct investigation on BMP-derived matrices was not possible. Therefore, it was decided realize mechanical environments that represent the ECM forming with and without BMP2 via 2D polyacrylamide gels and furthermore by 3D collagen scaffolds with distinct mechanical stiffness.

4.3.1 Synthetic niche to study BMP signaling

A key intrinsic feature that was reported earlier to affect cellular behavior is the substrate stiffness [3]. Individual stiffness environments can be simulated using synthetic 2D hydrogels such as functionalized polyacrylamide (PAA) [173], where a stiffness-dependent BMP responsiveness has been demonstrated previously [49].

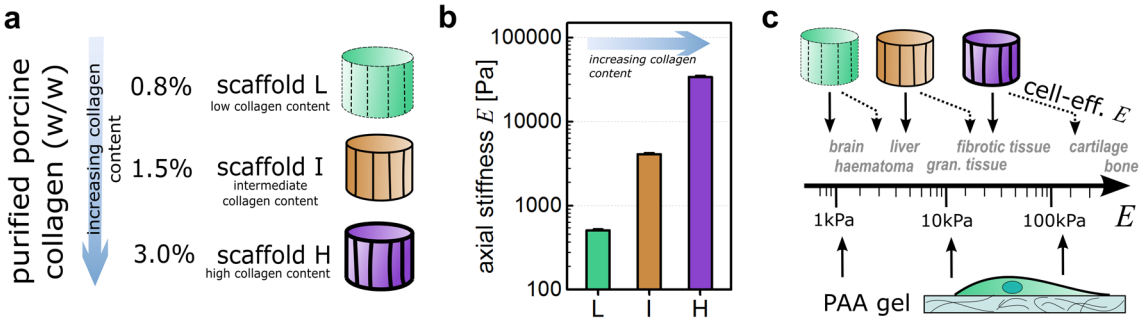

Figure 4-22: Natural and synthetic biomaterials varying in stiffness. Macroporous collagen scaffolds were produced with varying solid content (0.8% (w/v), low; 1.5% (w/v), intermediate; 3.0% (w/v), high) to obtain differences in macroscopic stiffness. 2D synthetic polyacrylamide gels of different stiffness were fabricated by varying the monomeric acrylamide content. Right: Stiffness regimes of various tissues. Dashed arrows indicate cell-effective stiffness of collagen scaffolds.

In order to simulate environments varying in stiffness in 3D, collagen scaffolds were fabricated from collagen dispersions of different solid content* (Figure 4-22). This resulted in three scaffolds that varied in macroscopic stiffness from 0.5kPa (0.8 wt.% collagen) to 4.1kPa (1.5 wt.% collagen) and 34kPa (3.0 wt.% collagen). In order to estimate the cell-effective stiffness of these biomaterials, a factor of 6.4 was applied based on a recently published approach using AFM measurements and *in silico* simulations [174]. Corresponding PAA hydrogels were fabricated to cover a range from 1.7 up to 160 kPa.

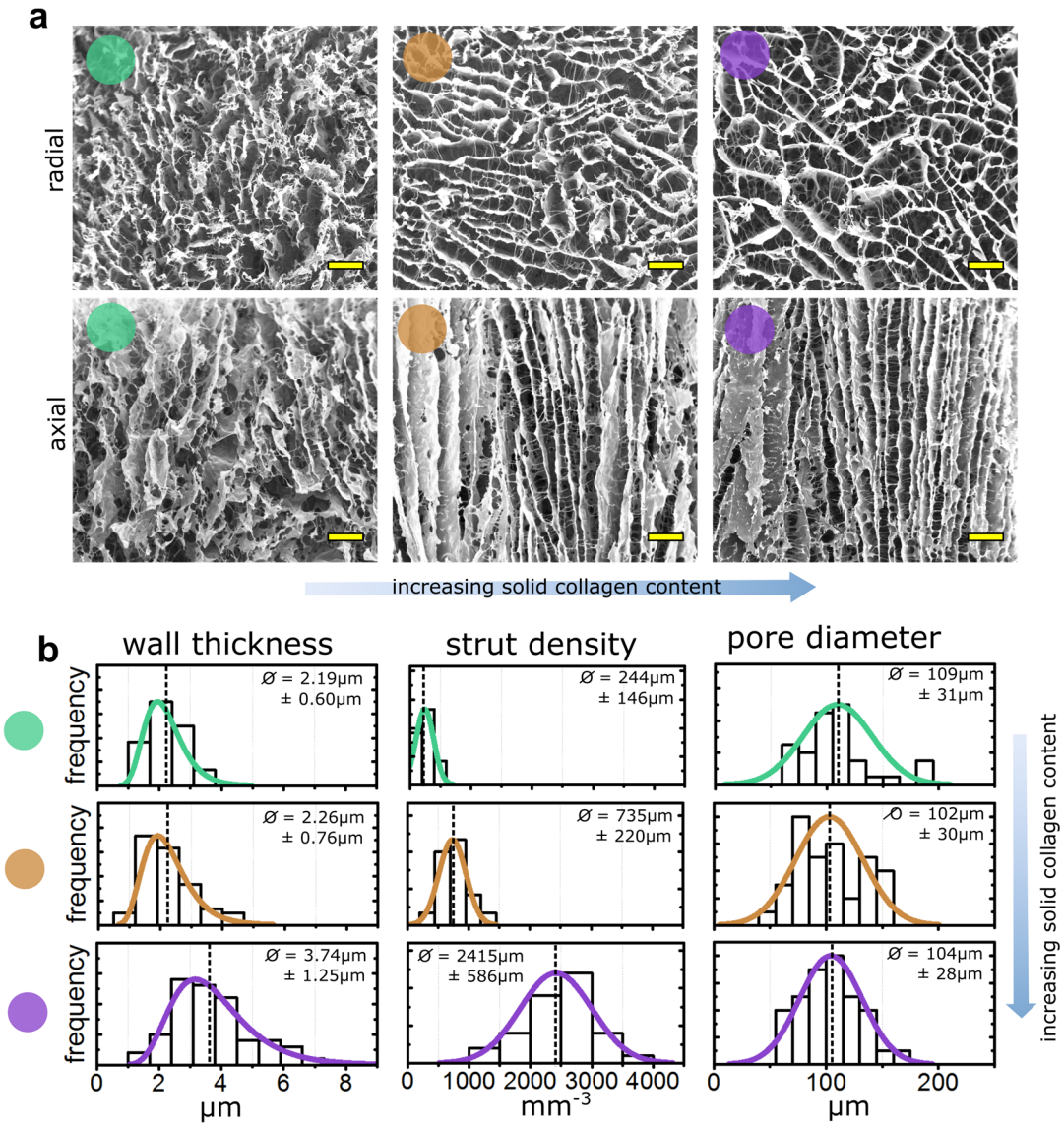

Figure 4-23: Collagen scaffold architecture. ***(a)*** *SEM images of collagen scaffolds with low (green sphere, 0.8%), intermediate (ocher, 1.5%) and high (purple, 3.0%) solid collagen content.* ***(b)*** *Quantification of wall thickness (left), strut density (middle) and pore diameter (right) presented as histograms. Colored lines represent log-normal (wall thickness) and normal distribution fit (strut density and pore diameter). Colored spheres and distribution curves indicate the corresponding solid collagen content.*

* Matricel GmbH, Herzogenrath, Germany

The structure of the macroporous collagen scaffolds was assessed by SEM and SHI (Figure 4-23, **a**). All three scaffolds showed a similar architecture of aligned, channel-like pores as shown before. Yet, the softest scaffold exhibited a higher degree of wall discontinuity and waviness of the collagen walls in both direction that partially deteriorates the anisotropic character of the material. Further characterization of several architectural parameters revealed a gradual increase in wall thickness and wall-interconnecting strut density with scaffold stiffness/solid collagen content. In contrast, the pore diameter remained constant (Figure 4-23**, b**).

4.3.2 Biomaterial stiffness affects BMP signaling response

For cell culture experiments, it was decided to work with human fetal osteoblasts [175] (hFOBs) as a model system that was reported to respond to BMP2 stimulation [23]. Cells seeded either onto 2D PAA substrates or 3D collagen scaffolds were stimulated with BMP2 (5nM or 135ng/ml) and Smad phosphorylation was analyzed after 60 minutes of stimulation (Figure 4-24).

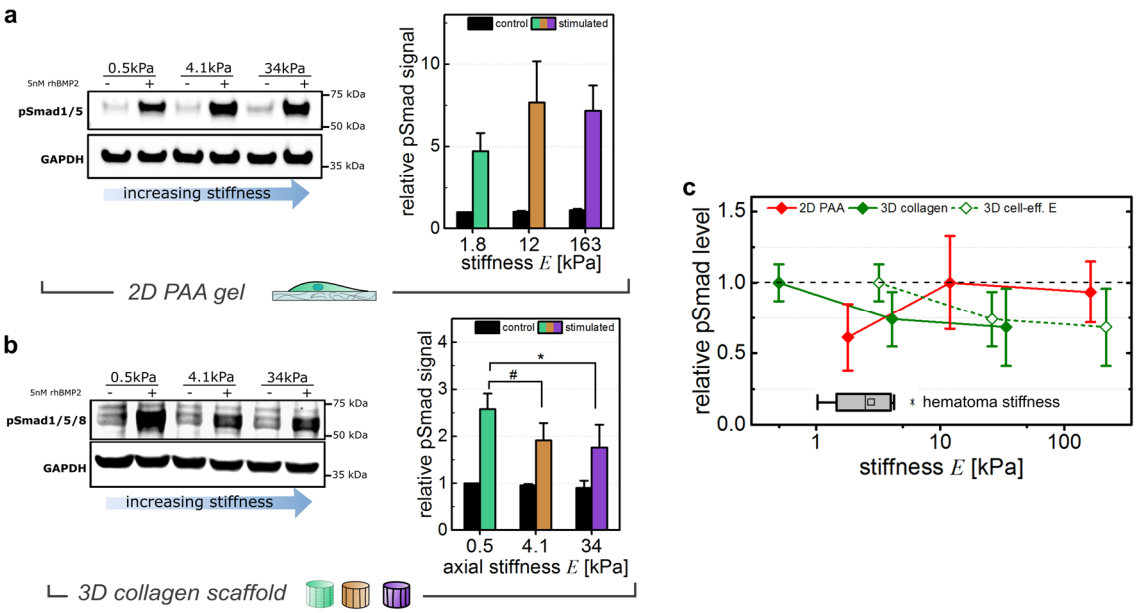

Figure 4-24: cells differently respond to BMP stimulation. ***(a)*** *Smad phosphorylation (Smads 1/5) after 60 minutes of stimulation of cells cultured on 2D PAA gels.* ***(b)*** *Smad phosphorylation (Smads 1/5/8) after 60 minutes of stimulation of cells cultured on 3D collagen scaffolds.* ***(c)*** *Comparison of stiffness-dependency of induction of normalized signals (normalized to maximum value).*

While the level of Smad phosphorylation increased with an increase in substrate stiffness on the 2D gel substrate in line with previous reports [49], surprisingly a decrease with increasing stiffness was observed when cells were cultured inside collagen scaffolds

(Figure 4-24, **a and b**). This strong antagonistic behavior is further highlighted by correlation of substrate stiffness and Smad phosphorylation (Figure 4-24, **c**). Intriguingly, the level of induction was rather constant between medium and high stiffness groups for 2D gels and 3D scaffolds. It becomes clear that a stiffness range from the hematoma stiffness up to 10-20 kPa seems to represent a "transition zone" in terms of BMP response where further stiffening not necessarily provoke further increase or decrease in Smad phosphorylation. In this context it has to be taken into account that the stiffness-range associated with the transition zone depends on whether the macroscopic or the calculated cell-effective stiffness is regarded.

In order to validate whether differences in phosphorylation transduce to the level of gene expression, the transcriptional response was analyzed after 6 hours of stimulation for cells seeded into collagen scaffolds (Figure 4-25).

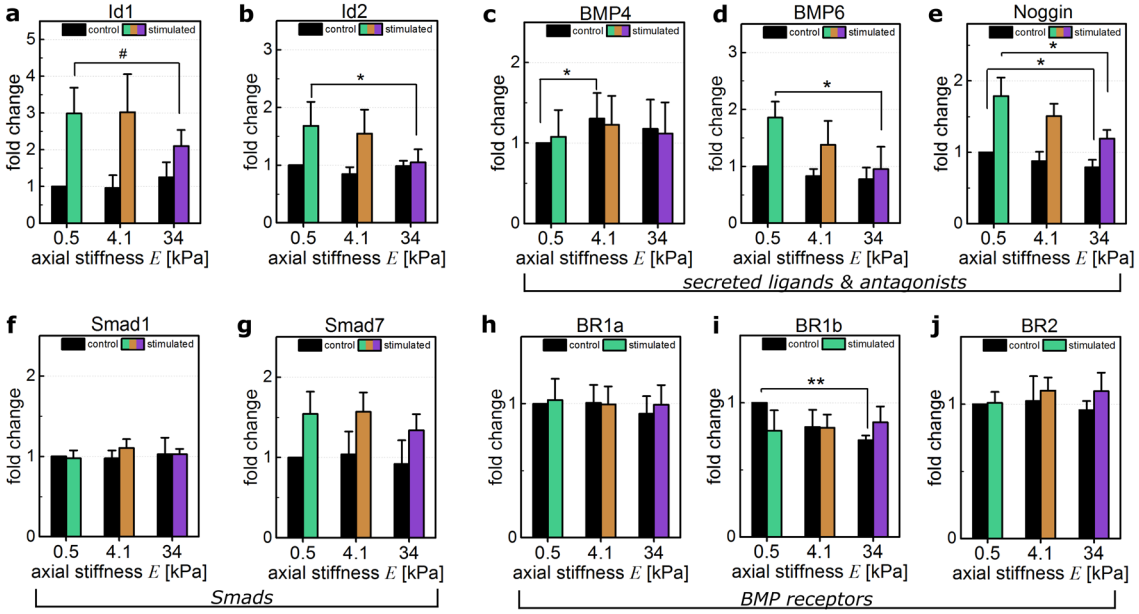

Figure 4-25: The substrate stiffness affects BMP2-mediated transcriptional response inside macroporous collagen scaffolds. ***(a-j)*** *gene expression levels after 6h of stimulation of selected BMP target genes (Id1, Id2), BMP ligands, Smads and BMP receptors presented as fold change relative to unstimulated 0.5kPa sample.*

The effect of decreasing BMP responsiveness with increasing substrate stiffness of the collagen scaffold could also be detected on gene expression level. Differences were most pronounced between the two softer (0.5 and 4.1kPa) in comparison to the stiffest material (34kPa) (Figure 4-25, **a and b**). A similar pattern was also visible for expression levels of BMP6 ligand and BMP antagonist Noggin showing higher levels of induction for the softest material (0.5kPa). Both, BMP6 and noggin are sensitive target genes that showed a gradual decline in their relative expression level with increasing scaffold stiffness.

While no differences were detected for R- and I-Smads, specifically BMP receptor type Ib showed a significantly increased basal expression level on the softest substrate. Although an increased expression level does not automatically imply an increased presence of receptors on the cell surface, it provides a potential regulatory factor since higher receptor levels would allow a stronger cell response to the BMP2 ligand.

Since these differences in BMP pathway activation were expected to be induced by a stiffness-dependent cell-material interaction, distinct mechanotransduction pathways were further studied. It was speculated that cellular mechanotransduction changes with stiffness which might correlate with BMP response.

4.3.3 Biomaterial stiffness affects mechanosensation

In a first step, cell adhesion and spreading was studied by confocal imaging (Figure 4-26, **a**). The images demonstrate that cells equally spread and adhere to all materials. Since it was shown that the density of wall-interconnecting struts increases with increasing solid collagen, the struts might offer additional adhesion sites for cells specifically in the stiff scaffold. However cells were preferentially localized on collagen walls independent of the amount of wall-interconnecting struts (Figure 4-26, **a**). It can be assumed that even with an increase in strut density at higher scaffold stiffness, the quantity of additional substrate area is low and only contributes to a minor extend.

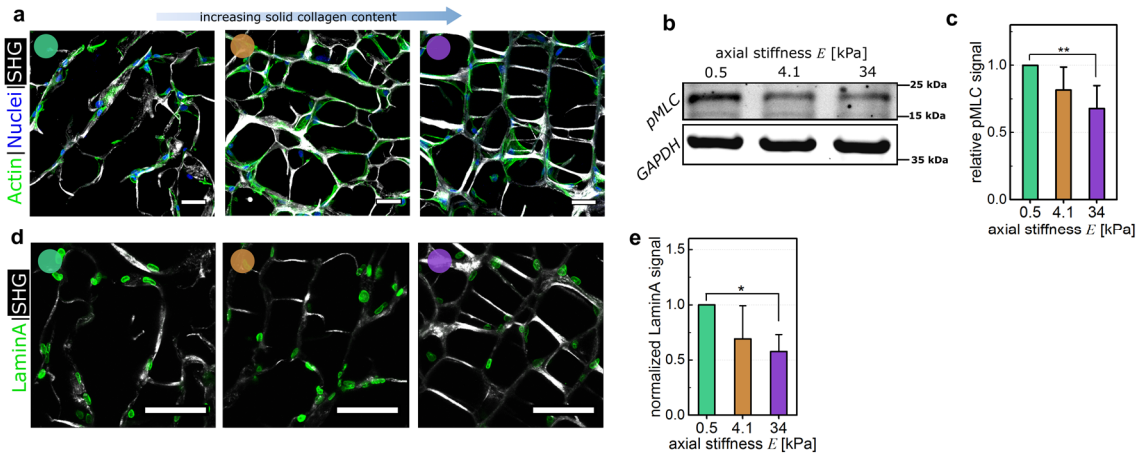

Figure 4-26: Cellular traction is influenced by the substrate stiffness. ***(a)*** *Confocal images of hFOBs seeded into collagen scaffolds and stained for actin (green) and nuclei (blue). The scaffold is visualized by SHG. Scale bar 50µm.* ***(b,c)*** *Phosphorylation of myosin light chain detected by immunoblotting. Signals were normalized to GAPDH.* ***(d)*** *Confocal images of hFOBs seeded into collagen scaffolds and stained for Lamin A. The scaffold is visualized by SHG. Scale bar 100µm.* ***(e)*** *Quantification of nuclear Lamin A presented as normalized signal relative to the softest scaffold.*

Various markers have been described over the last years to be responsive to a variation in substrate stiffness. In particular, it was demonstrated that cytoskeletal tension increases with substrate stiffness which is mediated through increased RhoA/ROCK signaling and higher phosphorylation of the regulatory myosin light chain (MLC) subunit [100,176]. Phosphorylation of MLC was analyzed by western blotting surprisingly revealing decreasing levels of the active phosphorylated protein with increasing substrate stiffness (Figure 4-26, **b and c**). Additionally, the level of nuclear Lamin A was analyzed by confocal imaging [177] (Figure 4-26, **d and e**). Again, a contradictory trend compared to literature could be observed showing a decreasing level of nuclear Lamin A with increasing scaffold stiffness.

From these observations it was concluded that cells cultured in a soft macroporous 3D environment adopted features (contractility, Lamin A mechanosensation marker) that are usually associated with a stiffer substrate. This antagonistic behavior could not be explained with the data obtained so far.

4.3.4 Cellular traction induces scaffold deformation on soft scaffolds

Since in particular increased MLC phosphorylation levels on the softest material (0.5kPa) point towards an increased contractility, it was speculated that cells might show a stiffness-dependent migration behavior. The generation of cell forces is a prerequisite for cell migration. Additionally, also the collagen scaffold was recorded by SHI since cell forces induce a deformation of the underlying substrate which was expected to vary in magnitude for different substrate stiffnesses (Figure 4-27).

Active migration of cells was observed for all three biomaterials with only little differences in the speed of movement. Intriguingly, while only little differences were observed for cell movement, the biomaterial was deformed due to cellular movement. This movement was found to gradually decrease with increasing scaffold stiffness. While for the softest material (0.5kPa), a continuous periodic wall deflection was visible for almost the entire scaffold, independent of the local wall thickness, for the stiffest material (34kPa) only sporadic events of individual fiber deformation were observed.

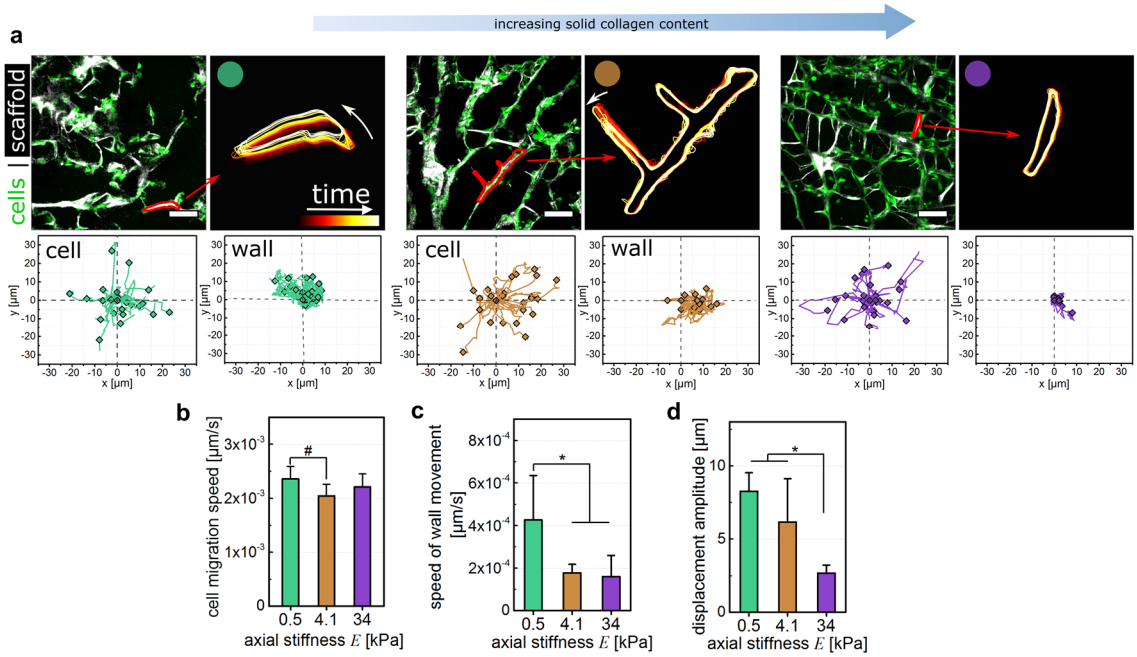

Figure 4-27: Cellular traction induces biomaterial deformation. ***(a)*** *Representative images from time-lapse recording of cells (green) seeded into collagen scaffolds (visualized by SHG). Scale bar 50µm. Cell and wall movement is presented as track trajectories. Local wall deformation is further shown as overlay of scaffold outline of different time points. White arrows indicate direction of movement.* ***(b)*** *Quantification of cell migration velocity.* ***(c)*** *Quantification of wall deformation velocity.* ***(d)*** *Quantification of amplitude of wall deformation.*

This mode of substrate deformation represents a strong difference to the situation where cell interact with a 2D elastic gel surface. In the latter, cell traction forces cause only a local material deformation around the points where the cell adheres to the substrate and deformation dissipates in all three dimensions with distance from the contact point (Figure 4-28). The elastic gel thus prohibits a long-range communication between cells via material straining [157]. In contrast to that, time-lapse experiments could demonstrate that in a soft macroporous 3D environment cellular traction lead to a systemic deformation. This suggests that the material architecture favors a transmission of cell-induced straining instead of dissipation. A deformation that was induced by a cell potentially can be sensed by other cells located at greater distance instead of proximal cells.

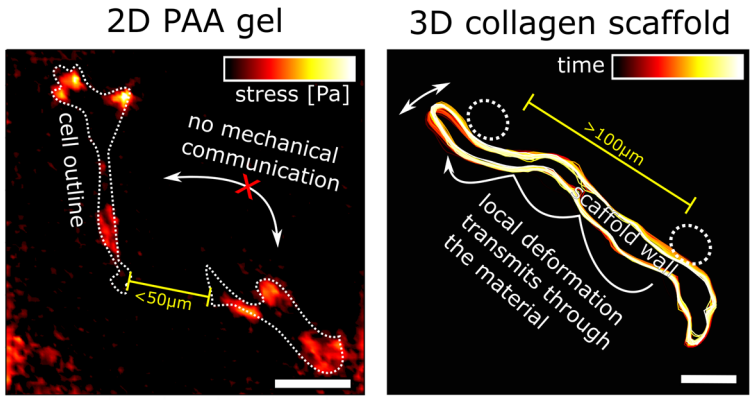

Figure 4-28: cellular communication via mechanical signals. ***Left:*** *Force magnitude map of cells seeded onto elastic 2D PAA gels. Heatmap represents the magnitude of local straining. The cell outline is indicated as white dashed lines.* ***Right:*** *Scaffold deformation over time illustrated by colored outline. Local deformations potentially transmit through the material and stimulate neighboring cells. Scale bar 50µm.*

In summary, it could be demonstrated that the mechanical as well as the dynamic cell-material interaction influences cellular responses, e.g. their contractility with further consequences for BMP signaling. A dynamic, soft environment of a constantly deforming substrate was found to correlate with an increased BMP response. Although there is no direct evidence, the biomaterial-mediated mechanical communication could represent a mechanism of inter-cell stimulation. A key feature of the material that caused described effects was the ability of the material to transmit mechanical signals. Together, these findings give novel insights how cell-material interactions and growth factor responses can be steered by the biomaterial properties which could improve future design and usage of biomaterials in regenerative medicine.

5 Discussion

As a result of the limited regenerative capacity of most of human tissues and organs, healing usually does not lead to restoration of the initial structure and functionality, but often to deposition of a collagen-rich fibrotic patch – referred to as scar. An exception is bone that exhibits a natural self-renewal and self-healing capacity with full restoration of the original architecture after damage. Using bone as a model system to better understand regenerative principles and processes might enable the development of novel therapy approaches for other tissues and organs with a poor intrinsic regenerative capacity, e.g. tendons, skin, cardiac & skeletal muscle and neuronal networks. However, also bone regeneration is limited by several constraints affecting the healing outcome [178] and more than 10% of all fractures result in a delayed healing or non-union [130]. Aside of the use of autologous bone graft for filling of the fracture gap, BMP growth factors are frequently used in clinical applications for the treatment of large bone defects [72]. While it is generally believed that BMPs mainly affect the healing outcome through their strong osteoinductive potential, little is known how early tissue formation events are affected. It was therefore hypothesized that BMPs steer the deposition of extracellular matrix at the onset of healing which was shown to have a structural guiding function for later mineralization processes [19]. A potential regulation of bone regeneration through information encoded into the ECM at early stages of healing would resemble a so-far unknown and neglected feature.

For the investigation of tissue formation *in vitro*, macroporous collagen scaffolds fabricated from a porcine collagen dispersion by directional freezing and freeze-drying [140] were selected as a model system. By tuning the solid collagen content in the initial dispersion, scaffolds of varying stiffness could be fabricated which all shared a similar architecture (Figure 4-23). Since it was shown that the material exhibited a highly elastic, spring-like behavior even over longer culture time, the scaffold could function as an *in situ* force sensor that allowed the conversion of scaffold contraction into quantitative values of deformation energy (Figure 4-1). Furthermore, the high porosity was favorable both for ECM deposition by fibroblast cells as well as reliable image quantification since cell-derived fibrillar collagen was spatially distinguishable from the thin scaffold walls (Figure 4-3). Using this system, it could be demonstrated that macroscopic contraction and tensioning was only visible once a fibrillar collagen network was deposited. The

amount of contraction and ultimately tension residing within the system potentially exceeded the sum of individual cell forces indicating a gradual transfer and storage inside pre-tensioned collagen fibers that leads to a consecutive multiplication of force. This principle can be illustrated by the deformation of stiff objects (e.g. a melon, but even coconuts and laptops) using rubber bands (Figure 5-1). In this example, forces applied to the melon by hand represent the forces exerted by cells to their underlying substrate. The maximum force that can be applied by a single hand is insufficient to efficiently deform the melon. When gradually transferring force into elastic elements (= stretching of rubber bands), the total force gradually increases with the amount of stretched/tensioned elements (Equation 1) which leads to a deformation of the melon.

Equation 1: Gradual increase of tissue tension.

$$F_{total} = \sum_{n} F_n$$

Figure 5-1: Illustration of an incremental tensioning process. Objects that are to stiff to be macroscopically deformed by a distinct force (e.g. grip force of a hand) can be deformed by an incremental transfer of force into pre-tensioned elements (stretching of rubber bands). A gradual transfer of tension allows a multiplication of the total acting force[*].

In the 3D *in vitro* culture system, cells are the objects that exert force to their environment. Without a gradual transfer of tension, contraction is limited to environments that exhibit a rather soft macroscopic stiffness (<4kPa) similar to the stiffness of a hematoma (Figure 4-9). Stiffer environments can only be macroscopically contracted with the aid of a load-bearing fibrillar collagen network. The permanent storage of forces inside collagen fibers could further be proven by decellularization of scaffold that were seeded with fibroblasts and cultured for two weeks. (Figure 4-12).

Together, these observations picture an incremental process of tissue formation and tensioning. Such a "slip-and-ratchet" model of tissue growth was proposed previously

[*] Images modified from https://www.youtube.com/watch?v=hEVw66Mv6Nw. Citation of copyright content according to terms and guidelines of §51 UrhG and YouTube fair use policy.

[159,179], but the work presented here gives first *in vitro* evidence for this model. In addition to that, also the essential role of collagen fibers was demonstrated.

A variety of different studies investigated the process of cellular self-organization, ECM deposition and tissue tensioning *in vitro* before. These studies utilized collagen gels [160,162,179] or stiff materials such as hydroxyapatite or PDMS [164,180,181]. While collagen gels are cheap and easy to handle, quantification of ECM synthesis and development of tissue tension in those materials is not trivial. Tissue tension in gels can be calculated based on the deflection of micro-posts of defined stiffness [162], but precise calculations are complicated by the poro-elastic behavior and non-linear strain-hardening of collagen gels [182,183]. Furthermore, observations are usually restricted to short time frames of 24-72 hours after which a typical saturation in contraction and tissue tension is observed [179]. Within this time frame matrix deposition particularly of fibrillar collagen cannot be expected. Collagen gels thus can be regarded as a suitable model system for mimicking the initial soft environment of a hematoma. In contrast to that, the macroporous character of the scaffold used in this study was favorable for cellular ECM deposition in a 3D environment and thus allowed to study *in vitro* wound healing processes beyond the hematoma phase (Figure 5-2).

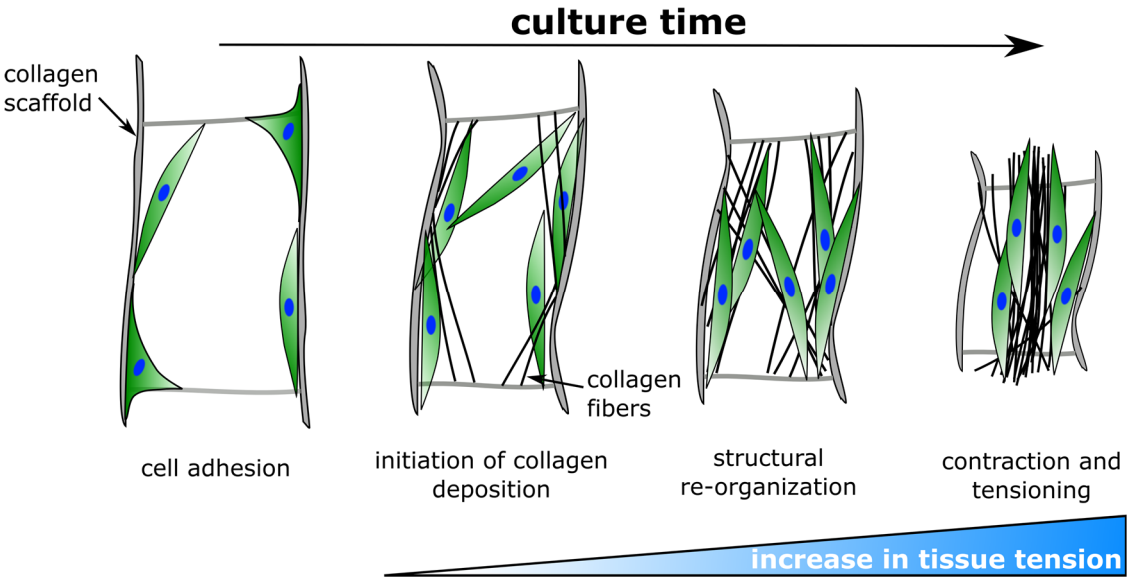

Figure 5-2: Graphical illustration of the described model. Cells adhere to the walls of a macroporous collagen scaffold and undergo a collective collagen deposition and structural re-organization process. This results in a highly aligned cell-ECM network. Tissue tension thereby increases linearly with the amount of tensioned collagen fibers deposited by cells.

Other systems, such as PDMS- or HA-based voids [164,180,184] provide a defined geometry with the potential to visualize local ECM patterning and straining, e.g. via a

FRET-probe or laser ablation. However, the stiff environment provided by these materials limits the potential of a quantitative assessment since material deformation usually is not measurable.

Although the biomaterial used in this study features several favorable properties compared to other established systems, it also faces several limitations: It was demonstrated that the material exhibits a stable and elastic behavior during culture (Figure 4-8) and calculations of strain energy per cell were based on macroscopic values of stiffness. Since the microscopic architecture of the scaffold is strongly heterogeneous, but calculated values of scaffold strain require a uniform material, values of acting forces might strongly vary on a microscopic level. Also, calculated strain energy values for scaffold deformation are purely based on the elastic properties of the empty scaffold and disregard additional mechanical contributions of cells and deposited ECM that might resist acting cell forces. The mechanical work that is delivered by each cell during the contraction process consequently is causing scaffold and ECM straining in an unknown proportion. Thus values of single cell force amplification in fact might be much higher since parts of the contraction process leading to the compression of ECM components other than the scaffold cannot be quantified.

Another factor that influences the calculations is the mode of single cell force combination. For this study, a tug-of-war-mode was assumed in which individual forces can be combined linearly (Figure 5-3). However, this represents the hypothetical maximum force output that can be reached by all cells present within the system. Although there is *in vitro*-evidence for a supra-cellular organization of the acto-myosin machinery during would closure [185], forces occurring during this process are not necessarily linearly aligned and might counteract and eliminate each other [186]. Furthermore, if cell forces, particularly at early stages of tissue formation, would not be transmitted through the ECM but via coordinated acto-myosin complexes between cells, the maximum force would be limited by the weakest element (human chain). Although a strong cellular alignment together with collagen deposition favors a tug-of-war mode, disregarding potential elimination of forces resembles another simplification.

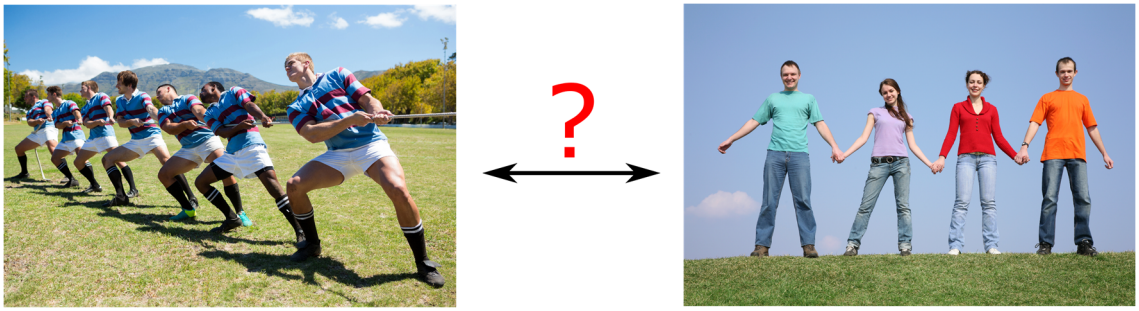

Figure 5-3: Different combination modes of mechanical elements. Tug-of-war-mode allows the linear addition of individual elements, while human chain-mode is limited by the weakest element[*].

Aside of these considerations another limitation that needs to be taken into account is the limited predictive capacity of 2D force measurements performed on thin PAA gels for actual forces occurring in 3D. Methods for the quantification of single cell forces in 3D are emerging [187–189], but are labor-intensive and require advanced *in silico* post-processing and simulation, whereas 2D approaches are well-established and allow a higher throughput. The latter represents a critical factor and was decisive for a preference of assessing single cell forces in 2D. As pointed out by Kurzawa and colleagues, the measurement of single cell forces is accompanied by a strong intrinsic variability, even when cell spreading is constraint to a defined geometry [190]. Similar observations were made also during this study and provoked the quantification of many cells to obtain a representative distribution for each donor. Despite the limited predictive capacity of actual 3D forces, 2D measurements could be used to assess differences between individual donors and compare them to macroscopic contraction patterns observed in 3D since single cell forces are expected to change in a similar manner for all donors during 3D culture. Furthermore, TFM could be used to assess the magnitude of potential regulations of single cell forces during culture, e.g. due to a pro-fibrotic stimulus such as TGF-β. It was shown that this growth factor drives myo-fibroblast activation and leads to an increased contractility of cells [97,191]. Myo-fibroblast activation naturally occurs during wound healing in a stiffness-dependent manner [192]. Since both autocrine TGF-β- and stiffness-mediated myo-fibroblast activation might occur during *in vitro* culture inside collagen scaffolds, 3D traction forces not only differ from 2D values but could dynamically change during culture and are disregarded in the presented calculations. However, fibroblasts activated by TGF- β in 2D only showed a 2-fold increase in their single cell forces compared to up to 17-fold differences in scaffold contraction and 100-fold in single cell force

[*] Picture sources: Images were licensed from Adobe Stock.

amplification factor (Figure 4-8). Although disregarding changes in cell forces might represent a limitation, it clearly demonstrates that it is mostly the ability to form a fibrillar collagen network that is decisive for macroscopic tensioning and contraction. Since myofibroblast activation also leads to increased collagen secretion [193], both factors potentially synergize in pathological wound contracture.

The model of incremental force amplification during tissue formation proposed in this study suggests a direct connection between collagen fiber alignment and directionality of tension. Since tension was shown to be gradually transferred and stored during ECM formation, maintenance of the tissue tensional state is independent of active cell forces. It was further demonstrated that an established collagen network has a guiding function on invading cells. Since also *in vivo* observations point to a strong structural guiding function of early ECM patterns for consecutive mineralization processes during bone healing [19], therapy approaches should aim to control these early organization processes.

During bone regeneration, the aforementioned process of tissue formation, tensioning and contraction would not occur under defined cell culture conditions but would be influenced by a variety of different factors such as cell localization, stiffness, oxygen and nutrient supply, mechanical loading (shear, compression) and growth factor gradients. Amongst the many growth factors, BMPs are described as potent inducers of bone formation. It was hypothesized that, in addition to their strong osteoinductive potential, BMPs steer early tissue formation processes and thus guide regeneration through a structural organization of the ECM. It was observed that BMP stimulation led to an enhanced tissue contraction. Intriguingly, BMP2-stimulated samples followed the same linear dependency of contraction and collagen density that was observed for unstimulated samples (Figure 4-15). Only for early time point of 7 days, a deviation from this dependency was observed since samples exhibited stronger contraction with less fibrillar collagen. This indicates a potential regulation of cellular contractility due to BMP stimulation which is supported by previous reports [22,194]. With an enhanced contractility, cells might be able to transfer more force into each element and could reach a similar or even higher contraction with less tensioned elements. However, it has to be mentioned that quantitative information on how BMP2 stimulation affects single cell forces is not available so far but can be expected to change since BMP stimulation was shown to directly affect regulatory myosin light chain phosphorylation [195].

While for unstimulated samples, fibrillar collagen formation and contraction followed a linear behavior over the whole culture time, BMP2 stimulation induced a strong acceleration of these processes particularly between 1 and 2 weeks of culture (Figure 4-15). After this time point, samples only experienced little changes between 2 and 3 week time points. As in particular collagen density was comparable at the end between stimulated and unstimulated samples, BMP seemed to lead to a strongly enhanced tissue formation process that resulted in a steady state situation. Furthermore, mechanical softening and increase in MMP expression point to the induction of a remodeling phase specifically in the BMP2-treated group (Figure 4-16 and Figure 4-17). Since tissue formation was not observed for longer culture time, it is unknown whether samples cultured without BMP2 stimulation eventually reach a steady state with consecutive remodeling as well or if this is exclusively due to BMP2 stimulation. MMP13 is a collagenase that is used as a marker of hypertrophic chondrocytes and promotes cartilage turnover and vascular invasion during endochondral ossification [196]. It could be shown that MMP13 induction is enhanced for cells encapsulated into spheroids compared to monolayer [106] which points to an environment-specific regulation of ECM assembly and disassembly by BMPs. A strong induction in MMP13 expression for BMP2-treated samples was observed after 7 and particularly 14 days of culture where also collagen density, scaffold contraction and stiffness was increased compared to unstimulated samples. This might prevent a too early degradation of ECM (atrophy) which would delay the process of regeneration, but on the other hand counteracts a potential “overshooting” and fibrotic stiffening of the granulation tissue (hypertrophy) that would drive further myo-fibroblast activation.

The considerations and observations were primarily focusing on changes in structural and mechanical properties that disregard differences in the ECM composition. It was hypothesized in the beginning of this thesis that an extracellular matrix build by cells under BMP2 stimulation has distinct properties which are beneficial for BMP2 stimulation again. This would ultimately establish a concept of feed forward signaling through ECM properties. This assumption regards the ECM in general but without specification of a distinct property (e.g. ECM structure, biochemical composition). Since it can be assumed that each property (structural organization, composition, tensile state) influences cellular behavior, it was tested whether decellularized samples can be homogeneously re-populated with cells (Figure 4-20). Decellularized constructs would provide an ideal model

system as the combined effect of differences in ECM organization, composition and tension can be studied at once. Yet, variations from a native ECM composition after perfusion decellularization can be expected (Figure 4-18) as ionic detergents used during the procedure remove some components (e.g. charged proteoglycans) more efficiently than others (covalently cross-linked collagens) [149].

However, it was observed that a homogeneous re-population of decellularized matrices with cells cannot be achieved as the pores of the scaffold seem to be blocked during the re-seeding process. In order to overcome this restriction, it was decided to separately study the influence of distinct ECM properties on cellular behavior. An increased collagen density after 2 weeks of culture in samples cultured with BMP2 stimulation point towards differences in the abundance of ECM proteins. In order to study the influence the biochemical composition of the ECM on cellular behavior, dECM was enzymatically digested to harvest a distinct peptide signature which was further used for tissue culture coating. In a proof-of-principle experiment, the osteogenic differentiation of hMSCs cultured on top of dECM coating was tested. Even without supplementation of BMP2, a clear effect was visible showing that dECM coating enhanced osteogenic differentiation and formation of a mineralized matrix compared to pure collagen coating (Figure 4-21). The beneficial effect might be caused by a more diverse composition featuring not only collagens but soft ECM components as demonstrated by mass spectrometry (Figure 4-19). Intriguingly, a dECM that was derived from samples stimulated with BMP2 showed a reduced matrix mineralization compared to dECM coating from unstimulated samples. This finding clearly supported the initial hypothesis that an ECM grown under BMP2 stimulation holds specific cell-instructive properties. Since the approach disregarded BMP2 supplementation in the final osteogenic differentiation assay, it remains unknown whether the biochemical composition of a matrix grown under BMP2 stimulation in turn also influences BMP signaling response. Furthermore, intrinsic limitations of the approach (e.g. selective removal of ECM components due to the decellularization procedure prior to enzyme digestion) might introduce or remove differences in the ECM composition and influence differentiation results. A more comprehensive analysis of changes in ECM protein secretion before and after decellularization, especially of changes introduced during detergent removal of cells might help to understand the obtained differentiation results.

BMP2 stimulation was found to not only affect the collagen density but dramatically tissue contraction and stiffness which was found to be increased for early time points of culture (7 and 14 days) and followed by a softening at later stages (21 days) compared to unstimulated samples. In order to investigate if changes in the stiffness of the ECM affects BMP signaling, it was decided to use macroporous collagen scaffolds as a simplified model system. By varying the solid collagen content, the macroscopic stiffness could be tuned to obtain a soft (0.8 wt.-% collagen, 0.5kPa), intermediate (1.5 wt.-% collagen, 4.1kPa) and stiff (3.0 wt.-% collagen, 34kPa) scaffold. Substrate stiffness is an intrinsic ECM property that was shown to affect cellular behavior in various fashions including adhesion, contractility, migration, proliferation and differentiation [3,87,88,176,197]. Furthermore, several studies could also demonstrate a stiffness-dependency in the response to growth factors, including to BMPs [49,94,95,97,99–101]. While all of these studies suggest a stronger growth factor response on stiffer substrates, an antagonistic behavior was observed for cells cultured in 3D. Both for Smad phosphorylation and BMP target gene expression, an increased response was found on the softest scaffold (0.5kPa) compared to the two stiffer ones. At least for Smad phosphorylation it was also visible that the stiffness-dependent response is not linear but there seems to be a threshold for Smad-phosphorylation with increasing substrate stiffness after which the response was not further increased (2D PAA gel) or reduced (3D collagen scaffold). Both, for 2D (PAA) and 3D (collagen scaffold), this range could be estimated to be between 10 and 30 kPa depending on the use of macroscopic stiffness or cell-effective stiffness for the collagen scaffold [174]. This implies that also the hematoma features mechanical properties (E=2.9±1.9kPa) that might be either favorable or obstructive for BMP signaling compared to matured callus tissue [163] (Figure 5-4).

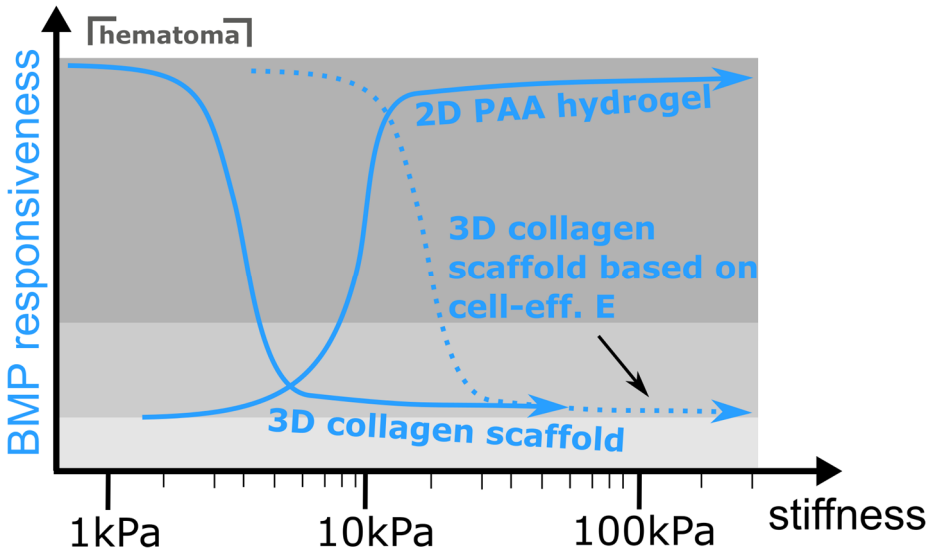

Figure 5-4: Stiffness-dependent BMP responsiveness. Findings described in section 4.3 are summarized to illustrate the antagonistic stiffness-dependent response to BMP2 stimulation on 2D polyacrylamide gels and 3D collagen scaffolds. The data suggest a "threshold" stiffness that either increases or decreases the response while further stiffening beyond that level does not provoke a further increased response.

It was further demonstrated by gene expression analysis that the expression of the BMP receptors is a potential regulatory feature since cell cultured inside soft collagen scaffolds (0.5kPa) exhibited significantly increased levels of the BMP type Ib receptor. This indicates that cell-material interactions directly affect the levels of cell surface receptors which further modulates the sensitivity to BMP2. Indeed, it could be observed that stimulation with a reduced concentration of BMP2 (1nM) provoked an induction in Id1 gene expression for the softer substrates, but not for the stiffest (Supplement 3). This shows that cells adopt a higher sensitivity, potentially due to enhanced BMP receptor expression. A connection between stiffness-dependent cell surface abundance of BMP receptors and BMP responsiveness has been established previously [49] and is described to be mediated through the interaction between BMP receptors and integrins. There are also various indications for a dependency of BMP signaling on integrin interaction, their activation and downstream signaling such as focal adhesion kinase [51,128,129,198]. Since stiffness is known to be a regulatory feature of cellular adhesion and contractility, it can be expected that differences found in BMP receptor expression and Smad phosphorylation correlate with differences in cell adhesion. An indirect hint has already been provided by the myosin light chain phosphorylation as a downstream effector of integrin signaling (Figure 4-26). Intriguingly, the phosphorylation of myosin light chain, but also the amount of nuclear Lamin A showed an antagonistic stiffness-dependent behavior compared to previous reports [177,199]. This unexpected behavior of cells cultured in a

soft macroporous scaffold adopting features of cells cultured on stiff 2D substrates was consistent for several markers and pathways (pMLC, nuclear Lamin A and BMP signaling).

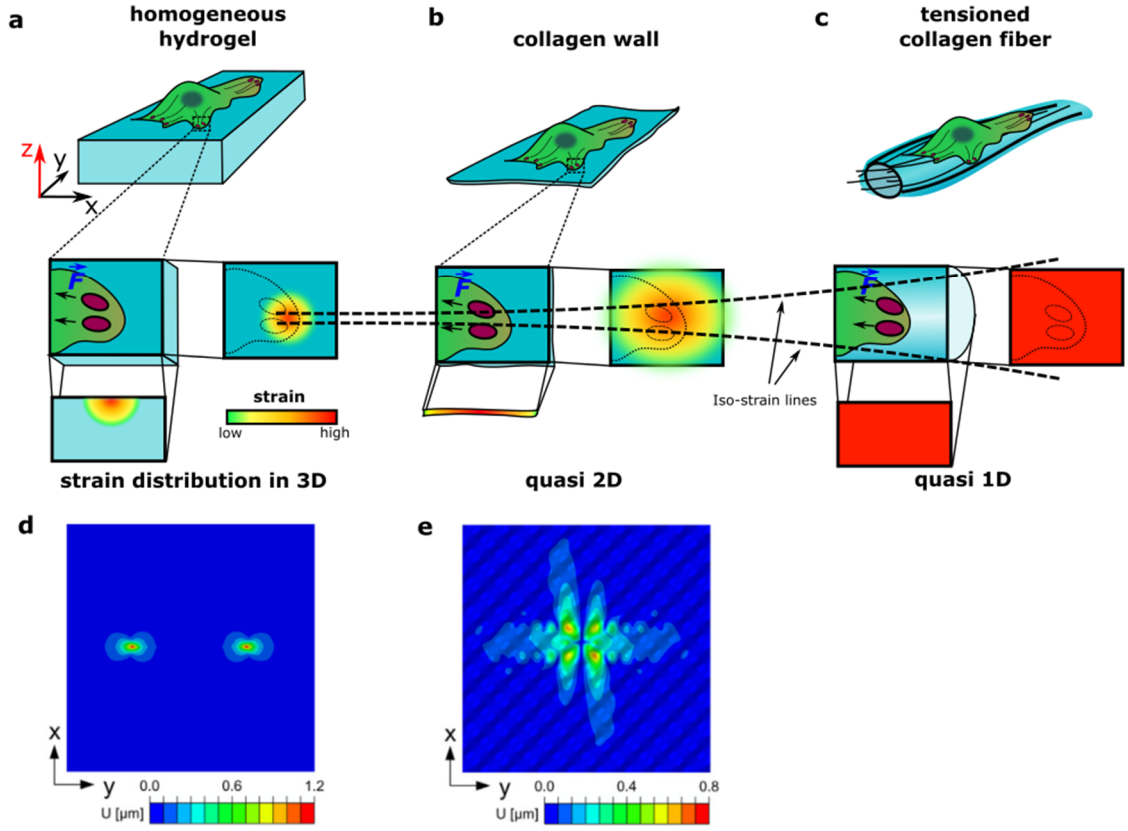

Figure 5-5: Dissipation of cell-induced material deformation. While tactile stress and the resulting deformation can dissipate in three dimensions for an elastic hydrogel ***(a)****, thin collagen walls permit a limited transmission of tactile stress via bending* ***(b)****. Tensioned collagen fibers are favorable to efficiently transmit local deformations over long ranges* ***(c)****. Simulation of material deformation produced by a unidirectional load (30pN) applied at 100µm distance for a 3D gel (d) and a quasi 2D scaffold wall (e). Simulations reproduced with permission from* [174].

Consequently, the stiffness characteristics of the macroporous collagen scaffolds not necessarily determine a distinct range that could be directly used as a blueprint for biomaterial design. Rather, the specific architecture of thin collagen walls provoked a distinct response via cell-material interaction which seems to be different than the interaction with an elastic hydrogel (Figure 5-5). An isotropic and elastic hydrogel such as polyacrylamide has only very limited potential to transmit mechanical signals between cells as gel deformation inversely scales with distance from the force contact point. A hypothetical application of a typical cell force of 10nN (10kPa gel) thereby would only lead to a deformation of 0.1µm at a distance of 100µm and usually is regarded as insignificant [157]. Consequently, cell force-induced material strain energy dissipates fast in all three dimensions of the hydrogel (Figure 5-5, **a and d**). In contrast to that, it was observed

particularly for the softest 3D collagen scaffold that it deformed systemically due to cell traction forces. Even regions of the scaffold that were not in direct proximity to cells showed a deformation. This suggests that cell traction-induced material strain potentially can be transmitted through the material and the resulting wall bending does not dissipate at short distances from the cell-material contact point (Figure 5-5, **b and e**). This even might permit the communication of cells via transmission of mechanical signals through the underlying substrate.

Although both macroporous collagen scaffolds and synthetic PAA hydrogels are highly elastic materials, only polyacrylamide provides an environment in which the application of force induces a strain field which dissipates fast into spatial dimensions and does not overlay or interfere with strain fields created by other cells. In contrast to that, cell-induced material deflection inside macroporous collagen scaffolds creates an altered topology of the surface for the cell itself as well as for neighboring cells. Cells are thus constantly adopting to the strain fields created by other cells. A daily life analog can be made by comparing movement on concrete (but also soft synthetic materials which can be found in sleeping mattresses) and movement on a thin surface, e.g. a trampoline (Figure 5-6). The latter particularly forces a person which is moving on top of the trampoline to continuously re-adopt its balance. This is even more pronounced when multiple people are moving as the movement of one influences its own but also everyone else's further movement. In contrast to that, walking or running on running tracks is not influenced by the movement of others on the same subgrade, even at high proximity.

Together, all these considerations indicate that the soft macroporous collagen scaffold, despite its highly elastic material properties, resembles a highly dynamic environment that seems to be favorable for BMP signaling. Most of all tissues in the human body exhibit a viscoelastic behavior [86]. Due to material creep cells naturally experience an environment that forces cells to continuously re-adopt – even disregarding the influence of others cell and active mechanical triggers (stretch, compression, shear, etc.). This potentially provokes a similar cellular behavior, even though caused by a different mechanical principle. An environment that permits the transmission of mechanical signals and thereby allows communication of cells through stress-induced material deformation could be a key feature of many tissues that is favored by cells. In fact, it was shown in section 4.1 that tissue formation by fibroblasts inside the pores of a macroporous collagen scaffold results in a highly aligned ECM network in which collagen bundles span through

the pores over long range (Figure 4-3). Furthermore, cells invading this cell-derived matrix after decellularization preferably adhered to the cell-derived matrix and not the collagen scaffold (Figure 4-13). However, secondary effects (e.g. high curvature of collagen bundles, differences in biochemical composition) might also influence this behavior and enforce cell adhesion to collagen bundles. Regarding the capacity to transduce mechanical strain, unidirectional tensioned collagen bundles are highly superior to homogeneous hydrogels and even 2D surfaces (Figure 5-5, **c**). The linearization of substrate straining that is restricted to one dimension results in a much slower dissipation. A similar principle enables the operating mode of a cans phone in which the acoustic noise induces a vibration within a can which can be transmitted by a longitudinal wave through a tensioned cord towards a second can. Similarly, it can be speculated that cell-induced straining of aligned collagen bundles leads to a longitudinal transmission of mechanical strain. Cells might be able to communicate and coordinate their behavior over large distances, e.g. the size of a fracture gap. Indications that the structural organization of these collagen bundles has a strong influence on the healing outcome have been published recently [19].

Figure 5-6: mechanical communication on different substrates[*].

Hints that such an environment again might be beneficial for BMP signaling were found during this thesis. As shown in section 4.2.1, BMP target genes, particularly Id2 showed a mild response directly after initial stimulation with BMP. After 14 days of culture, a strong increase in the Id1 and Id2 gene expression was detected (Figure 4-14). This is even more remarkable as it (in the case of Id2) exceeds even absolute expression levels (mean normalized expression) detected after 6 hours of stimulation. This indicates a strongly increased BMP signaling response after 14 days of culture. Regarding collagen density analysis (Figure 4-15), this was also the time point, where a strong increase in

[*] Picture sources: left – private image; middle and right: licensed from Adobe stock.

collagen density was observed. A highly increased BMP responsiveness thus co-occurred with the establishment of a dense and tensioned fibrillar collagen network. Based on this observation, it can be speculated that the ECM that was formed by cells inside the macroporous collagen scaffolds is beneficial for BMP signaling. A critical aspect of this ECM is the high tensional state of deposited collagen fibers which allow a transmission of mechanical signals. This feature is inherent to an ECM that was formed without as well as with additional supplementation with BMP2. A matrix grown under BMP2 stimulation, at least in the presented *in vitro* approach, thus might not be superior for BMP signaling per se compared to an ECM grown without BMP2 stimulation. However, as collagen deposition and contraction were found to be enhanced, the time that is needed to establish such an ECM network could be reduced.

So far, it was reported that BMP signaling can be enhanced by mechanical loading applied extrinsically. [23]. Similar observations were also obtained from *in vivo* experiments that could even show that the degree of fixator stiffness for an osteotomy gap loaded with BMP2 influences callus formation and mineralization [22]. This thesis could provide first *in vitro* evidence that a similar response can be induced by specific material properties as well without extrinsic application of force. The findings indicate an inter-cell mechano-stimulation through cell force-induced material deformation. Together, these observations imply distinct requirements for biomaterials for bone regeneration which might help to overcome limitations and drawbacks of current therapy approaches.

6 Conclusion & Further Prospects

The aim of this thesis was to investigate how BMPs affect tissue formation, in particular during early stages of bone regeneration. The thesis was divided into three consecutive parts: (i) to investigate and architectural blueprint cells follow to restore tissue structure and tensional state, (ii) to analyze the effect of BMP stimulation on tissue formation and finally, (iii) to validate if an ECM assembled under BMP stimulation exhibits properties which are beneficial for BMP signaling.

It could be demonstrated that (i) cells undergo a collective tissue formation and tensioning process inside the pores of a macroporous collagen scaffold. During this, cells incrementally transfer force into tensioned collagen fibers which results in a multiplication of single cell forces. Furthermore, it was shown that (ii) BMP2 stimulation positively affects processes essential for tissue healing and regeneration, namely collagen deposition and tissue tensioning. Finally (iii), an altered stiffness of the underlying substrate was simulated using collagen scaffold of varying collagen content. Cells that were cultured on a soft material (0.5kPa) showed an increased response in BMP signaling compared to stiffer materials (4 and 34 kPa). This observation correlated with a cell-induced material deformation which suggests an autocrine and/or paracrine mechanical stimulation. These findings suggest distinct requirements for biomaterials used for bone regeneration.

Biomaterials for bone tissue engineering can be fabricated from various natural (e.g. collagen, fibrin) or synthetic materials (e.g. PCL) and even metals (titanium). Every material allows distinct properties of stiffness, porosity, biocompatibility, biodegradability and osteoconductive/-inductive potential [200]. While several approaches, e.g. using natural or synthetic ceramics or titanium structures focus on the macroscopic mechanical stabilization and support of the defect area [201,202], this thesis emphasizes that providing a macroporous soft tissue environment similar to the early stages of healing leads to a strong activation of cells in terms of tissue formation and growth factor response. This is based on the assumption that mechanical inter-cell communication on soft elastic substrates contributes to ECM formation and maturation processes during tissue healing and regeneration. However, a biomaterial that is too soft to withstand macroscopically occurring loads easily can be displaced or strongly compressed. This results in an antagonism

of the mechanical requirements for a biomaterial between the cell (soft environment with a high porosity) and the tissue level (optimal mechanical support with controlled interfragmentary movement).

One possible way to solve this antagonism is the integration of different materials to form a composite structure. It could be suggested that a secondary support, e.g. a titanium cage [202] or degradable polymer, is filled with a softer and biologically active material. Although the collagen scaffold used for this thesis already is a suitable candidate, other material systems could be considered as well. One promising candidate might be biomaterials derived from alginate which show a high versatility and can be chemically modified to tune stiffness, stress relaxation behavior, degradation and cell adhesion [86,203,204]. Furthermore, alginate can be used as a delivery platform for ceramic particles, bioactive glass ("bioglass"), growth factors and cells in order to enhance the osteoinductive potential. The appropriate selection and modification of all of these parameters is of greatest relevance not only to the specific aspects of ECM formation and tensioning and BMP signaling which were addressed during this thesis. Other processes which are taking place during bone regeneration such as inflammation/ immune cell recruitment and revascularization integrate into or counteract tissue formation processes. The integration of these factors should be evaluated in order to assess or further optimize the biomaterials' true translational potential.

Together, these considerations are expected to contribute and improve biomaterial-based approaches for bone regeneration and thereby overcome limitations of current therapy approaches.

References

[1] R.O. Hynes, Integrins: A family of cell surface receptors, Cell. 48 (1987) 549–554. doi:10.1016/0092-8674(87)90233-9.

[2] D.E. Discher, P. Janmey, Y.-L. Wang, Tissue cells feel and respond to the stiffness of their substrate., Science. 310 (2005) 1139–43. doi:10.1126/science.1116995.

[3] A.J. Engler, S. Sen, H.L. Sweeney, D.E. Discher, Matrix Elasticity Directs Stem Cell Lineage Specification, Cell. 126 (2006) 677–689. doi:10.1016/j.cell.2006.06.044.

[4] E. Cukierman, D.E. Bassi, Physico-mechanical aspects of extracellular matrix influences on tumorigenic behaviors, Semin. Cancer Biol. 20 (2010) 139–145. doi:10.1016/j.semcancer.2010.04.004.

[5] T. Rozario, D.W. DeSimone, The extracellular matrix in development and morphogenesis: A dynamic view, Dev. Biol. 341 (2010) 126–140. doi:10.1016/j.ydbio.2009.10.026.

[6] G. Charras, E. Sahai, Physical influences of the extracellular environment on cell migration, Nat. Rev. Mol. Cell Biol. 15 (2014) 813–824. doi:10.1038/nrm3897.

[7] J. Henkel, M.A. Woodruff, D.R. Epari, R. Steck, V. Glatt, I.C. Dickinson, P.F.M. Choong, M.A. Schuetz, D.W. Hutmacher, Bone Regeneration Based on Tissue Engineering Conceptions — A 21st Century Perspective, Bone Res. 1 (2013) 216–248. doi:10.4248/BR201303002.

[8] L.W. Lau, R. Cua, M.B. Keough, S. Haylock-Jacobs, V.W. Yong, Pathophysiology of the brain extracellular matrix: a new target for remyelination., Nat. Rev. Neurosci. 14 (2013) 722–9. doi:10.1038/nrn3550.

[9] S. Calve, S.J. Odelberg, H.G. Simon, A transitional extracellular matrix instructs cell behavior during muscle regeneration, Dev. Biol. 344 (2010) 259–271. doi:10.1016/j.ydbio.2010.05.007.

[10] S.E. Mercer, S.J. Odelberg, H.G. Simon, A dynamic spatiotemporal extracellular matrix facilitates epicardial-mediated vertebrate heart regeneration, Dev. Biol. 382 (2013) 457–469. doi:10.1016/j.ydbio.2013.08.002.

[11] K. Schmidt-Bleek, A. Petersen, A. Dienelt, C. Schwarz, G.N. Duda, Initiation and early control of tissue regeneration – bone healing as a model system for tissue regeneration, Expert Opin. Biol. Ther. 14 (2014) 247–259. doi:10.1517/14712598.2014.857653.

[12] J.-H. Chen, C. Liu, L. You, C. a. Simmons, Boning up on Wolff's Law: Mechanical regulation of the cells that make and maintain bone, J. Biomech. 43 (2010) 108–118. doi:10.1016/j.jbiomech.2009.09.016.

[13] C. Schlundt, T. El Khassawna, A. Serra, A. Dienelt, S. Wendler, H. Schell, N. van Rooijen, A. Radbruch, R. Lucius, S. Hartmann, G.N. Duda, K. Schmidt-Bleek, Macrophages in bone fracture healing: Their essential role in endochondral ossification., Bone. 106 (2018) 78–89. doi:10.1016/j.bone.2015.10.019.

[14] F.A. Sass, K. Schmidt-Bleek, A. Ellinghaus, S. Filter, A. Rose, B. Preininger, S. Reinke, S. Geissler, H.D. Volk, G.N. Duda, A. Dienelt, CD31+ Cells From Peripheral Blood Facilitate Bone Regeneration in Biologically Impaired Conditions Through Combined Effects on Immunomodulation and Angiogenesis, J. Bone Miner. Res. 32 (2017) 902–912. doi:10.1002/jbmr.3062.

[15] S. Reinke, S. Geissler, W.R. Taylor, K. Schmidt-Bleek, K. Juelke, V. Schwachmeyer, M. Dahne, T. Hartwig, L. Akyuz, C. Meisel, N. Unterwalder, N.B. Singh, P. Reinke, N.P.

Haas, H.-D. Volk, G.N. Duda, Terminally Differentiated CD8+ T Cells Negatively Affect Bone Regeneration in Humans, Sci. Transl. Med. 5 (2013) 177ra36-177ra36. doi:10.1126/scitranslmed.3004754.

[16] A. Schindeler, M.M. McDonald, P. Bokko, D.G. Little, Bone remodeling during fracture repair: The cellular picture, Semin. Cell Dev. Biol. 19 (2008) 459–466. doi:10.1016/j.semcdb.2008.07.004.

[17] C. Colnot, S. Huang, J. Helms, Analyzing the cellular contribution of bone marrow to fracture healing using bone marrow transplantation in mice, Biochem. Biophys. Res. Commun. 350 (2006) 557–561. doi:10.1016/j.bbrc.2006.09.079.

[18] K.N. Malizos, L.K. Papatheodorou, The healing potential of the periosteum, Injury. 36 (2005) S13–S19. doi:10.1016/j.injury.2005.07.030.

[19] A. Petersen, A. Princ, G. Korus, A. Ellinghaus, H. Leemhuis, A. Herrera, A. Klaumünzer, S. Schreivogel, A. Woloszyk, K. Schmidt-Bleek, S. Geissler, I. Heschel, G.N. Duda, A biomaterial with a channel-like pore architecture induces endochondral healing of bone defects., Nat. Commun. 9 (2018) 4430. doi:10.1038/s41467-018-06504-7.

[20] T.A. Einhorn, L.C. Gerstenfeld, Fracture healing: mechanisms and interventions, Nat. Rev. Rheumatol. 11 (2014) 45–54. doi:10.1038/nrrheum.2014.164.

[21] C. Schwarz, D. Wulsten, A. Ellinghaus, J. Lienau, B.M. Willie, G.N. Duda, Mechanical Load Modulates the Stimulatory Effect of BMP2 in a Rat Nonunion Model, Tissue Eng. Part A. 19 (2013) 247–254. doi:10.1089/ten.tea.2012.0265.

[22] C. Schwarz, C.-E. Ott, D. Wulsten, E. Brauer, S. Schreivogel, A. Petersen, K. Hassanein, L. Roewer, T. Schmidt, B.M. Willie, G.N. Duda, The interaction of BMP2-induced defect healing in rat and fixator stiffness modulates matrix alignment and contraction, JBMR Plus. 2 (2018) 174–186. doi:10.1002/jbm4.10031.

[23] J. Kopf, A. Petersen, G.N. Duda, P. Knaus, BMP2 and mechanical loading cooperatively regulate immediate early signalling events in the BMP pathway, BMC Biol. 10 (2012) 37. doi:10.1186/1741-7007-10-37.

[24] H. Järveläinen, A. Saino, M. Koulu, T. Wight, R. Penttinen, Extracellular matrix molecules: potential targets in pharmacotherapy, Pharmacol Rev. 61 (2009) 198–223. doi:10.1124/pr.109.001289.provided.

[25] M.D. Shoulders, R.T. Raines, Collagen Structure and Stability, Annu. Rev. Biochem. 78 (2009) 929–958. doi:10.1146/annurev.biochem.77.032207.120833.

[26] D.J. Prockop, K.I. Kivirikko, Collagens: molecular biology, diseases, and potentials for therapy., Annu. Rev. Biochem. 64 (1995) 403–34. doi:10.1146/annurev.bi.64.070195.002155.

[27] J.C. Forlino, A., Cabral, W.A., Barnes, A.M., Marini, New Perspectives on Osteogenesis Imperfecta, Nat. Rev. Endocrinol. 7 (2011) 540–557. doi:10.1038/nrendo.2011.81.New.

[28] J.A.M. Ramshaw, N.K. Shah, B. Brodsky, Gly-X-Y tripeptide frequencies in collagen: A context for host-guest triple-helical peptides, J. Struct. Biol. 122 (1998) 86–91. doi:10.1006/jsbi.1998.3977.

[29] S. Baud, L. Duca, B. Bochicchio, B. Brassart, N. Belloy, A. Pepe, M. Dauchez, L. Martiny, L. Debelle, Elastin peptides in aging and pathological conditions, Biomol. Concepts. 4 (2013) 65–76. doi:10.1515/bmc-2011-0062.

[30] R. Pankov, Fibronectin at a glance, J. Cell Sci. 115 (2002) 3861–3863. doi:10.1242/jcs.00059.

[31] R. V. Iozzo, L. Schaefer, Proteoglycan form and function: A comprehensive nomenclature of proteoglycans, Matrix Biol. 42 (2015) 11–55. doi:10.1016/j.matbio.2015.02.003.

[32] C. Frantz, K.M. Stewart, V.M. Weaver, The extracellular matrix at a glance, J. Cell Sci. 123 (2010) 4195–4200. doi:10.1242/jcs.023820.

[33] R. Fridman, Matrix metalloproteinases., Biochim. Biophys. Acta. 1803 (2010) 1–2. doi:10.1016/j.bbamcr.2010.01.016.

[34] H. Nagase, R. Visse, G. Murphy, Structure and function of matrix metalloproteinases and TIMPs, Cardiovasc. Res. 69 (2006) 562–573. doi:10.1016/j.cardiores.2005.12.002.

[35] E.L. George, E.N. Georges-Labouesse, R.S. Patel-King, H. Rayburn, R.O. Hynes, Defects in mesoderm, neural tube and vascular development in mouse embryos lacking fibronectin., Development. 119 (1993) 1079–1091. doi:10.1083/jcb.200107107.

[36] C. Bonnans, J. Chou, Z. Werb, Remodelling the extracellular matrix in development and disease, Nat. Rev. Mol. Cell Biol. 15 (2014) 786–801. doi:10.1038/nrm3904.

[37] L. Louzao-Martinez, A. Vink, M. Harakalova, F.W. Asselbergs, M.C. Verhaar, C. Cheng, Characteristic adaptations of the extracellular matrix in dilated cardiomyopathy, Int. J. Cardiol. 220 (2016) 634–646. doi:10.1016/j.ijcard.2016.06.253.

[38] M.W. Parker, D. Rossi, M. Peterson, K. Smith, K. Sikstroḿ, E.S. White, J.E. Connett, C.A. Henke, O. Larsson, P.B. Bitterman, Fibrotic extracellular matrix activates a profibrotic positive feedback loop, J. Clin. Invest. 124 (2014) 1622–1635. doi:10.1172/JCI71386.

[39] J.D. Humphrey, E.R. Dufresne, M.A. Schwartz, Mechanotransduction and extracellular matrix homeostasis, Nat. Rev. Mol. Cell Biol. 15 (2014) 802–812. doi:10.1038/nrm3896.

[40] R.O. Hynes, Integrins: Bidirectional, allosteric signaling machines, Cell. 110 (2002) 673–687. doi:10.1016/S0092-8674(02)00971-6.

[41] B. Sinha, D. Köster, R. Ruez, P. Gonnord, M. Bastiani, D. Abankwa, R. V. Stan, G. Butler-Browne, B. Vedie, L. Johannes, N. Morone, R.G. Parton, G. Raposo, P. Sens, C. Lamaze, P. Nassoy, Cells respond to mechanical stress by rapid disassembly of caveolae., Cell. 144 (2011) 402–13. doi:10.1016/j.cell.2010.12.031.

[42] J.D. Humphries, A. Byron, M.J. Humphries, Integrin ligands at a glance, J. Cell Sci. 119 (2006) 3901–3903. doi:10.1242/jcs.03098.

[43] D.A. Calderwood, I.D. Campbell, D.R. Critchley, Talins and kindlins: partners in integrin-mediated adhesion, Nat. Rev. Mol. Cell Biol. 14 (2013) 503–517. doi:10.1038/nrm3624.

[44] E. Goksoy, Y.Q. Ma, X. Wang, X. Kong, D. Perera, E.F. Plow, J. Qin, Structural Basis for the Autoinhibition of Talin in Regulating Integrin Activation, Mol. Cell. 31 (2008) 124–133. doi:10.1016/j.molcel.2008.06.011.

[45] B. Wehrle-Haller, Assembly and disassembly of cell matrix adhesions., Curr. Opin. Cell Biol. 24 (2012) 569–81. doi:10.1016/j.ceb.2012.06.010.

[46] R. Zaidel-Bar, S. Itzkovitz, A. Ma'ayan, R. Iyengar, B. Geiger, Functional atlas of the integrin adhesome., Nat. Cell Biol. 9 (2007) 858–67. doi:10.1038/ncb0807-858.

[47] G. Hannigan, A.A. Troussard, S. Dedhar, Integrin-linked kinase: A cancer therapeutic target unique among its ILK, Nat. Rev. Cancer. 5 (2005) 51–63. doi:10.1038/nrc1524.

[48] M. Delcommenne, C. Tan, V. Gray, L. Rue, J. Woodgett, S. Dedhar, Phosphoinositide-3-OH kinase-dependent regulation of glycogen synthase kinase 3 and protein kinase B/AKT by the integrin-linked kinase., Proc. Natl. Acad. Sci. U. S. A. 95 (1998) 11211–11216. doi:10.1073/pnas.95.19.11211.

[49] J. Du, X. Chen, X. Liang, G. Zhang, J. Xu, L. He, Q. Zhan, X.-Q. Feng, S. Chien, C. Yang, Integrin activation and internalization on soft ECM as a mechanism of induction of stem cell differentiation by ECM elasticity, Proc. Natl. Acad. Sci. 108 (2011) 9466–9471. doi:10.1073/pnas.1106467108.

[50] J. Zhou, P.-L. Lee, C.-I. Lee, S.-Y. Wei, S.H. Lim, T.-E. Lin, S. Chien, J.-J. Chiu, BMP receptor-integrin interaction mediates responses of vascular endothelial Smad1/5 and proliferation to disturbed flow, J. Thromb. Haemost. 11 (2013) 741–755. doi:10.1111/jth.12159.

[51] C.-F. Lai, S.-L. Cheng, αvβ Integrins Play an Essential Role in BMP-2 Induction of Osteoblast Differentiation, J. Bone Miner. Res. 20 (2004) 330–340. doi:10.1359/JBMR.041013.

[52] C. Hiepen, a Benn, a Denkis, I. Lukonin, C. Weise, J.H. Boergermann, P. Knaus, BMP2-induced chemotaxis requires PI3K p55gamma/p110alpha-dependent phosphatidylinositol (3,4,5)-triphosphate production and LL5beta recruitment at the cytocortex, BMC Biol. 12 (2014) 43. doi:10.1186/1741-7007-12-43.

[53] B. Shen, M.K. Delaney, X. Du, Inside-out, outside-in, and inside-outside-in: G protein signaling in integrin-mediated cell adhesion, spreading, and retraction, Curr. Opin. Cell Biol. 24 (2012) 600–606. doi:10.1016/j.ceb.2012.08.011.

[54] V. Conte, D.T. Tambe, J.P. Butler, J.J. Fredberg, E. Anon, E. Bazellieres, R. Vincent, X. Trepat, X. Serra-Picamal, Mechanical waves during tissue expansion, Nat. Phys. 8 (2012) 628–634. doi:10.1038/nphys2355.

[55] Y. Park, K.J.C. Utuje, J. Shin, S. Banerjee, H. Jang, B. Gweon, M.C. Marchetti, J. Notbohm, J.P. Butler, J.J. Fredberg, Cellular Contraction and Polarization Drive Collective Cellular Motion, Biophys. J. 110 (2016) 2729–2738. doi:10.1016/j.bpj.2016.05.019.

[56] M.R. Urist, Bone: formation by autoinduction., Science. 150 (1965) 893–899. doi:10.1126/science.150.3698.893.

[57] T.D. Mueller, J. Nickel, Promiscuity and specificity in BMP receptor activation, FEBS Lett. 586 (2012) 1846–1859. doi:10.1016/j.febslet.2012.02.043.

[58] C. Sieber, J. Kopf, C. Hiepen, P. Knaus, Recent advances in BMP receptor signaling., Cytokine Growth Factor Rev. 20 (2009) 343–55. doi:10.1016/j.cytogfr.2009.10.007.

[59] V.S. Salazar, L.W. Gamer, V. Rosen, BMP signalling in skeletal development, disease and repair., Nat. Rev. Endocrinol. advance on (2016) 203–221. doi:10.1038/nrendo.2016.12.

[60] K.J. Gordon, G.C. Blobe, Role of transforming growth factor-β superfamily signaling pathways in human disease, Biochim. Biophys. Acta - Mol. Basis Dis. 1782 (2008) 197–228. doi:10.1016/j.bbadis.2008.01.006.

[61] K. Ishida, C. Acharya, B. a. Christiansen, J.H.N. Yik, P.E. DiCesare, D.R. Haudenschild, Cartilage oligomeric matrix protein enhances osteogenesis by directly binding and activating bone morphogenetic protein-2, Bone. 55 (2013) 23–35. doi:10.1016/j.bone.2013.03.007.

[62] T. Gründer, C. Gaissmaier, J. Fritz, R. Stoop, P. Hortschansky, J. Mollenhauer, W.K. Aicher, Bone morphogenetic protein (BMP)-2 enhances the expression of type II collagen and aggrecan in chondrocytes embedded in alginate beads, Osteoarthr. Cartil. 12 (2004) 559–567. doi:10.1016/j.joca.2004.04.001.

[63] S.C. Fu, Y.P. Wong, B.P. Chan, H.M. Pau, Y.C. Cheuk, K.M. Lee, K.-M. Chan, The roles of bone morphogenetic protein (BMP) 12 in stimulating the proliferation and matrix production of human patellar tendon fibroblasts, Life Sci. 72 (2003) 2965–2974. doi:10.1016/S0024-3205(03)00169-3.

[64] F. Klatte-Schulz, G. Giese, C. Differ, S. Minkwitz, K. Ruschke, R. Puts, P. Knaus, B. Wildemann, An investigation of BMP-7 mediated alterations to BMP signalling components in human tenocyte-like cells., Sci. Rep. 6 (2016) 29703.

doi:10.1038/srep29703.

[65] X. Yang, L. Long, M. Southwood, N. Rudarakanchana, P.D. Upton, T.K. Jeffery, C. Atkinson, H. Chen, R.C. Trembath, N.W. Morrell, Dysfunctional Smad signaling contributes to abnormal smooth muscle cell proliferation in familial pulmonary arterial hypertension, Circ. Res. 96 (2005) 1053–1063. doi:10.1161/01.RES.0000166926.54293.68.

[66] R.X. Li, W.H. Yiu, S.C.W. Tang, Role of bone morphogenetic protein-7 in renal fibrosis, Front. Physiol. 6 (2015) 1–9. doi:10.3389/fphys.2015.00114.

[67] C. Atkinson, S. Stewart, P.D. Upton, R. Machado, J.R. Thomson, R.C. Trembath, N.W. Morrell, Primary pulmonary hypertension is associated with reduced pulmonary vascular expression of type II bone morphogenetic protein receptor, Circulation. 105 (2002) 1672–1678. doi:10.1161/01.CIR.0000012754.72951.3D.

[68] A. Benn, C. Bredow, I. Casanova, S. Vukičević, P. Knaus, VE-Cadherin facilitates BMP-induced endothelial cell permeability and signaling., J. Cell Sci. 129 (2015) 206–218. doi:10.1242/jcs.179960.

[69] J. Zhong, H. Zou, BMP signaling in axon regeneration, Curr. Opin. Neurobiol. 27C (2014) 127–134. doi:10.1016/j.conb.2014.03.009.

[70] S.J. Newfeld, R.G. Wisotzkey, S. Kumar, Molecular evolution of a developmental pathway: phylogenetic analyses of transforming growth factor-beta family ligands, receptors and Smad signal transducers., Genetics. 152 (1999) 783–95. http://www.ncbi.nlm.nih.gov/pubmed/10353918.

[71] K.J. Gordon, G.C. Blobe, Role of transforming growth factor-β superfamily signaling pathways in human disease., Biochim. Biophys. Acta. 1782 (2008) 197–228. doi:10.1016/j.bbadis.2008.01.006.

[72] O.P. Gautschi, S.P. Frey, R. Zellweger, Bone morphogenetic proteins in clinical applications., ANZ J. Surg. 77 (2007) 626–31. doi:10.1111/j.1445-2197.2007.04175.x.

[73] S.N. Lissenberg-Thunnissen, D.J.J. De Gorter, C.F.M. Sier, I.B. Schipper, Use and efficacy of bone morphogenetic proteins in fracture healing, Int. Orthop. 35 (2011) 1271–1280. doi:10.1007/s00264-011-1301-z.

[74] A.W. James, G. LaChaud, J. Shen, G. Asatrian, V. Nguyen, X. Zhang, K. Ting, C. Soo, A Review of the Clinical Side Effects of Bone Morphogenetic Protein-2, Tissue Eng. Part B Rev. 22 (2016) 284–297. doi:10.1089/ten.teb.2015.0357.

[75] D. Horbelt, A. Denkis, P. Knaus, A portrait of Transforming Growth Factor β superfamily signalling: Background matters, Int. J. Biochem. Cell Biol. 44 (2012) 469–474. doi:10.1016/j.biocel.2011.12.013.

[76] A. Nohe, S. Hassel, M. Ehrlich, F. Neubauer, W. Sebald, Y.I. Henis, P. Knaus, The mode of bone morphogenetic protein (BMP) receptor oligomerization determines different BMP-2 signaling pathways, J. Biol. Chem. 277 (2002) 5330–5338. doi:10.1074/jbc.M102750200.

[77] B.M. Chacko, B.Y. Qin, A. Tiwari, G. Shi, S. Lam, L.J. Hayward, M. de Caestecker, K. Lin, Structural Basis of Heteromeric Smad Protein Assembly in TGF-b Signaling Benoy, Mol. Cell. 15 (2004) 813–823. http://ac.els-cdn.com/S1097276504004381/1-s2.0-S1097276504004381-main.pdf?_tid=0a0494ee-d6b0-11e5-8afc-00000aab0f01&acdnat=1455848907_4527d2b6b05f4052e75c96817afda67c.

[78] Y. Shi, Y.F. Wang, L. Jayaraman, H. Yang, J. Massagué, N.P. Pavletich, Crystal structure of a Smad MH1 domain bound to DNA: Insights on DNA binding in TGF-β signaling, Cell. 94 (1998) 585–594. doi:10.1016/S0092-8674(00)81600-1.

[79] J. Groppe, J. Greenwald, E. Wiater, J. Rodriguez-Leon, A.N. Economides, W.

Kwiatkowski, M. Affolter, W.W. Vale, J.C. Izpisua Belmonte, S. Choe, Structural basis of BMP signalling inhibition by the cystine knot protein Noggin., Nature. 420 (2002) 636–42. doi:10.1038/nature01245.

[80] D. Onichtchouk, Y.G. Chen, R. Dosch, V. Gawantka, H. Delius, J. Massagué, C. Niehrs, Silencing of TGF-β signalling by the pseudoreceptor BAMBI, Nature. 401 (1999) 480–485. doi:10.1038/46794.

[81] M. Sammar, S. Stricker, G.C. Schwabe, C. Sieber, A. Hartung, M. Hanke, I. Oishi, J. Pohl, Y. Minami, W. Sebald, S. Mundlos, P. Knaus, Modulation of GDF5/BRI-b signalling through interaction with the tyrosine kinase receptor Ror2, Genes to Cells. 9 (2004) 1227–1238. doi:10.1111/j.1365-2443.2004.00799.x.

[82] P.J. Halbrooks, R. Ding, J.M. Wozney, G. Bain, Role of RGM coreceptors in bone morphogenetic protein signaling, J. Mol. Signal. 2 (2007) 1–10. doi:10.1186/1750-2187-2-4.

[83] T. Imamura, M. Takase, A. Nishihara, E. Oeda, J.I. Hanai, M. Kawabata, K. Miyazono, Smad6 inhibits signalling by the TGF-β superfamily, Nature. 389 (1997) 622–626. doi:10.1038/39355.

[84] A. Nakao, M. Afrakhte, A. Morén, T. Nakayama, J.L. Christian, R. Heuchel, S. Itoh, M. Kawabata, N.-E. Heldin, C.-H. Heldin, P. ten Dijke, Identification of Smad7, a TGFbeta-inducible antagonist of TGF-beta signalling., Nature. 389 (1997) 631–635. doi:10.1038/39369.

[85] L.C. Fuentealba, E. Eivers, A. Ikeda, C. Hurtado, H. Kuroda, E.M. Pera, E.M. De Robertis, Integrating Patterning Signals: Wnt/GSK3 Regulates the Duration of the BMP/Smad1 Signal, Cell. 131 (2007) 980–993. doi:10.1016/j.cell.2007.09.027.

[86] O. Chaudhuri, L. Gu, D. Klumpers, M. Darnell, S.A. Bencherif, J.C. Weaver, N. Huebsch, H.-P. Lee, E. Lippens, G.N. Duda, D.J. Mooney, Hydrogels with tunable stress relaxation regulate stem cell fate and activity., Nat. Mater. 15 (2016) 326–34. doi:10.1038/nmat4489.

[87] A. Shkumatov, M. Thompson, K.M. Choi, D. Sicard, K. Baek, D.H. Kim, D.J. Tschumperlin, Y.S. Prakash, H. Kong, Matrix stiffness-modulated proliferation and secretory function of the airway smooth muscle cells., Am. J. Physiol. Lung Cell. Mol. Physiol. 308 (2015) L1125-35. doi:10.1152/ajplung.00154.2014.

[88] T. Yeung, P.C. Georges, L. a. Flanagan, B. Marg, M. Ortiz, M. Funaki, N. Zahir, W. Ming, V. Weaver, P. a. Janmey, Effects of substrate stiffness on cell morphology, cytoskeletal structure, and adhesion, Cell Motil. Cytoskeleton. 60 (2005) 24–34. doi:10.1002/cm.20041.

[89] Y.H. Zhang, C.Q. Zhao, L.S. Jiang, L.Y. Dai, Substrate stiffness regulates apoptosis and the mRNA expression of extracellular matrix regulatory genes in the rat annular cells, Matrix Biol. 30 (2011) 135–144. doi:10.1016/j.matbio.2010.10.008.

[90] N. Rosa, R. Simoes, F.D. Magalhães, A.T. Marques, From mechanical stimulus to bone formation: A review, Med. Eng. Phys. 37 (2015) 719–728. doi:10.1016/j.medengphy.2015.05.015.

[91] Q. Kang, M.H. Sun, H. Cheng, Y. Peng, A.G. Montag, A.T. Deyrup, W. Jiang, H.H. Luu, J. Luo, J.P. Szatkowski, P. Vanichakarn, J.Y. Park, Y. Li, R.C. Haydon, T.C. He, Characterization of the distinct orthotopic bone-forming activity of 14 BMPs using recombinant adenovirus-mediated gene delivery, Gene Ther. 11 (2004) 1312–1320. doi:10.1038/sj.gt.3302298.

[92] P. De Biase, R. Capanna, Clinical applications of BMPs., Injury. 36 Suppl 3 (2005) S43–S46. doi:10.1016/j.injury.2005.07.034.

[93] M. Ronga, A. Fagetti, G. Canton, E. Paiusco, M.F. Surace, P. Cherubino, Clinical

applications of growth factors in bone injuries: Experience with BMPs, Injury. 44 (2013) S34–S39. doi:10.1016/S0020-1383(13)70008-1.

[94] J.L. Allen, M.E. Cooke, T. Alliston, ECM stiffness primes the TGF pathway to promote chondrocyte differentiation, Mol. Biol. Cell. 23 (2012) 3731–3742. doi:10.1091/mbc.E12-03-0172.

[95] H.N. Chia, M. Vigen, A.M. Kasko, Effect of substrate stiffness on pulmonary fibroblast activation by TGF- b, Acta Biomater. 8 (2012) 2602–2611. doi:10.1016/j.actbio.2012.03.027.

[96] Z. Li, J.A. Dranoff, E.P. Chan, M. Uemura, J. Sévigny, R.G. Wells, Transforming growth factor-beta and substrate stiffness regulate portal fibroblast activation in culture, Hepatology. 46 (2007) 1246–1256. doi:10.1002/hep.21792.

[97] A. Marinkovic, J.D. Mih, J.-A. Park, F. Liu, D.J. Tschumperlin, Improved throughput traction microscopy reveals pivotal role for matrix stiffness in fibroblast contractility and TGF- responsiveness, AJP Lung Cell. Mol. Physiol. 303 (2012) L169–L180. doi:10.1152/ajplung.00108.2012.

[98] J.S. Park, J.S. Chu, A.D. Tsou, R. Diop, Z. Tang, A. Wang, S. Li, The effect of matrix stiffness on the differentiation of mesenchymal stem cells in response to TGF-??, Biomaterials. 32 (2011) 3921–3930. doi:10.1016/j.biomaterials.2011.02.019.

[99] X.Q. Brown, E. Bartolak-Suki, C. Williams, M.L. Walker, V.M. Weaver, J.Y. Wong, Effect of substrate stiffness and PDGF on the behavior of vascular smooth muscle cells: Implications for atherosclerosis, J. Cell. Physiol. 225 (2010) 115–122. doi:10.1002/jcp.22202.

[100] J. Huynh, F. Bordeleau, C. Kraning-Rush, C.A. Reinhart-King, Substrate Stiffness Regulates PDGF-Induced Circular Dorsal Ruffle Formation Through MLCK, Cell Mol Bioeng. 75 (2013) 1781–1791. doi:10.1007/s11103-011-9767-z.Plastid.

[101] M.L. Previtera, A. Sengupta, Substrate stiffness regulates proinflammatory mediator production through TLR4 activity in macrophages, PLoS One. 10 (2015). doi:10.1371/journal.pone.0145813.

[102] E. Davidson, E.L. Vitters, P.L. van Lent, F.A. van de Loo, W.B. van den Berg, P.M. van der Kraan, Elevated extracellular matrix production and degradation upon bone morphogenetic protein-2 (BMP-2) stimulation point toward a role for BMP-2 in cartilage repair and remodeling, Arthritis Res. Ther. 9 (2007) R102. doi:10.1186/ar2305.

[103] a Haaijman, R.N. D'Souza, a L. Bronckers, S.W. Goei, E.H. Burger, OP-1 (BMP-7) affects mRNA expression of type I, II, X collagen, and matrix Gla protein in ossifying long bones in vitro., J. Bone Miner. Res. 12 (1997) 1815–23. doi:10.1359/jbmr.1997.12.11.1815.

[104] J. Li, S.T. Yoon, W.C. Hutton, Effect of Bone Morphogenetic Protein-2 (BMP-2) on Matrix Production, Other BMPs, and BMP Receptors in Rat Intervertebral Disc Cells, J. Spinal Disord. Tech. 17 (2004) 423–428. doi:10.1097/01.bsd.0000112084.85112.5d.

[105] J. Li, K.S. Kim, J.S. Park, W. a. Elmer, W.C. Hutton, S.T. Yoon, BMP-2 and CDMP-2: stimulation of chondrocyte production of proteoglycan, J. Orthop. Sci. 8 (2003) 829–835. doi:10.1007/s00776-003-0719-6.

[106] T. Rothhammer, S. Braig, A.-K. Bosserhoff, Bone morphogenetic proteins induce expression of metalloproteinases in melanoma cells and fibroblasts, Eur. J. Cancer. 44 (2008) 2526–2534. doi:10.1016/j.ejca.2008.07.029.

[107] X. Wang, R.E. Harris, L.J. Bayston, H.L. Ashe, Type IV collagens regulate BMP signalling in Drosophila, Nature. 455 (2008) 72–77. doi:nature07214 [pii]\r10.1038/nature07214.

[108] X.-D. Chen, The small leucine-rich proteoglycan biglycan modulates BMP-4-induced osteoblast differentiation, FASEB J. 18 (2004) 948–958. doi:10.1096/fj.03-0899com.

[109] Y. Du, Y. Wang, L. Wang, B. Liu, Q. Tian, C. -j. Liu, T. Zhang, Q. Xu, Y. Zhu, O. Ake, Y. Qi, C. Tang, W. Kong, X. Wang, Cartilage Oligomeric Matrix Protein Inhibits Vascular Smooth Muscle Calcification by Interacting With Bone Morphogenetic Protein-2, Circ. Res. 108 (2011) 917–928. doi:10.1161/CIRCRESAHA.110.234328.

[110] O. Fromigué, P.J. Marie, a Lomri, Bone morphogenetic protein-2 and transforming growth factor-β2 interact to modulate human bone marrow stromal cell proliferation and differentiation, J Cell Biochem. 68 (1998) 411–426. doi:10.1002/(SICI)1097-4644(19980315)68:4<411::AID-JCB2>3.0.CO;2-T.

[111] L. Gilbertson, S.-H. Ahn, P.-N. Teng, R.K. Studer, C. Niyibizi, J.D. Kang, The effects of recombinant human bone morphogenetic protein-2, recombinant human bone morphogenetic protein-12, and adenoviral bone morphogenetic protein-12 on matrix synthesis in human annulus fibrosis and nucleus pulposus cells, Spine J. 8 (2008) 449–456. doi:10.1016/j.spinee.2006.11.006.

[112] K.E. Gregory, R.N. Ono, N.L. Charbonneau, C.L. Kuo, D.R. Keene, H.P. Bächingeri, L.Y. Sakai, The prodomain of BMP-7 targets the BMP-7 complex to the extracellular matrix, J. Biol. Chem. 280 (2005) 27970–27980. doi:10.1074/jbc.M504270200.

[113] W. Hu, Glycosaminoglycan chains of biglycan promote bone morphogenetic protein-4-induced osteoblast differentiation, Int. J. Mol. Med. (2012) 1075–1080. doi:10.3892/ijmm.2012.1091.

[114] R. Jasuja, B.L. Allen, W.N. Pappano, a. C. Rapraeger, D.S. Greenspan, Cell-surface Heparan Sulfate Proteoglycans Potentiate Chordin Antagonism of Bone Morphogenetic Protein Signaling and Are Necessary for Cellular Uptake of Chordin, J. Biol. Chem. 279 (2004) 51289–51297. doi:10.1074/jbc.M408129200.

[115] a. Krase, R. Abedian, E. Steck, C. Hurschler, W. Richter, BMP activation and Wnt-signalling affect biochemistry and functional biomechanical properties of cartilage tissue engineering constructs, Osteoarthr. Cartil. 22 (2014) 284–292. doi:10.1016/j.joca.2013.11.011.

[116] C. Laflamme, M. Rouabhia, Effect of BMP-2 and BMP-7 homodimers and a mixture of BMP-2/BMP-7 homodimers on osteoblast adhesion and growth following culture on a collagen scaffold, Biomed. Mater. 3 (2008) 15008. doi:10.1088/1748-6041/3/1/015008.

[117] F. Lecanda, L. V Avioli, S.-L. Cheng, Regulation of Bone Matrix Protein Expression and Induction of Differentiation of Human Osteoblasts and Human Bone Marrow Stromal Cells by Bone Morhogenetic Protein-2, J Cell Biochem. 67 (1997) 386–398.

[118] M. Moreno, R. Muñoz, F. Aroca, M. Labarca, E. Brandan, J. Larraín, Biglycan is a new extracellular component of the Chordin–BMP4 signaling pathway, EMBO J. 24 (2005) 1397–1405. doi:10.1038/sj.emboj.7600615.

[119] E.R. Neptune, P. a. Frischmeyer, D.E. Arking, L. Myers, T.E. Bunton, B. Gayraud, F. Ramirez, L.Y. Sakai, H.C. Dietz, Dysregulation of TGF-β activation contributes to pathogenesis in Marfan syndrome, Nat. Genet. 33 (2003) 407–411. doi:10.1038/ng1116.

[120] P. Owens, H. Polikowsky, M.W. Pickup, A.E. Gorska, B. Jovanovic, A.K. Shaw, S. V. Novitskiy, C.C. Hong, H.L. Moses, Bone Morphogenetic Proteins Stimulate Mammary Fibroblasts to Promote Mammary Carcinoma Cell Invasion, PLoS One. 8 (2013) e67533. doi:10.1371/journal.pone.0067533.

[121] F. Ramirez, D.B. Rifkin, Extracellular microfibrils: contextual platforms for TGF?? and BMP signaling, Curr. Opin. Cell Biol. 21 (2009) 616–622. doi:10.1016/j.ceb.2009.05.005.

[122] G. Sengle, V. Carlberg, S.F. Tufa, N.L. Charbonneau, S. Smaldone, E.J. Carlson, F.

Ramirez, D.R. Keene, L.Y. Sakai, Abnormal Activation of BMP Signaling Causes Myopathy in Fbn2 Null Mice, PLoS Genet. 11 (2015) 1–25. doi:10.1371/journal.pgen.1005340.

[123] Y. Shintani, M. Maeda, N. Chaika, K.R. Johnson, M.J. Wheelock, Collagen I Promotes Epithelial-to-Mesenchymal Transition in Lung Cancer Cells via Transforming Growth Factor–β Signaling, Am. J. Respir. Cell Mol. Biol. 38 (2008) 95–104. doi:10.1165/rcmb.2007-0071OC.

[124] A.L. Sieron, N. Louneva, A. Fertala, Site-Specific Interaction of Bone Morphogenetic Protein 2 With Procollagen Ii, Cytokine. 18 (2002) 214–221. doi:10.1006/cyto.2002.1035.

[125] M. Suzawa, Y. Tamura, S. Fukumoto, K. Miyazono, T. Fujita, S. Kato, Y. Takeuchi, Stimulation of Smad1 transcriptional activity by Ras-extracellular signal-regulated kinase pathway: a possible mechanism for collagen-dependent osteoblastic differentiation., J. Bone Miner. Res. 17 (2002) 240–8. doi:10.1359/jbmr.2002.17.2.240.

[126] J.T. Thomas, P. Canelos, F.P. Luyten, M. Moos, Xenopus SMOC-1 Inhibits Bone Morphogenetic Protein Signaling Downstream of Receptor Binding and Is Essential for Postgastrulation Development in Xenopus, J. Biol. Chem. 284 (2009) 18994–19005. doi:10.1074/jbc.M807759200.

[127] X. Yang, S.K. Trehan, Y. Guan, C. Sun, D.C. Moore, C.T. Jayasuriya, Q. Chen, Matrilin-3 Inhibits Chondrocyte Hypertrophy as a Bone Morphogenetic Protein-2 Antagonist, J. Biol. Chem. 289 (2014) 34768–34779. doi:10.1074/jbc.M114.583104.

[128] H.L. Ashe, Modulation of BMP signalling by integrins, Biochem. Soc. Trans. 44 (2016) 1465–1473. doi:10.1042/BST20160111.

[129] Y. Tamura, Y. Takeuchi, M. Suzawa, S. Fukumoto, M. Kato, K. Miyazono, T. Fujita, Focal Adhesion Kinase Activity Is Required for Bone Morphogenetic Protein-Smad1 Signaling and Osteoblastic Differentiation in Murine MC3T3-E1 Cells, J. Bone Miner. Res. 16 (2001) 1772–1779.

[130] L. Audigé, D. Griffin, M. Bhandari, J. Kellam, T.P. Rüedi, Path analysis of factors for delayed healing and nonunion in 416 operatively treated tibial shaft fractures., Clin. Orthop. Relat. Res. 438 (2005) 221–32. doi:10.1097/01.blo.0000163836.66906.74.

[131] R. Dimitriou, E. Jones, D. McGonagle, P. V. Giannoudis, Bone regeneration: current concepts and future directions., BMC Med. 9 (2011) 1–10. doi:10.1186/1741-7015-9-66.

[132] P. V Giannoudis, H. Dinopoulos, E. Tsiridis, Bone substitutes: an update., Injury. 36 Suppl 3 (2005) S20-7. doi:10.1016/j.injury.2005.07.029.

[133] P. V. Giannoudis, T.A. Einhorn, Bone morphogenetic proteins in musculoskeletal medicine., Injury. 40 Suppl 3 (2009) S1-3. doi:10.1016/S0020-1383(09)00642-1.

[134] K.R. Garrison, S. Donell, J. Ryder, I. Shemilt, M. Mugford, I. Harvey, F. Song, Clinical effectiveness and cost-effectiveness of bone morphogenetic proteins in the non-healing of fractures and spinal fusion: a systematic review, Health Technol. Assess. (Rockv). 11 (2007).

[135] E. Huber, A.-M. Pobloth, N. Bormann, N. Kolarczik, K. Schmidt-Bleek, H. Schell, P. Schwabe, G.N. Duda, B. Wildemann, * Demineralized Bone Matrix as a Carrier for Bone Morphogenetic Protein-2: Burst Release Combined with Long-Term Binding and Osteoinductive Activity Evaluated In Vitro and In Vivo., Tissue Eng. Part A. 23 (2017) 1321–1330. doi:10.1089/ten.TEA.2017.0005.

[136] B.R. Seo, P. Bhardwaj, S. Choi, J. Gonzalez, R.C.A. Eguiluz, K. Wang, S. Mohanan, P.G. Morris, B. Du, X.K. Zhou, L.T. Vahdat, A. Verma, O. Elemento, C.A. Hudis, R.M. Williams, D. Gourdon, A.J. Dannenberg, C. Fischbach, Obesity-dependent changes in interstitial ECM mechanics promote breast tumorigenesis, Sci. Transl. Med. 7 (2015).

doi:10.1126/scitranslmed.3010467.

[137] K.E. Kubow, R. Vukmirovic, L. Zhe, E. Klotzsch, M.L. Smith, D. Gourdon, S. Luna, V. Vogel, Mechanical forces regulate the interactions of fibronectin and collagen I in extracellular matrix., Nat. Commun. 6 (2015) 8026. doi:10.1038/ncomms9026.

[138] S. Arnoldini, A. Moscaroli, M. Chabria, M. Hilbert, S. Hertig, R. Schibli, M. Béhé, V. Vogel, Novel peptide probes to assess the tensional state of fibronectin fibers in cancer, Nat. Commun. 8 (2017). doi:10.1038/s41467-017-01846-0.

[139] B. Herrera, G.J. Inman, A rapid and sensitive bioassay for the simultaneous measurement of multiple bone morphogenetic proteins. Identification and quantification of BMP4, BMP6 and BMP9 in bovine and human serum., BMC Cell Biol. 10 (2009) 20. doi:10.1186/1471-2121-10-20.

[140] H. Schoof, J. Apel, I. Heschel, G. Rau, Control of Pore Structure and Size in Freeze-Dried Collagen Sponges, Biomed Mater Res. 58 (2001) 352–357. doi:10.1002/jbm.1028.

[141] M.W. Pfaffl, A new mathematical model for relative quantification in real-time RT-PCR., Nucleic Acids Res. 29 (2001) e45. doi:10.1093/nar/29.9.e45.

[142] C. Ramakers, J.M. Ruijter, R.H. Lekanne Deprez, A.F.M. Moorman, Assumption-free analysis of quantitative real-time polymerase chain reaction (PCR) data, Neurosci. Lett. 339 (2003) 62–66. doi:10.1016/S0304-3940(02)01423-4.

[143] B. Kappler, P. Anic, M. Becker, A. Bader, K. Klose, O. Klein, B. Oberwallner, Y.H. Choi, V. Falk, C. Stamm, The cytoprotective capacity of processed human cardiac extracellular matrix, J. Mater. Sci. Mater. Med. 27 (2016) 1–13. doi:10.1007/s10856-016-5730-5.

[144] M.L. Jarman-Smith, T. Bodamyali, C. Stevens, J.A. Howell, M. Horrocks, J.B. Chaudhuri, Porcine collagen crosslinking , degradation and its capability for fibroblast adhesion and proliferation, J. Mater. Sci. Mater. Med. 15 (2004) 925–932. doi:10.1023/B:JMSM.0000036281.47596.cc.

[145] E.G. Canty, K.E. Kadler, Procollagen trafficking, processing and fibrillogenesis., J. Cell Sci. 118 (2005) 1341–1353. doi:10.1242/jcs.01731.

[146] A. Petersen, P. Joly, C. Bergmann, G. Korus, G.N. Duda, The Impact of Substrate Stiffness and Mechanical Loading on Fibroblast-Induced Scaffold Remodeling, Tissue Eng. Part A. 18 (2012) 1804–1817. doi:10.1089/ten.tea.2011.0514.

[147] T.W. Gilbert, T.L. Sellaro, S.F. Badylak, Decellularization of tissues and organs, Biomaterials. 27 (2006) 3675–3683. doi:10.1016/j.biomaterials.2006.02.014.

[148] T.J. Keane, I.T. Swinehart, S.F. Badylak, Methods of tissue decellularization used for preparation of biologic scaffolds and in vivo relevance, Methods. 84 (2015) 25–34. doi:10.1016/j.ymeth.2015.03.005.

[149] P.M. Crapo, T.W. Gilbert, S.F. Badylak, An overview of tissue and whole organ decellularization processes, Biomaterials. 32 (2011) 3233–3243. doi:10.1016/j.biomaterials.2011.01.057.

[150] M.C. Prewitz, F.P. Seib, M. von Bonin, J. Friedrichs, A. Stißel, C. Niehage, K. Müller, K. Anastassiadis, C. Waskow, B. Hoflack, M. Bornhäuser, C. Werner, Tightly anchored tissue-mimetic matrices as instructive stem cell microenvironments, Nat. Methods. 10 (2013) 788–794. doi:10.1038/nmeth.2523.

[151] X. Chen, O. Nadiarynkh, S. Plotnikov, P.J. Campagnola, Second harmonic generation microscopy for quantitative analysis of collagen fibrillar structure, Nat. Protoc. 7 (2012) 654–669. doi:10.1038/nprot.2012.009.

[152] R. Rezakhaniha, A. Agianniotis, J.T.C. Schrauwen, A. Griffa, D. Sage, C.V.C. Bouten, F.N. Van De Vosse, M. Unser, N. Stergiopulos, Experimental investigation of collagen

waviness and orientation in the arterial adventitia using confocal laser scanning microscopy, Biomech. Model. Mechanobiol. 11 (2012) 461–473. doi:10.1007/s10237-011-0325-z.

[153] A. Boudaoud, A. Burian, D. Borowska-Wykręt, M. Uyttewaal, R. Wrzalik, D. Kwiatkowska, O. Hamant, FibrilTool, an ImageJ plug-in to quantify fibrillar structures in raw microscopy images., Nat. Protoc. 9 (2014) 457–463. doi:10.1038/nprot.2014.024.

[154] M. Doube, M.M. Klosowski, I. Arganda-Carreras, F.P. Cordelières, R.P. Dougherty, J.S. Jackson, B. Schmid, J.R. Hutchinson, S.J. Shefelbine, BoneJ: Free and extensible bone image analysis in ImageJ, Bone. 47 (2010) 1076–1079. doi:10.1016/j.bone.2010.08.023.

[155] J.Y. Tinevez, N. Perry, J. Schindelin, G.M. Hoopes, G.D. Reynolds, E. Laplantine, S.Y. Bednarek, S.L. Shorte, K.W. Eliceiri, TrackMate: An open and extensible platform for single-particle tracking, Methods. 115 (2017) 80–90. doi:10.1016/j.ymeth.2016.09.016.

[156] S. Plotnikov, B. Sabass, U. Schwarz, C.M. Waterman, High-Resolution Traction Force Microscopy, Methods Cell Biol. 123 (2014) 367–394. doi:10.1016/B978-0-12-420138-5.00020-3.

[157] J.L. Martiel, A. Leal, L. Kurzawa, M. Balland, I. Wang, T. Vignaud, Q. Tseng, M. Théry, Measurement of cell traction forces with ImageJ, Methods Cell Biol. 125 (2015) 269–287. doi:10.1016/bs.mcb.2014.10.008.

[158] Q. Tseng, E. Duchemin-Pelletier, A. Deshiere, M. Balland, H. Guillou, O. Filhol, M. Thery, Spatial organization of the extracellular matrix regulates cell-cell junction positioning, Proc. Natl. Acad. Sci. 109 (2012) 1506–1511. doi:10.1073/pnas.1106377109.

[159] J.J. Tomasek, G. Gabbiani, B. Hinz, C. Chaponnier, R. a Brown, Myofibroblasts and mechano-regulation of connective tissue remodelling., Nat. Rev. Mol. Cell Biol. 3 (2002) 349–63. doi:10.1038/nrm809.

[160] M.S. Sakar, J. Eyckmans, R. Pieters, D. Eberli, B.J. Nelson, C.S. Chen, Cellular forces and matrix assembly coordinate fibrous tissue repair., Nat. Commun. 7 (2016) 11036. doi:10.1038/ncomms11036.

[161] K.S. Midwood, L.V. Williams, J.E. Schwarzbauer, Tissue repair and the dynamics of the extracellular matrix, Int. J. Biochem. Cell Biol. 36 (2004) 1031–1037. doi:10.1016/j.biocel.2003.12.003.

[162] W.R. Legant, A. Pathak, M.T. Yang, V.S. Deshpande, R.M. McMeeking, C.S. Chen, Microfabricated tissue gauges to measure and manipulate forces from 3D microtissues., Proc. Natl. Acad. Sci. U. S. A. 106 (2009) 10097–102. doi:10.1073/pnas.0900174106.

[163] E. Brauer, E. Lippens, O. Klein, G. Nebrich, S. Schreivogel, G. Korus, G.N. Duda, A. Petersen, Collagen Fibrils Mechanically Contribute to Tissue Contraction in an In Vitro Wound Healing Scenario., Adv. Sci. (Weinheim, Baden-Wurttemberg, Ger. 6 (2019) 1801780. doi:10.1002/advs.201801780.

[164] C.M. Bidan, P. Kollmannsberger, V. Gering, S. Ehrig, P. Joly, A. Petersen, V. Vogel, P. Fratzl, J.W.C. Dunlop, Gradual conversion of cellular stress patterns into pre-stressed matrix architecture during in vitro tissue growth., J. R. Soc. Interface. 13 (2016) 20160136. doi:10.1098/rsif.2016.0136.

[165] H. Duong, B. Wu, B. Tawil, Modulation of 3D Fibrin Matrix Stiffness by Intrinsic Fibrinogen–Thrombin Compositions and by Extrinsic Cellular Activity, Tissue Eng. Part A. 15 (2009) 1865–1876. doi:10.1089/ten.tea.2008.0319.

[166] L. Van De Water, S. Varney, J.J. Tomasek, Mechanoregulation of the Myofibroblast in Wound Contraction, Scarring, and Fibrosis: Opportunities for New Therapeutic Intervention, Adv. Wound Care. 2 (2013) 122–141. doi:10.1089/wound.2012.0393.

[167] B. Hinz, Formation and function of the myofibroblast during tissue repair, J. Invest.

Dermatol. 127 (2007) 526–537. doi:10.1038/sj.jid.5700613.

[168] X. Wang, W. Song, N. Kawazoe, G. Chen, The osteogenic differentiation of mesenchymal stem cells by controlled cell-cell interaction on micropatterned surfaces, J. Biomed. Mater. Res. - Part A. 101 (2013) 3388–3395. doi:10.1002/jbm.a.34645.

[169] M.T. Wolf, K.A. Daly, E.P. Brennan-Pierce, S.A. Johnson, C.A. Carruthers, A. D'Amore, S.P. Nagarkar, S.S. Velankar, S.F. Badylak, A hydrogel derived from decellularized dermal extracellular matrix, Biomaterials. 33 (2012) 7028–7038. doi:10.1016/j.biomaterials.2012.06.051.

[170] M.J. Sawkins, W. Bowen, P. Dhadda, H. Markides, L.E. Sidney, A.J. Taylor, F.R.A.J. Rose, S.F. Badylak, K.M. Shakesheff, L.J. White, Hydrogels derived from demineralized and decellularized bone extracellular matrix, Acta Biomater. 9 (2013) 7865–7873. doi:10.1016/j.actbio.2013.04.029.

[171] M.F. Pittenger, A.M. Mackay, S.C. Beck, R.K. Jaiswal, R. Douglas, J.D. Mosca, M.A. Moorman, D.W. Simonetti, S. Craig, D.R. Marshak, Multilineage potential of adult human mesenchymal stem cells., Science. 284 (1999) 143–7. http://www.ncbi.nlm.nih.gov/pubmed/10102814.

[172] C. Vater, P. Kasten, M. Stiehler, Culture media for the differentiation of mesenchymal stromal cells, Acta Biomater. 7 (2011) 463–477. doi:10.1016/j.actbio.2010.07.037.

[173] R.S. Fischer, K.A. Myers, M.L. Gardel, C.M. Waterman, Stiffness-controlled three-dimensional extracellular matrices for high-resolution imaging of cell behavior, Nat. Protoc. 7 (2012) 2056–2066. doi:10.1038/nprot.2012.127.

[174] A. Herrera, J. Hellwig, H. Leemhuis, R. von Klitzing, I. Heschel, G.N. Duda, A. Petersen, From macroscopic mechanics to cell-effective stiffness within highly aligned macroporous collagen scaffolds, Mater. Sci. Eng. C. 103 (2019) 109760. doi:10.1016/j.msec.2019.109760.

[175] S.A. Harris, R.J. Enger, B.L. Riggs, T.C. Spelsberg, Development and characterization of a conditionally immortalized human fetal osteoblastic cell line., J. Bone Miner. Res. 10 (1995) 178–86. doi:10.1002/jbmr.5650100203.

[176] R. McBeath, D.M. Pirone, C.M. Nelson, K. Bhadriraju, C.S. Chen, Cell shape, cytoskeletal tension, and RhoA regulate stem cell lineage commitment, Dev. Cell. 6 (2004) 483–495. doi:10.1016/S1534-5807(04)00075-9.

[177] J. Swift, I.L. Ivanovska, A. Buxboim, T. Harada, P.C.D.P. Dingal, J. Pinter, J.D. Pajerowski, K.R. Spinler, J.W. Shin, M. Tewari, F. Rehfeldt, D.W. Speicher, D.E. Discher, Nuclear lamin-A scales with tissue stiffness and enhances matrix-directed differentiation, Science (80-.). 341 (2013). doi:10.1126/science.1240104.

[178] K. Schmidt-Bleek, A. Petersen, A. Dienelt, C. Schwarz, G.N. Duda, Initiation and early control of tissue regeneration - bone healing as a model system for tissue regeneration., Expert Opin. Biol. Ther. 14 (2014) 247–59. doi:10.1517/14712598.2014.857653.

[179] M. Marenzana, N. Wilson-Jones, V. Mudera, R.A. Brown, The origins and regulation of tissue tension: Identification of collagen tension-fixation process in vitro, Exp. Cell Res. 312 (2006) 423–433. doi:10.1016/j.yexcr.2005.11.005.

[180] P. Kollmannsberger, C.M. Bidan, J.W.C. Dunlop, P. Fratzl, V. Vogel, Tensile forces drive a reversible fibroblast-to-myofibroblast transition during tissue growth in engineered clefts., Sci. Adv. 4 (2018) eaao4881. doi:10.1126/sciadv.aao4881.

[181] M. Rumpler, A. Woesz, J.W.. Dunlop, J.T. van Dongen, P. Fratzl, The effect of geometry on three-dimensional tissue growth, J. R. Soc. Interface. 5 (2008) 1173–1180. doi:10.1098/rsif.2008.0064.

[182] C. Storm, J.J. Pastore, F.C. MacKintosh, T.C. Lubensky, P.A. Janmey, Nonlinear

elasticity in biological gels., Nature. 435 (2005) 191–4. doi:10.1038/nature03521.

[183] O. Moreno-Arotzena, J.G. Meier, C. Del Amo, J.M. García-Aznar, Characterization of Fibrin and Collagen Gels for Engineering Wound Healing Models., Mater. (Basel, Switzerland). 8 (2015) 1636–1651. doi:10.3390/ma8041636.

[184] P. Joly, G.N. Duda, M. Schöne, P.B. Welzel, U. Freudenberg, C. Werner, A. Petersen, Geometry-Driven Cell Organization Determines Tissue Growths in Scaffold Pores: Consequences for Fibronectin Organization, PLoS One. 8 (2013) e73545. doi:10.1371/journal.pone.0073545.

[185] M. Tamada, T.D. Perez, W.J. Nelson, M.P. Sheetz, Two distinct modes of myosin assembly and dynamics during epithelial wound closure., J. Cell Biol. 176 (2007) 27–33. doi:10.1083/jcb.200609116.

[186] A. Brugués, E. Anon, V. Conte, J.H. Veldhuis, M. Gupta, J. Colombelli, J.J. Muñoz, G.W. Brodland, B. Ladoux, X. Trepat, Forces driving epithelial wound healing., Nat. Phys. 10 (2014) 683–690. doi:10.1038/nphys3040.

[187] J. Steinwachs, C. Metzner, K. Skodzek, N. Lang, I. Thievessen, C. Mark, S. Münster, K.E. Aifantis, B. Fabry, Three-dimensional force microscopy of cells in biopolymer networks., Nat. Methods. 13 (2016) 171–6. doi:10.1038/nmeth.3685.

[188] W.R. Legant, C.K. Choi, J.S. Miller, L. Shao, L. Gao, E. Betzig, C.S. Chen, Multidimensional traction force microscopy reveals out-of-plane rotational moments about focal adhesions., Proc. Natl. Acad. Sci. U. S. A. 110 (2013) 881–6. doi:10.1073/pnas.1207997110.

[189] W.R. Legant, J.S. Miller, B.L. Blakely, D.M. Cohen, G.M. Genin, C.S. Chen, Measurement of mechanical tractions exerted by cells in three-dimensional matrices., Nat. Methods. 7 (2010) 969–71. doi:10.1038/nmeth.1531.

[190] L. Kurzawa, B. Vianay, F. Senger, T. Vignaud, L. Blanchoin, M. Théry, Dissipation of contractile forces: the missing piece in cell mechanics., Mol. Biol. Cell. 28 (2017) 1825–1832. doi:10.1091/mbc.E16-09-0672.

[191] R. Montesano, L. Orci, Transforming growth factor beta stimulates collagen-matrix contraction by fibroblasts : Implications for wound healing, Proc. Natl. Acad. Sci. U. S. A. 85 (1988) 4894–4897.

[192] I. Darby, O. Skalli, G. Gabbiani, Alpha-smooth muscle actin is transiently expressed by myofibroblasts during experimental wound healing., Lab. Invest. 63 (1990) 21–9. http://www.ncbi.nlm.nih.gov/pubmed/2197503.

[193] T.A. Wynn, Cellular and molecular mechanisms of fibrosis., J. Pathol. 214 (2008) 199–210. doi:10.1002/path.2277.

[194] N. Ghosh-Choudhury, S.L. Abboud, B. Chandrasekar, G. Ghosh Choudhury, BMP-2 regulates cardiomyocyte contractility in a phosphatidylinositol 3 kinase-dependent manner., FEBS Lett. 544 (2003) 181–4. doi:10.1016/S0014-5793(03)00507-6.

[195] G. Konstantinidis, A. Moustakas, C. Stournaras, Regulation of myosin light chain function by BMP signaling controls actin cytoskeleton remodeling., Cell. Physiol. Biochem. 28 (2011) 1031–44. doi:10.1159/000335790.

[196] R. Pogue, K. Lyons, BMP Signaling in the Cartilage Growth Plate, Curr. Top. Dev. Biol. 76 (2006) 1–48. doi:10.1016/S0070-2153(06)76001-X.

[197] A. Buxboim, I.L. Ivanovska, D.E. Discher, Matrix elasticity, cytoskeletal forces and physics of the nucleus: how deeply do cells “feel” outside and in?, J. Cell Sci. 123 (2010) 297–308. doi:10.1242/jcs.041186.

[198] Y.-K. Wang, X. Yu, D.M. Cohen, M. a. Wozniak, M.T. Yang, L. Gao, J. Eyckmans, C.S.

Chen, Bone Morphogenetic Protein-2-Induced Signaling and Osteogenesis Is Regulated by Cell Shape, RhoA/ROCK, and Cytoskeletal Tension, Stem Cells Dev. 21 (2012) 1176–1186. doi:10.1089/scd.2011.0293.

[199] B.F. Kennedy, M.L. McFetridge, D.D. Sampson, A.J. Engler, B.-N. Vo, K. Bieback, J.L. Young, H. Taylor-Weiner, D.Y. Kim, A.W. Holle, P. Wijesinghe, Y.S. Choi, J.H. Wen, A.R. Lee, J.P. Spatz, W.J. Hadden, Stem cell migration and mechanotransduction on linear stiffness gradient hydrogels, Proc. Natl. Acad. Sci. 114 (2017) 5647–5652. doi:10.1073/pnas.1618239114.

[200] A.J. Salgado, O.P. Coutinho, R.L. Reis, Bone tissue engineering: State of the art and future trends, Macromol. Biosci. 4 (2004) 743–765. doi:10.1002/mabi.200400026.

[201] A.-M. Pobloth, H. Schell, A. Petersen, K. Beierlein, C. Kleber, K. Schmidt-Bleek, G.N. Duda, Tubular open-porous β-tricalcium phosphate polycaprolactone scaffolds as guiding structure for segmental bone defect regeneration in a novel sheep model., J. Tissue Eng. Regen. Med. 12 (2018) 897–911. doi:10.1002/term.2446.

[202] A.-M. Pobloth, S. Checa, H. Razi, A. Petersen, J.C. Weaver, K. Schmidt-Bleek, M. Windolf, A.Á. Tatai, C.P. Roth, K.-D. Schaser, G.N. Duda, P. Schwabe, Mechanobiologically optimized 3D titanium-mesh scaffolds enhance bone regeneration in critical segmental defects in sheep., Sci. Transl. Med. 10 (2018) eaam8828. doi:10.1126/scitranslmed.aam8828.

[203] A. Lueckgen, D.S. Garske, A. Ellinghaus, R.M. Desai, A.G. Stafford, D.J. Mooney, G.N. Duda, A. Cipitria, Hydrolytically-degradable click-crosslinked alginate hydrogels., Biomaterials. 181 (2018) 189–198. doi:10.1016/j.biomaterials.2018.07.031.

[204] M. Pumberger, T.H. Qazi, M.C. Ehrentraut, M. Textor, J. Kueper, G. Stoltenburg-Didinger, T. Winkler, P. von Roth, S. Reinke, C. Borselli, C. Perka, D.J. Mooney, G.N. Duda, S. Geißler, Synthetic niche to modulate regenerative potential of MSCs and enhance skeletal muscle regeneration, Biomaterials. 99 (2016) 95–108. doi:10.1016/j.biomaterials.2016.05.009.

Supplemental Information

Supplement 1

Table modified from Shoulders et al.[25]. Subscripts indicate abundance in triple helix. Colors refer to classes of collagens: fibrillar (grey), network forming collagens (light yellow), FACITs (light blue), MACITs (light green), MULTIPLEXINs (light red).

type	Isoforms & composition	Distribution	pathology
I	$\alpha1[I]_2\alpha2[I]$	Tendon, bone, dermis, ligament	OI, Ehlers-Danlos, osteoporosis
II	$\alpha1[II]_3$	Cartilage	Osteoarthrosis, chondrodysplasis
III	$\alpha1[III]_3$	Skin, blood vessels, intestine	Ehlers-Danlos
IV	$\alpha1[IV]_2\alpha2[IV]$ $\alpha3[IV]\alpha4[IV]$ $\alpha5[IV]$ $\alpha5[IV]_2\alpha6[IV]$	Basement membrane	Alport syndrome
V	$\alpha1[V]_3$ $\alpha1[V]_2\alpha2[V]$ $\alpha1[V]\alpha2[V]$ $\alpha3[V]$	Dermis, bone, cornea, placenta	Ehlers-Danlos
VI	$\alpha1[VI]\alpha2[VI]$ $\alpha3[VI]$ $\alpha1[VI]\alpha2[VI]$ $\alpha4[VI]$	Bone, cartilage, dermis	Bethlem myopathy
VII	$\alpha1[VII]_2\alpha2[VII]$	Dermis, bladder	Epidermolysis bullosa acquisita
VIII	$\alpha1[VIII]_3$ $\alpha2[VIII]_3$ $\alpha1[VIII]_2\alpha2[VIII]$	Dermis, brain, heart, kidney	Fuchs endothelia corneal dystrophy
IX	$\alpha1[IX]\alpha2[IX]$ $\alpha3[IX]$	Cartilage, cornea, vitreous	Osteoarthrosis
X	$\alpha1[X]_3$	Cartilage	Chondrodysplasia
XI	$\alpha1[XI]\alpha2[XI]$ $\alpha3[XI]$	Cartilage, IVDs	Chondrodysplasia
XII	$\alpha1[XII]_3$	Dermis, tendon	-
XIII	-	Endothelial cells, dermis, eye, heart	-
XIV	$\alpha1[XIV]_3$	Bone, dermis, cartilage	-
XV	-	Capillaries, testis, kidney, heart	-
XVI	-	Dermis, kidney	-
XVII	$\alpha1[XVII]_3$	-	-
XVIII	-	Basement membrane	Knobloch syndrome
XIX	-	Basement membrane	-
XX	-	Cornea	-
XXI	-	Stomach, kidney	-
XXII	-	Tissue junctions	-
XXIII	-	Heart, retina	-
XXIV	-	Bone, cornea	-

type	Isoforms & composition	Distribution	pathology
XXV	-	Brain, heart, testis	-
XXVI	-	Testis, ovary	-
XXVII	-	Cartilage	-
XXVIII	-	Dermis, sciatic nerve	-

Supplement 2

Summary of different staining protocols.

Target protein	Cat. | manufacturer	reactivity	host species	clonality
Fibronectin	#ab23750 | abcam	mouse, human	rabbit	polyclonal

All steps were conducted at room temperature if not otherwise stated. For buffer recipes, check other sources.

General volumes: all washing steps in a 24well plate with 1ml, blocking/staining solutions in a 48well with 300µl

	Step	Time	Description		
Day 1	washing	3 x 5 min	TBS-T/0.025%		
	washing	1 x 5 min	TBS		
	blocking I	1 x 10 min	**1% BSA**/TBS		
	blocking II	1 x 30 min	**5% NDS/1% BSA**/TBS		
	1st antibody	o/n at 4°C	**rbαFibronectin pAb 1:150** in **Ab diluent** (Dako)		
Day 2	washing	3 x 5 min	TBS-T/0.025%		
	2nd antibody	2h	**dαrb pAb-Cy3** conjugate (biolegend) **1:200** + **Phalloidin-A488** conjugate (Invitrogen) **1:400** in **5%NDS/1%BSA**/TBS		**dαrb pAb-Alexa488** conjugate (Invitrogen) **1:400** + **Phalloidin-A633** conjugate (Invitrogen) **1:100** in **5%NDS/1%BSA**/TBS
	washing	3 x 5 min	TBS-T/0.025%		
	equilibration	1 x 5 min	TBS	1 x 5 min	AMPUWA
	Draq5	1h	**Draq5 1:1000** in **TBS**	15 min	**DAPI 1:1500** in **AMPUWA**
	washing	3 x 5 min	TBS	3 x 10 min	AMPUWA
	storage	4°C	TBS		

Target protein	Cat. | manufacturer
Actin|Nuclei	Alexa Fluor® 488 Phalloidin (Invitrogen, A12379), 633 Phalloidin (Invitrogen, A22284), DAPI (Invitrogen, D3571), Draq5 (Biolegend, 424101)

All steps were conducted at room temperature if not otherwise stated. For buffer recipes, check other sources.

General volumes: all washing steps in a 24well plate with 1ml, staining solutions in a 48well with 300µl

	Step	Time	Description		
Day 1	washing	3 x 10 min	TBS-T/0.025%		
	washing	1 x 5 min	TBS		
	staining	2h	Alexa Fluor® **488 Phalloidin 1:400** + **Draq5 1:1000** in TBS	Alexa Fluor® **633 Phalloidin 1:100** in TBS	
	washing	3 x 10 min	TBS-T/0.025%		
	equilibration		DAPI staining can also be combined with Alexa-488 Phalloidin as well.	1 x 5 min	AMPUWA
	DAPI			15 min	**DAPI 1:1500** in **AMPUWA**
	washing			3 x 10 min	AMPUWA
	storage	4°C	TBS		

Supplement 3

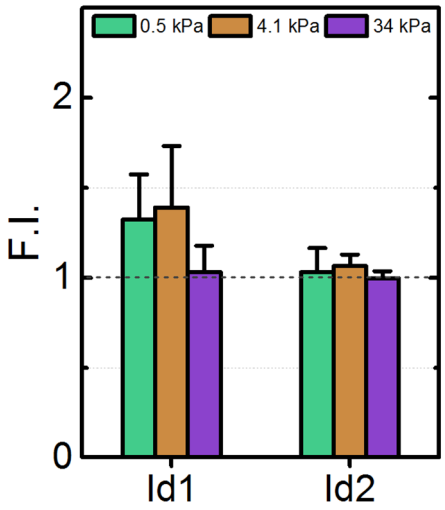

Gene expression analysis after 6h of BMP2 stimulation (1nM). Data are presented as fold change for each biomaterial stiffness relative to the unstimulated control (grey dashed line).

Abbreviations

A

APS *ammonium persulfate*

APTMS *(3-Aminopropyl)trimethoxysilane*

B

BMP *bone morphogenetic protein*

BRE *BMP response element*

BSA *bovine serum albumin*

C

CAD *computer-aided design*

D

ddH2O *double distilled water*

DMEM *Dulbecco's modified Eagle medium*

DMSO *dimethyl sulfoxide*

E

e.g. *exempli gratia*

ECM *extracellular matrix*

EDTA *ethylenediaminetetraacetic acid*

F

FACITs *fibril-associated collagens with interrupted helices*

FAK focal adhesion kinase

FBS *fetal bovine serum*

FDA *food and drug administration*

FGF *Fibroblast growth factor*

G

GAG *gylcosaminoglycan, glycosaminoglycan*

GAPDH *Glyceraldehyde 3-phosphate dehydrogenase*

GDF *Growth/Differentiation factor*

H

hdFs *human dermal fibroblasts*

hFOBs *human fetal osteoblasts*

hMSCs *human mesenchymal stromal cells*

I

IF *immunofluorescence*

IHH *Indian hedgehog, Indian Hedgehog*

IL *Interleukin*

ILK *integrin-linked kinase*

IVMTs *in vitro-grown micro-tissues*

L

LDS *Lithium dodecyl sulfate*

M

MACITs *membrane-associated collagens with interrupted helices*

MES *2-(N-Morpholino)ethanesulfonic acid*

MLC *myosin light chain*

mM *milli molar*

MMPs *matrix metalloproteinases*

MNE *mean normalized expression*

mRNA *messenger RNA*

MSC *Mesenchymal stem cell*

N

NDD *non descanned detectors*

NEA *non-essential amino acids*

P

P/S *Penicillin/Streptomycin*

PAA *polyacrylamide*

PBS *Phosphate buffered saline*

PCR *polymerase chain reaction*

PDMS *polydimethylsiloxane*

PEEK *polyether ether ketone*

PFA *paraformaldehyde*

PGs *proteoglycans*

PI3K *phosphatidylinositol 3-kinase*

POM *polyoxymethylene*

PTHrP *parathyroid hormone-related peptide*

Q

qPCR *quantitative PCR*

q-RT-PCR *quantitative reverse transcription PCR*

R

ROI *region of interest*

S

SHG *second harmonic generation*

T

TCP *tissue culture plastic*

TFM *traction force microscopy*

TGF *Transforming growth factor*

TIMPs *tissue inhibitor of metalloproteinase*

TNF *tumor necrosis factor*

U

UV *ultraviolet*

Danksagung

An dieser Stelle möchte ich mich zunächst bei Ansgar Petersen bedanken. Zum einen für den Einsatz dieses Projekt und deren Finanzierung zu ermöglichen, zum anderen aber vor allem für seine Unterstützung, ohne welche diese Arbeit nicht im Ansatz seine gegenwärtige Qualität aufweisen würde. Es war und ist mir eine Freude und ein Privileg mit dir zusammen zu arbeiten sowie die Freiheiten zu genießen die du zur Entfaltung der individuellen Forschungsinteressen gewährst.

Ein besonderer Dank geht auch an Georg Duda und Petra Knaus, welche mich als Betreuer während dieser Zeit begleitet haben und ebenfalls großen Anteil an der Umsetzung dieser Doktorarbeit haben. Ihr gabt stets Hilfe, wenn ich sie benötigte und habt durch eine unterstützende und konstruktive Arbeitsumgebung zur Entwicklung sowohl meinerseits als auch des Projektes beigetragen.

Unter den zahllosen Personen, die ich während dieser Zeit kennen gelernt habe, möchte ich mich allen voran bei Aaron und Sophie bedanken. Ihr habt mich nicht nur im Labor unterstützt wo immer es euch möglich war. Vielmehr sind es die zahllosen Abende und Mittagspausen, die aus uns mehr als nur Arbeitskollegen gemacht haben. Es war eine tolle Zeit, die ich für immer in Erinnerung behalten werde.

Mein Dank gilt natürlich auch allen gegenwärtigen und ehemaligen Mitgliedern des CBM Teams, insbesondere aber meinen Studenten Laura, Simone und Tobias. Ihr habt Wunderbares geleistet während eurer Zeit und mit euren Arbeiten entscheidend zu den verschiedensten einzelnen Kapiteln dieser Dissertation beigetragen.

Darüber hinaus all die Menschen, die meinen Arbeitsalltag nicht nur wissenschaftlich, sondern auch menschlich bereichert haben. In dieser Hinsicht geht besonderer Dank an Oliver Klein welcher die MS Messungen vorgenommen hat.

Zu guter Letzt möchte ich mich bei all den Menschen Bedanken die mich privat immer unterstützt haben. Meine Freunde, mit denen man nach all den Jahren einfach nur auf den Moment anstoßen kann um die alltäglichen Probleme und Sorgen auszublenden. Meine Eltern, die mich immer unterstützt haben so gut sie konnten. Und am meisten jedoch danke ich meiner Frau Jana. Die vergangenen Jahre haben uns nicht nur weiter zusammen geschweißt bei all dem was wir erlebt und durchgemacht haben. Sie haben auch das Beste

was uns bisher passiert ist hervorgebracht – unseren kleinen (und doch schon so erschreckend großen) Sohn Theo der mit seiner Lebensfreude und seinem Grinsen jeden noch so grauen Tag mit Sonne flutet. Ihr seid das was zählt.

Curriculum Vitae

Der Lebenslauf ist in der Online-Version aus Gründen des Datenschutzes nicht enthalten.

Freie Universität Berlin

Selbstständigkeitserklärung

Name: BRAUER	(Nur Block- oder Maschinenschrift verwenden.)
Vorname: ERIK	
geb.am:	
Matr.Nr.: 4287893	

Ich erkläre gegenüber der Freien Universität Berlin, dass ich die vorliegende DISSERTATION selbstständig und ohne Benutzung anderer als der angegebenen Quellen und Hilfsmittel angefertigt habe.

Die vorliegende Arbeit ist frei von Plagiaten. Alle Ausführungen, die wörtlich oder inhaltlich aus anderen Schriften entnommen sind, habe ich als solche kenntlich gemacht.

Diese Arbeit wurde in gleicher oder ähnlicher Form noch bei keiner anderen Universität als Prüfungsleistung eingereicht.

Datum: 13.01.2020 Unterschrift: _____